Title
INFRARED SPECTROSCOPY OF WEAKLY BOUND MOLECULAR IONS

Author
Yeh, L.I.-C.

Publication Date
1988-11-01

Lawrence Berkeley Laboratory
UNIVERSITY OF CALIFORNIA

Materials & Chemical Sciences Division

Infrared Spectroscopy of Weakly Bound Molecular Ions

L.I.-C. Yeh
(Ph.D. Thesis)

November 1988

Prepared for the U.S. Department of Energy under Contract Number DE-AC03-76SF00098.

DISCLAIMER

LBL-26331

Infrared Spectroscopy of Weakly Bound Molecular Ions

Lisa I-Ching Yeh
(Ph.D. Thesis)

Materials and Chemical Sciences Division
Lawrence Berkeley Laboratory
1 Cyclotron Road
Berkeley, California 94720
USA

November 1988

This thesis is dedicated to all professional women who struggle for equal opportunity, equal acceptance, and equal respect.

Infrared Spectroscopy of Weakly Bound Molecular Ions

by

Lisa I-Ching Yeh

Abstract

The infrared spectra of a series of hydrated hydronium cluster ions and of protonated ethane ion are presented. A tandem mass spectrometer is ideally suited to obtaining the spectra of such weakly bound molecular ions. Traditional absorption spectroscopy is not feasible in these situations, so the techniques described in this thesis make use of some consequence of photon absorption with higher sensitivity than simply attenuation of laser power. That consequence is dissociation. By first mass selecting the parent ion under study and then mass selecting the fragment ion formed from dissociation, the near unit detection efficiency of ion counting methods has been used to full advantage.

A brief introduction to the field of ion spectroscopy is the subject of Chapter I. Chapters II and III present spectra of the series of hydrated hydronium cluster ions, $H_3O^+ \cdot (H_2O)_n$ (n = 1, 2, 3). In Chapter II, the spectra of $H_5O_2^+$, $H_7O_3^+$, and $H_9O_4^+$ are compared to the spectra taken

using a "messenger" weakly bound to the water cluster ion under investigation. These "messenger" species are bound loosely enough that only a single infrared photon is needed to induce dissociation. The hydrated hydronium ions, on the other hand, have a binding energy exceeding the energy of an infrared photon and require a multiphoton absorption process to induce dissociation. Both one-color and two-color laser schemes were used, as described in Chapter II. Chapter III discusses the Doppler limited spectra obtained of $H_5O_2^+$ and $H_9O_4^+$ and gives the reader an introduction to permutation-inversion group theory, which is used to treat the large amplitude motions permissible in these floppy cluster ions.

The infrared spectrum of $C_2H_7^+$ is the subject of Chapter IV. The controversy over whether various carbonium ions exist in the classical or the nonclassical bridging structure is briefly reviewed. Evidence is presented that the spectra of both the classical and the bridging geometries of $C_2H_7^+$ have been obtained and preliminary assignments are given for all observed features.

ACKNOWLEDGEMENTS

Being a graduate student in Berkeley has sometimes been enjoyable, sometimes depressing, but never boring. Many people have contributed positively to my graduate experience and I would like to thank them here.

First, I need to thank Yuan Lee for giving me the opportunity to do good science and providing me with constant challenges. It has been a privilege to work for such a great scientist and have the benefit of his ideas. Yuan's hands off management style sometimes led to problems, but overall was beneficial. He gave the students in his group a great deal of responsibility and freedom in the laboratory. This allowed us the chance to try out our own ideas and learn from our successes and failures.

Of the many people I have worked with, my collaboration with Mitchio Okumura was the most extensive and I am deeply indebted to him. I want to thank him for teaching me about ion spectroscopy and for his patience with me through the years. The data on the hydrated hydronium ionic clusters using a hydrogen messenger was taken by him.

I only overlapped briefly with Sandy Bustamente, but his encouragement and kindness will long be appreciated. Sandy also was the predecessor most responsible for building the spectrometer and writing the data acquisition

program. Didier Normand lent his laser expertise to our early experiments on CH_2^- and CH^- lifetimes and came in at 6 AM to relieve me from all night data scans.

I also want to thank Jim Myers, who worked with me on the 2-color IRMPD studies of the water cluster ions. John Price helped with the $H_7O_3^+ \cdot Ne$ spectrum and had the insight to go back and take the $H_9O_4^+$ spectrum using a one-color MPD approach after we accidentally discovered it would work. He also kept the laser system going in the $C_2H_7^+$ studies. Mark Crofton joined the ion spectroscopy effort after I was off the machine, so I missed the opportunity of working with him. Even so, we have had many interesting spectroscopy discussions and I want to thank him for that. It's sometimes difficult being a spectroscopist in a non-spectroscopy group.

I have also had the benefit of working with many theoreticians outside of the group. Richard Remington and Fritz Schaefer did the calculations on the structures, energies, and frequencies of the hydrated hydronium ions. Michel Dupuis calculated vibrational frequencies for $C_2H_7^+$ and his results are quoted extensively in the last chapter. Jon Hougen helped immensely in my understanding of permutation-inversion group theory and was amazingly patient and fun to work with. Tim Lee calculated vibrational lifetimes for CH_2^-. Martin Gruebele, while not a

theorist, is appreciated for all the conversations on $H_5O_2^+$ and spectroscopy in general.

Many other people in the Lee group have also helped me out. I want to thank Eric Hintsa for his willingness to talk to me about science, China, politically correct causes, and for being my friend. I've also enjoyed talking with Pam Chu who kept our group computer system going. Gil Nathanson was always willing to answer my questions and I wish him the best of luck at Wisconsin. Present office-mates Zhao Xinsheng, Mike Covinsky, and Arthur Suits have all contributed to enriching my graduate experience. Thanks for the Chinese lessons, Xinsheng. My first office-mates Tom Turner and Peter Felder helped me assimilate into the Lee group. Thanks for all the car work lessons, Tom. Other people in the group I want to thank include Anne-Marie Schmoltner, Alec Wodtke, Rick Brudzynski, Laurie Butler, Jeremy Frey, and Gary Robinson.

I want to thank Tony Moscarelli for all the late night machining assistance he cheerfully gave me. George Weber built the corona discharge source that all of the data in this thesis was taken with. Fred Wolff and Andy Anderson also gave valuable assistance on shop projects. I especially want to thank Charalambos "Harry" Chiladakis for his assistance when we moved down to campus.

These acknowledgements would not be complete without thanking E. Ann Weightman for keeping the group running

when Yuan was out of town. She also did many things outside of her job description for me and for that I am grateful.

Going back to Illinois, I would like to thank Larry Faulkner, Steve Zumdahl, and Gilbert Haight for the opportunities they gave me, the encouragement I received, and the complete confidence they had in me. David Chandler taught an excellent PChem course and sparked my interest. I am grateful to my high school chemistry and physics teachers, Clyde Smith and Al Smith, for introducing me to how interesting and fun science can be.

Finally, I thank my family for their continuing support and encouragement over the years. I thank Doug Krajnovich for loving me with all of his stubbornness.

This work was supported by the Director, Office of Energy Research, Office of Basic Energy Sciences, Chemical Sciences Division of the U. S. Department of Energy under Contract No. DE-AC-0376SF00098.

Table of Contents

Chapter I

Introduction

Research in the field of ion spectroscopy has made remarkable progress in recent years.[1-4] Initial spectra were constrained to the visible wavelength range and are described in the review by Herzberg.[5] An early exception was the work by Dehmelt and Jefferts on H_2^+ which used an rf-optical double resonance technique to obtain a relatively high resolution rf spectrum.[6-8]

Spectroscopy of ions in the microwave range was developed in the early 1970's. The first rotational spectra was obtained by radio astronomers of HCO+ and N_2H^+ through emission.[9-11] This was soon followed by laboratory absorption spectra of HCO^+, N_2H^+, and CO^+ from Wood's group.[12-14]

Infrared spectroscopy of molecular ions was pioneered by Wing in his study of HD^+.[15] He used a fast ion beam to take advantage of kinematic compression followed by charge exchange as the method of detection. This technique has the advantage of high detection sensitivity since it uses ion detection, but has the disadvantage of relying on a small change in the charge exchange cross section upon vibrational excitation. Carrington et al. also used the

fast ion beam coupled with charge exchange in their study of CO^+.[16] Indirect detection schemes such as the above, that rely on ion counting, have often been advantageous over direct detection approaches, that rely on photon absorption or emission.

Another indirect detection scheme makes use of a change in the ion-molecule reaction cross section upon excitation. Carrington et al. used this technique in their study of H_2O^+.[17] In order to increase the difference in reaction rate between ground state H_2O^+ and electronically excited H_2O^+, they found it necessary to retard the fast ion beam after interacting with the laser but before colliding with the H_2 target gas. A loss of beam intensity was caused by the deceleration process. The ideal application of this approach is to a system where the ground state reaction is endothermic and the excited state reaction is exothermic.

Electronic predissociation is another indirect detection scheme, and was used by Carrington[18] and Cosby[19] to study the $b^4\Sigma_g^-$ <- $a^4\Pi_u$ transition in O_2^+. Predissociative lifetimes are often long enough that narrow spectral features can be seen. This method also utilizes the sensitivity of ion detection. A difficulty with this technique is that some prior knowledge of the electronic states or vibrational states is necessary in order to design the experiment.

Photodissociation and photodetachment processes have also been used to study ion spectroscopy. Lineberger used a two-photon process to study the negative ion C_2^-, one of the few negative ions with a bound electronic state.[20] Carrington used a one-photon dissociation process to study highly vibrationally excited HD^+.[21]

The first infrared direct absorption spectrum of a molecular ion was taken by Oka in 1980 of H_3^+.[22] He combined a liquid nitrogen cooled multiple-reflection discharge cell with a difference frequency laser system. The estimated density of H_3^+ in the discharge was 3×10^{10} ions/cm^3. The infrared spectrum of D_3^+ was also reported in 1980, and was obtained using a fast ion beam with indirect detection by charge-exchange.[23]

Direct absorption spectroscopy of molecular ions in the infrared region became more widely applicable with the advent of the velocity modulation technique.[24,25] One of the overriding difficulties when studying ions is that they are greatly outnumbered by the neutrals also present. The velocity modulation approach makes use of the fact that the velocity of ions can be readily controlled by an applied electric field. As in the fast ion beam work where the ions are Doppler shifted into resonance, the velocity modulation method makes use of the Doppler effect to shift an ion into resonance. However, the applied field is modulated so that the ions are alternately

accelerated in opposing directions in the discharge cell whereas the neutrals remain comparatively unperturbed. This means that the neutral signals can be fairly effectively discriminated against using ac detection techniques.

Infrared spectroscopy of negative ions has also been making advances. Using vibrational autodetachment, the vibrational spectrum of NH^- was obtained by Neumark et al.[26] Velocity modulation was used to obtain the direct absorption spectrum of OH^- by Owrutsky et al.[27] Also from Saykally's group, the first infrared direct absorption spectrum in an ion beam was obtained by Coe et al. of N_2H^+.[28]

The indirect technique of vibrational predissociation has been used to study the hydrogen cluster ions and other weakly bound ions as described in the next chapter and in Refs. 29-32. The indirect technique of photodissociation has also shown new promise.[33] As described in subsequent chapters, it has been developed into a two-color approach. Although direct absorption techniques have improved drastically in the last decade, a fundamental limitation is the need for ion currents in the microamps range. By using more sensitive ion detection techniques we are able to study exotic molecular ions that are formed with only picoamps of ion current and that may be partitioned over a large number of initial states.

REFERENCES

1. A. Carrington, Proc. R. Soc. Lond. A **367**, 433 (1979).

2. R. J. Saykally, and R. C. Woods, Annu. Rev. Phys. Chem. **32**, 403 (1981).

3. Molecular Ions: Spectroscopy, Structure, and Chemistry, T. A. Miller, and V. E. Bondybey, eds. (North-Holland, Amsterdam, 1983).

4. J. V. Coe and R. J. Saykally, in Spectroscopy and Structures of Molecular Clusters and Molecular Ions, John Myer, ed. (Elsevier Science Publishers, Amsterdam, 1988), to be published.

5. G. Herzberg, Rev. Chem. Soc. **25**, 201 (1971).

6. H. G. Dehmelt, and K. B. Jefferts, Phys. Ref. **125**, 1318 (1962).

7. K. B. Jefferts, Phys. Rev. Lett. **20**, 39 (1968).

8. K. B. Jefferts, Phys. Rev. Lett. **23**, 1476 (1969).

9. W. Klemperer, Nature, Lond. **227**, 1230 (1970).

10. D. Buhl and L. E. Snyder, Astrophys. J. **180**, 791 (1973).

11. S. Green, J. A. Montgomery, and P. Thaddeus, Astrophys. J. **193**, L 89 (1974).

12. R. C. Woods, T. A. Dixon, R. J. Saykally, and P. G. Szanto, Phys. Rev. Lett. **35**, 1269 (1975).

13. T. A. Dixon and R. C. Woods, Phys. Rev. Lett. **34**, 61 (1975).

14. R. J. Saykally, T. A. Dixon, T. G. Anderson, P. G. Szanto, and R. C. Woods, Astrophys. J. **205**, L 101 (1976).

15. W. H. Wing, G. A. Ruff, W. E. Lamb, and J. J. Spezeski, Phys. Rev. Lett. **36**, 1488 (1976).

16. A. Carrington, D. R. J. Milverton, and P. J. Sarre, Mol. Phys. **35**, 1505 (1978).

17. A. Carrington, D. R. J. Milverton, P. G. Roberts, and P. J. Sarre, J. Chem. Phys. **68**, 5659 (1978).

18. A. Carrington, P. G. Roberts, and P. J. Sarre, Mol. Phys. **35**, 1523 (1978).

19. P. C. Cosby, J.-B. Ozenne, and J. T. Moseley, J. Mol. Spectrosc. **79**, 203 (1980).

20. W. C. Lineberger and T. A. Patterson, Chem. Phys. Lett. **13**, 40 (1972).

21. A. Carrington and J. Buttenshaw, Mol. Phys. **44**, 267 (1981).

22. T. Oka, Phys. Rev. Lett. **45**, 531 (1980).

23. J.-T. Shy, J. W. Farley, W. E. Lamb, and W. H. Wing, Phys. Rev. Lett. **45**, 535 (1980).

24. R. J. Saykally and C. S. Gudeman, Annu. Rev. Phys. Chem. **35**, 387 (1984).

25. C. S. Gudeman, M. H. Begemann, J. Pfaff, and R. J. Saykally, Phys. Rev. Lett. **50**, 727 (1983).

26. D. M. Neumark, K. R. Lykke, T. Andersen, and W. C. Lineberger, J. Chem. Phys. **83**, 4364 (1985).

27. J. C. Owrutsky, N. H. Rosenbaum, L. M. Tack, and R. J. Saykally, J. Chem. Phys. **83**, 2426 (1985).

28. J. V. Coe, J. Owrutsky, E. Keim, N. Agman, and R. J. Saykally, J. Chem. Phys. (in press).

29. M. Okumura, L. I. Yeh, and Y. T. Lee, J. Chem. Phys. **83**, 3705 (1985).

30. M. Okumura, L. I. Yeh, and Y. T. Lee, J. Chem. Phys. **88**, 79 (1988).

31. M. Okumura, L. I. Yeh, J. D. Myers, and Y. T. Lee, J. Chem. Phys. **85**, 2328 (1986).

32. M. Okumura, Ph.D. Thesis, University of California, Berkeley, 1986.

33. L. I. Yeh, M. Okumura, J. D. Myers, J. M. Price, and Y. T. Lee, to be published.

Chapter II

Vibrational Spectroscopy of the Hydrated Hydronium Cluster Ions, $H_3O^+ \cdot (H_2O)_n$ (n = 1, 2, 3)

I. Introduction

Properties of the hydrated hydronium ions are of broad interest in chemistry.[1] The hydronium ion and its hydrated analogues are present throughout our natural environment. Narcisi and Bailey identified H_3O^+ and $H_5O_2^+$ in the D region of the ionosphere in their pioneering rocket-borne mass-spectrometer flights.[2] Since then, it has been shown that $H_3O^+ \cdot (H_2O)_n$ ions are the dominant ions in the D region.[3] Not only are water cluster ions important in atmospheric studies, they are also important components of aqueous solutions and govern the proton transfer process.

Much of the early work attempted to determine the structure of these ions in crystals by using x-ray[4-6] or neutron diffraction[6-8] data. Soon after Nakahara, Saito, and Kuroya first suggested the existence of $H_5O_2^+$ in crystals of organic acids,[9] a central question became whether this ion existed as the asymmetric $H_3O^+ \cdot H_2O$ structure or the symmetric $H_2O \cdot H^+ \cdot OH_2$ structure. Evidence

to support both conclusions was found among the many crystal environments studied.[7,8]

Spectroscopic work was also initially constrained to liquid or crystalline phases. Infrared absorption was used to confirm the presence of dioxonium ion ($H_5O_2^+$) in several different salts.[10] One of the earliest IR spectra of $H_9O_4^+$ was taken in an HBr crystalline hydrate.[11] Many other spectroscopic studies soon followed.[12-17] All of these studies share the problems of low resolution and ambiguity in assigning absorption features.

Gas phase studies were carried out on hydrated protons by Searcy and Fenn, who used a quadrupole mass spectrometer to detect $H^+(H_2O)_n$ (n=1-28) formed in a corona discharge source.[18] Lancaster et al. detected large water clusters of n = 1 to 180 from the secondary ion mass spectrum of ice.[19] Beuhler and Friedman used mass spectrometric detection to study formation of water cluster ions of m/e < 59000.[20] Important thermodynamic work was done by Kebarle's group in studying the temperature dependence of the equilibrium constants for reactions involving the successive addition of a water molecule to determine heats of reaction. They obtained binding energies of $H_3O^+ \cdot (H_2O)_n$ to be 31.6, 19.5, and 17.9 kcal/mole (11050, 6820, and 6260 cm^{-1}) for n = 1, 2, and 3, respectively.[21-23] An independent investigation by

Meot-Ner and Field found binding energies of 33.0, 21.0, and 16.0 kcal/mole for n = 1, 2, and 3, respectively.[24]

Gas phase spectroscopic work on the hydrated hydronium ions was carried out by Schwarz.[25] He used a 2.1 MeV electron beam pulse produced by a Van de Graaff accelerator to ionize argon. The argon then transferred the ionization to a small amount of water vapor, which was also present in the reaction cell. Absorption spectra from 2000-4000 cm^{-1} of the ions $H_3O^+ \cdot (H_2O)_n$ (n = 3, 4, 5) were obtained at 40 cm^{-1} resolution by monitoring the attenuation of light, produced by a globar operated at 1450°C, as a function of frequency. By varying the partial pressure of water vapor, the relative abundances of different size clusters could be changed. Equilibrium constants from Kebarle et al.[21] were used to estimate these abundances and decompose the data into individual spectra for each cluster ion. Spectral features assigned to $H_9O_4^+$ occurred at 3710 and 3620 cm^{-1}, corresponding to the antisymmetric and symmetric modes of the three outer water molecules, and at 3000 and 2660 cm^{-1}, corresponding to the symmetric and antisymmetric modes of the central H_3O^+.

High resolution infrared absorption spectra have recently been taken on the predecessor of these ions, H_3O^+.[26-31] This work found the inversion splitting of the

ground state to be 55.3 cm^{-1}.[29,31] These experimental searches were complemented by theoretical efforts.[32-35]

Theoretical efforts have also attempted to determine the structure and vibrational spectra of the larger hydrated hydronium ions.[36-38] SCF-LCGO calculations by Potier, Leclercq, and Allavena found $H_5O_2^+$ to have C_2 symmetry.[39] They systematically varied the ∠HOH of the two end waters, the angle between the O-O direction and the bisecting line of the ∠HOH angle, and the relative orientation of the two water groups to find the lowest energy structure. They calculated a barrier height of ~1.1 kcal/mole for rotation of the end waters, and ~1.2 kcal/mole to bend the plane of the end water groups. The binding energy of $H_5O_2^+$ relative to the sum of the energies for separated H_2O and H_3O^+ was calculated to be 32.06 kcal/mole. Potier et al. also addressed the ease with which the $H_5O_2^+$ structure adjusts to its environment. They report that the range of experimental structures found in crystals are practically all within kT of the lowest energy structure. Unpublished results by Remington and Schaefer predict structures and vibrational frequencies and intensities for $H_3O^+ \cdot (H_2O)_n$ (n = 1, 2, 3).[40] Their calculations were done at the SCF level using a DZP basis set for all three ions. In addition, $H_5O_2^+$ was treated at the Configuration Interaction level including single and double excitations (CISD) with a DZP basis set. Calcu-

lated structures at the highest level of theory used for these three water cluster ions are shown in Fig. 1. These cluster ions can be viewed as an H_3O^+ core which has been solvated by H_2O groups. This interpretation of the structures becomes more accurate as the cluster size increases. Their results will be presented in detail below.

Studying the vibrational spectroscopy of cluster ions, such as the hydrated hydronium ions, $H_3O^+ \cdot (H_2O)_n$, is an inherently difficult problem. Although one may study these species in the liquid phase or in a gas cell where their densities are relatively high, these methods have the disadvantage of ambiguity in assigning absorption features to a given species (see, for example, Ref. 25). The velocity modulation technique[41] in gaseous discharge plasmas has provided important information on high resolution infrared absorption spectra of molecular ions, but weakly bound ionic clusters are practically impossible to study in high temperature plasmas, even if they can be formed with high densities, due to the partition function. Using an ion beam has the advantage of mass selection capability, but at the expense of orders of magnitude in ion density. In most cases, this makes traditional absorption spectroscopy impossible.[42] Thus, one has to depend on the observation of the consequence of photon absorption, rather than the attenuation of photon inten-

sity due to absorption, when studying cluster ion spectroscopy.

For very weakly bound ionic clusters such as H_5^+, H_7^+, H_9^+, etc. excitation of vibrational degrees of freedom induces dissociation and one can use the vibrational predissociation process to obtain vibrational spectra[43,44] as has been done in the investigation of neutral molecular clusters.[45,46] But there are many cluster ions, such as the hydrated hydronium ions, whose binding energy far exceeds the energy of vibrational quanta, and the vibrational predissociation process will not occur after excitation of the fundamental molecular vibration. In our recent ion beam study of the hydrated hydronium ions, we have overcome this obstacle by utilizing two complementary techniques. Both methods take advantage of the inherently high sensitivity of ion detection.

The first approach, which has been reported previously,[47-49] is to attach a weakly bound "messenger" to the hydrated hydronium ions. Because the goal is to study the hydrated hydronium ions, the attached messenger is hoped to have only a small effect on the spectrum. The scheme is as follows. A tunable infrared laser is used to excite the O-H stretch of the cluster ion. That vibrational energy gets transferred to the weakest coordinate which is the bond to the messenger. This causes the cluster ion to undergo vibrational predissociation, losing

the messenger. The role of the messenger is to indicate when an absorption has taken place. By monitoring the dissociation product as a function of laser frequency, the absorption spectra of these $H_3O^+ \cdot (H_2O)_n \cdot$messenger (n = 1, 2, 3) ions have been found. Initially, hydrogen molecule was used as the messenger.[47-49] More recently, spectra have been taken for $H_7O_3^+$ using neon as a messenger.[50]

The second approach is to detect the vibrationally excited $H_3O^+ \cdot (H_2O)_n$ (n = 1, 2, 3) ions using an infrared multiphoton dissociation process. The procedure is to first excite from v = 0 to v = 1 in the O-H stretch using a tunable IR laser. We then make use of the fact that the density of states near v = 0 and v = 1 are very different, and the vibrationally excited ionic clusters, which contain many low frequency vibrations, are likely to be in a region with a high enough density of states for the sequential excitation by a fixed frequency laser. This means that one can distinguish between ground state and vibrationally excited $H_3O^+ \cdot (H_2O)_n$ by using a multiphoton dissociation (MPD) process to selectively dissociate the latter using a CO_2 laser. Once again, we monitor the dissociation product ion signal as a function of the excitation frequency of the first laser to get the absorption spectra of the $H_3O^+ \cdot (H_2O)_n$ ions.

This chapter presents the spectra of $H_5O_2^+$, $H_7O_3^+$, and $H_9O_4^+$ from 3550 to 3800 cm^{-1} and compares them to the

spectra of $H_5O_2^+ \cdot H_2$, $H_7O_3^+ \cdot H_2$, $H_9O_4^+ \cdot H_2$,[47-49] and $H_7O_3^+ \cdot Ne$.[50] A comparison with vibrational frequencies calculated using ab initio methods by Remington and Schaefer[40] is also made and implications regarding the structures and the messenger binding sites are discussed.

II. Experimental Details

An unusual feature of this experiment arises from the ubiquitous nature of water. The proton affinity of H_2O is 167 kcal/mole, which is 66 kcal/mole higher than the carrier gas H_2. Thousands of collisions occur at 100 torr before the supersonic expansion, allowing the predominant ion to be determined by energetics rather than kinetics or neutral abundance. Therefore, protonated water ions will be the dominant ion species even with very little neutral water present. Because only trace amounts of water are necessary for this experiment, we found the residual water on the walls of the 1/4 in. copper tubing was sufficient as the source of water. In fact, even this was too much even though the inlet line was routinely pumped and Matheson ultra-high purity H_2 (99.999%) was generally used. Therefore, a molecular sieve trap filled with Linde 13X 1/8 in. pellets was used in the inlet line. For $H_5O_2^+$, the sieve trap was cooled using liquid nitrogen. $H_7O_3^+$ production was optimized with the sieve trap cooled in an ice bath. The larger $H_9O_4^+$ cluster was produced in large

quantities by bypassing the sieve trap and running the gas directly into the source.

The source used to create these ions is a high pressure corona discharge source[18,51,52] as shown in Fig. 2. For these experiments, the body of the source itself was not cooled and was probably only slightly above room temperature due to heat from the discharge. Typical discharge conditions behind the nozzle are 1.2 kV from cathode to anode, 20-40 μA discharge current, and 200 torr of H_2 gas containing trace amounts of H_2O. The cathode, which is floated at 350 V, is the copper wall of the source which is located 0.150 ± 0.003 in. away from the nickel plated iron needle which serves as the anode. The nozzle, which is silver soldered into the source body is therefore also floated at 350 V. The beam containing various ionic clusters is formed by expanding the plasma through a 75 μm nozzle. 6.4 mm downstream from the nozzle is a 1.5 mm diameter skimmer which is floated such that the difference in potential between the nozzle and skimmer is 1 V or less. This is to prevent collisional heating of the nascent cluster ions. A grid which is also floated at 350 V surrounds the nozzle/skimmer area to keep this area relatively field free. In the chamber before the skimmer an operating pressure of 1-2 x 10^{-4} torr is achieved using a liquid nitrogen trapped 10 in. diffusion pump backed by a Roots pump.

After the skimmer, the ions pass into a second differential region, with pressures normally at least an order of magnitude lower than in the first region. Here, they are focused and deflected in one of two possible directions. One direction is toward a quadrupole mass filter with electron multiplier system which is used for source characterization and optimization. The other direction is to a third differential region (at 2×10^{-8} torr) where mass selection is achieved using a 60° sector magnet as shown schematically in Fig. 3. The process of mass selection allows us to eliminate the background ions completely as well as to unambiguously ascertain the identity of the ion being studied. Because the magnet acts as a momentum selector, only ions of a particular mass, which is determined by the strength of the magnetic field, follow the arc of 20 cm radius for a given source energy. The mass resolution of the sector magnet is about $M/\Delta M \approx 150$. To aid in achieving high transmission, a set of quadrupole lens pairs is placed before the magnet which changes a rectangular ion beam to one which is parallel in one plane and convergent in the other plane.[53-56] This focusses the ions to a line perpendicular to the magnetic field lines, compensating for the sector magnet which has no focussing in the z direction. Another set of eight short rods is placed after the magnet in order to defocus the ions and collimate them into a 3.2 mm inner diameter

tube. This tube, which is 36 mm long, leads to the ultra-high vacuum section of the machine, which has a pressure generally about 1×10^{-9} torr.

Upon entering the UHV region, the ion of interest is bent 90° by an electrostatic field. The primary motivation for bending the ion path is to have the capability of monitoring the laser power after it has passed through the machine. This field is generated by an electrostatic quadrupole field deflector as described by Zeman.[57] There are two major advantages to this selection. First, by choosing an electrostatic deflector all masses will be transmitted equally since, in our source, it is a good approximation to assume all masses have the same energy. Second, the quadrupole field deflector geometry has its rods spaced such that the laser beam can exit the machine without hitting the electrodes. This obviates the need to cut holes in the electrodes which would perturb the electric field.

The ions are then decelerated from 350 V to about 5 V and focused into a 50 cm long radio-frequency octopole ion trap. The ion trap consists of eight molybdenum rods of 0.32 cm diameter evenly spaced on a 1.25 cm diameter circle. An rf of 7.4 MHz and 200-300 V peak-to-peak is applied with adjacent rods having opposite phases. While the ions are trapped, they interact with a tunable infra-

red laser. Additional experimental details can be found in Ref. 58.

Two different laser schemes were needed depending on the approach taken. When studying $H_3O^+ \cdot (H_2O)_n \cdot$messenger, a single tunable infrared laser was needed.[47-50] The system used was a Quanta-Ray infrared wavelength extender (IR-WEX), which is a difference frequency laser. The IR-WEX generates infrared at the difference between the fundamental of a YAG laser and the output from a pulsed dye laser. The laser path between the output of the tunable infrared laser and the entrance of the machine was enclosed and continually flushed with dry nitrogen to reduce atmospheric water absorptions. The laser path was flushed in both laser schemes.

The second laser scheme consists of two lasers and is used to investigate the more strongly bound $H_3O^+ \cdot (H_2O)_n$. The first laser is a Burleigh cw F-center laser which is scanned from 3550 to 3800 cm^{-1} with a linewidth of 0.5 cm^{-1}. This is the O-H stretching region. The second laser, used to dissociate (through a multiphoton process) the vibrationally excited $H_5O_2^+$, $H_7O_3^+$, or $H_9O_4^+$ ions, is an MPB Technologies Inc. cw CO_2 laser. The frequency and intensity of the CO_2 laser are determined by trying to reach the ideal situation where none of the ground state $H_3O^+ \cdot (H_2O)_n$ ions absorb enough photons to dissociate, but those in v = 1 do dissociate into $H_3O^+ \cdot (H_2O)_{n-1}$ and H_2O.

This ideal situation is different for the three cluster ions studied and is described below. In $H_5O_2^+$, as opposed to $H_7O_3^+$ and $H_9O_4^+$, the ground state ions do not readily absorb enough photons to dissociate. In order to estimate the density of vibrational states, the direct count method with 7-9 frequency groups was used.[59] Around 3750 cm^{-1}, $H_5O_2^+$ is estimated to have 38 states/cm^{-1}, $H_7O_3^+$ has 65,000 states/cm^{-1}, and $H_9O_4^+$ has 2×10^8 states/cm^{-1}. Thus, the density of states for $H_5O_2^+$ is rather sparse, and it is not in the quasicontinuum region, making the multiphoton dissociation process less facile. Therefore, the CO_2 laser is run full power (8 W out of the laser) on R(24) of the 00^o1-02^o0 transition. Since a cw CO_2 laser is used, the length of time the $H_5O_2^+$ ions reside in the octopole ion trap is a third variable which is optimized to achieve a low H_3O^+ background from those $H_5O_2^+$ ions that do not absorb an IR photon from the F-center laser and a high H_3O^+ signal from those $H_5O_2^+$ that do. In this case, 100 msec was found to be optimal. The residence time of the ions and the laser intensity together determine the energy fluence of the laser irradiation of the ions in the trap. Both the F-center laser and the CO_2 laser were run cw into the ion trap of the machine. Typical $H_5O_2^+$ ion count rates with a 100 msec trap time were 2000 - 2500 cps. RRKM lifetimes of $H_5O_2^+$ excited 0.1 kcal/mole above the dissociation limit are estimated to be <1 μsec.

When studying $H_7O_3^+$, the CO_2 laser was set on R(20) of the $00^0 1 - 10^0 0$ band. The laser power output was just over 6 W, and the power after the beam exited the machine through the electrostatic bending field electrodes was generally 2.2 W. The trapping time chosen was 57.5 msec. This gave 6000-9000 cps of mass-selected $H_7O_3^+$ at the detector. A chopper was used to separate in time the FCL and CO_2 beams. The timing sequence was as follows. The lens at the entrance of the octopole trap was gated low for 1.0 msec to allow the $H_7O_3^+$ ions into the trap. The chopper then allowed the FCL into the trap for 25 msec. The CO_2 laser, starting 2.0 msec after the FCL was blocked, interacted with the ions for 30.5 msec. The lens at the exit of the octopole was then pulsed low for 5.0 msec to allow all of the ions out of the trap.

The CO_2 laser was run on the same line (R(20) of $00^0 1 - 10^0 0$) for $H_9O_4^+$. The intensity was attenuated by passing the beam through a gas cell containing ethylene. The gas cell was made out of brass with NaCl windows on either side placed at Brewster's angle in a non-parallel geometry to minimize both reflection losses and beam walk. The CO_2 intensity after passing through the gas cell was 2.0 W. Power measured at the opposite end of the machine was 0.6 W. Again, a trapping time of 57.5 msec was selected. $H_9O_4^+$ was the easiest ion to make, and we obtained 30,000-40,000 cps at the detector after trapping. The timing

sequence used for $H_9O_4^+$ was the same as that used for $H_7O_3^+$. The primary reason the chopper was not used in the $H_5O_2^+$ experiment was the lower signal levels obtained when chopping. This is likely due to radiative relaxation of the initially excited O-H stretch before the CO_2 laser was unblocked. Theorists have calculated vibrational radiative lifetimes of OH, OH^-, and OH^+ to be 82.0, 7.3, and 3.8 msec, respectively.[60] The lifetime of the O-H stretches excited in $H_5O_2^+$ should be between 82 and 3.8 msec. In the scheme using the chopper, the FCL is unblocked for 25 msec, and the CO_2 laser is unblocked 2 msec afterwards. This means that any $H_5O_2^+$ excited in the first msec, for example, waits 26 msec before the CO_2 laser can pump it up to the dissociation limit. It seems reasonable to conclude that the lower signal implies that many of the vibrationally excited $H_5O_2^+$ ions have relaxed back to ground state before the CO_2 laser was unblocked. The very low $H_5O_2^+$ ion counts obtained necessitated maximizing the signal. We could not afford any reductions to this already very low signal. Of course, the minimal absorption of CO_2 photons by $H_5O_2^+$ in the ground state allows us to use this scheme. Otherwise, the spectra could be substantially contaminated by those $H_5O_2^+$ which are first excited by a CO_2 photon.

After the F-center and CO_2 laser irradiation, all of the ions are ejected from the rf ion trap. It is the

creation of fragment ions, not the decrease of parent ions, that is monitored by an Extranuclear quadrupole mass filter equipped with a Daly-type ion detector.[61] Specifically, when studying $H_5O_2^+ \cdot H_2$, the quadrupole mass filter selects $H_5O_2^+$ fragment ions; when studying $H_5O_2^+$, the H_3O^+ ions are detected. By monitoring the fragment ion signal as a function of the tunable IR laser frequency, the vibrational spectrum is obtained.

III. Results

The previously presented hydrated hydronium spectra obtained by using a hydrogen molecule as a messenger[47-49] are shown in Fig. 4. Each spectrum will be compared in turn with the appropriate two color IRMPD spectrum.

A. $H_5O_2^+$

The smallest ion studied using the two color scheme was $H_5O_2^+$. The infrared spectrum obtained from 3550 to 3770 cm^{-1} is presented in Fig. 5. Two features are seen. At lower frequency is a broad, featureless band centered at 3608.8 cm^{-1} with a width of ~15 cm^{-1}. The higher frequency band, centered at 3684.4 cm^{-1}, is composed of many peaks, separated by ~11.6 cm^{-1}. Contrast this spectrum with the $H_5O_2^+ \cdot H_2$ spectrum shown in Fig. 4. Rather than two features, four are now evident with two of these bands being centered within 8 cm^{-1} of the two bands

seen by the IRMPD method. The very dissimilar spectra calls into question the validity of using H_2 as a messenger to obtain the spectrum of $H_5O_2^+$.

To understand the origin of the disparate spectra, one needs to consider the possible structures of $H_5O_2^+$. Remington and Schaefer calculated structures, energies, and frequencies for $H_5O_2^+$ at both the SCF and CISD levels. Two structures, which are very close in energy at both levels, are the C_s and C_2 structures. One of the primary differences between them is that the C_2 structure has a H in the center, making it resemble two H_2O units equally sharing a proton, whereas the C_s structure has the central H off to one side, making the $H_3O^+ \cdot H_2O$ picture more appropriate. The other major difference is that, in the C_s structure, the H_3O^+ is pyramidal whereas, in the C_2 structure, the $H_2O \cdot H^+$ is almost planar. The initial calculation, done at the SCF level, with a DZP basis set, found the C_s geometry to be lower in energy by 0.27 kcal/mole. The higher level CISD, also with a DZP basis set, found the C_2 structure lower in energy by 0.19 kcal/mole. The geometries also changed: the $H_2O \cdot H^+$ portion in the C_2 structure is more pyramidal at the CISD level than at the SCF level, and the central proton for the C_s structure is closer to the center at the CISD level than at the SCF level. In addition to structures, vibrational frequencies and intensities were calculated

for both the C_s and the C_2 geometries in the harmonic approximation with a semi-empirical scaling factor.

The fact that the C_2 and C_s structures are separated in energy by less than 0.2 kcal/mole indicates that the potential is very flat and that there is almost no barrier to motion of the central proton from its center position to the side. The estimated binding energy of the H_2 molecule to the $H_5O_2^+$, as discussed in Ref. 48, is less than 4 kcal/mole. This bond seems to be strong enough to shift the relative energies of the C_2 and C_s structures to favor the asymmetric C_s structure when the hydrogen molecule is attached.

This hypothesis is substantiated by comparing the spectra of $H_5O_2^+$ and $H_5O_2^+ \cdot H_2$ with the scaled frequencies calculated for the C_2 and C_s geometries. The two highest frequencies for the C_2 geometry, which correspond to antisymmetric O-H stretches of the two H_2O groups either in-phase or out-of-phase, are predicted to have the same frequency. The next two highest frequencies for the C_2 geometry correspond to the symmetric O-H stretch in- and out-of-phase. While they are predicted to be separated by 12 cm^{-1}, the intensity for the out-of-phase mode is predicted to be >30 times larger than the in-phase mode. Thus, theory predicts only three strong bands in this frequency region, two of which are accidentally degenerate. This is in agreement with the experimental $H_5O_2^+$

spectrum. The symmetric O-H stretch, calculated to occur at 3624 cm^{-1}, is seen at 3609 cm^{-1}. The antisymmetric O-H stretch, which is calculated at 3710 cm^{-1}, is found at 3684 cm^{-1}. These values are listed in Table I. The red shift from the symmetric and antisymmetric O-H stretches as seen in free water compared to the experimentally observed peaks is 43 and 72 cm^{-1}, respectively.

The spectrum of $H_5O_2^+ \cdot H_2$ cannot be fully assigned by comparing to either the $H_5O_2^+$ spectrum or the calculated frequencies for the C_2 geometry. Rather, the frequencies calculated using a C_s geometry fit the messenger spectrum better. The frequencies at 3617 and 3696 cm^{-1} have been assigned to the symmetric and antisymmetric O-H stretch. The band at 3660 cm^{-1}, which is, similar to the symmetric and antisymmetric O-H stretch, ~20 cm^{-1} higher than theoretically predicted, is assigned primarily to a free O-H stretch of the H_3O^+ and is an asymmetric stretch. The fourth band at 3528 cm^{-1}, however, is lower than theory by ~20 cm^{-1}. This band has also been assigned to a free O-H of the H_3O^+, but is a symmetric stretch. Although there is probably a substantial mixing of these normal modes, the discrepancy is explained by postulating that the H_2 messenger is located at this site.

In order to understand the origin of the sharp peaks seen in the 3684 cm^{-1} feature, it is helpful to realize that $H_5O_2^+$ is a near symmetric top. The rotational

constants from the ab initio C_2 structure are A = 6.120, B = 0.2936, and C = 0.2923 cm^{-1}. The progression seen is characteristic of a perpendicular band progression where the transition moment lies perpendicular to the symmetric top axis. For $H_5O_2^+$, the top axis lies along the O-H-O bond (not to be confused with the C_2 rotation axis which lies perpendicular to the O-H-O bond). Theory predicts two transitions at the same frequency of species A and species B, which would both give perpendicular bands, with an 8.6 to 6.5 intensity ratio. A perpendicular band would be dominated by a prominent series of Q branches from the different sub-bands, especially when A >> B,[62] as in this case. The separation of the Q branches should be 2(A'-B') which is 11.65 cm^{-1}. This is in good agreement with the experimentally observed spacing of ~11.6 cm^{-1}. Thus, we have assigned the spectrum shown in Fig. 5 to a progression of Q branches using the notation as described by Herzberg.[62] (The superscript P or R indicates ΔK, the large Q gives ΔJ, and the subscript is the K value for the lower state.) The possibility exists that the assignments should be shifted one position, i.e. the peak currently assigned to the $^RQ_0$ sub-band may actually be the $^PQ_1$ sub-band. A rotational temperature in the K quantum number of ~40 K is found.

An estimate of the legitimacy of using the symmetric top approximation can be made by using the b asymmetry

parameter. From Allen and Cross,[63]

$$b = \frac{C - B}{2A - B - C}$$

where b is expanded in a power series to give the energy correction terms. Using rotational constants calculated by Remington and Schaefer,[40] we obtain $b = 1.1 \times 10^{-4}$. This will give, except for very high J states, correction terms well below the resolution we are capable of obtaining due to the Doppler width of the ions moving back and forth in the ion trap. The Doppler width can be obtained from the formula,[64]

$$\delta\omega_D = 2\sqrt{\ln 2}\ \omega_0\ v_p / c$$

by estimating the most probable velocity in the trap. If an ion energy in the trap of 0.5 eV is used, which is actually an upper bound, a Doppler width of 0.028 cm^{-1} is obtained.

Data were also obtained at much higher resolution for the K'=1 <-- K"=0 and K'=2 <-- K"=1 sub-bands. The spectrum, which was Doppler limited, is discussed in the next chapter.

B. $H_7O_3^+$

The infrared spectrum obtained when H_3O^+ is solvated by two water groups is shown in Fig. 6. The three bands are located at 3637.4, 3667.0, and 3721.6 cm^{-1}. The bands at 3637.4 and 3721.6 cm^{-1} are assigned to the symmetric and antisymmetric O-H stretch of the outer water groups. The feature at 3667.0 cm^{-1} is due to the O-H stretch of the H_3O^+ core at the unoccupied site. The dashed lines in the figure correspond to the vibrational frequencies and intensities of the lowest energy C_s structure as calculated in Ref. 40. The solid lines correspond to the frequencies and intensities for the C_{2v} structure which is predicted to be higher in energy by 0.516 kcal/mole at the SCF level using a DZP basis set. The fact that the scaled frequencies from the C_{2v} geometry match our observed bands better implies that the C_{2v} structure may actually be the lowest energy geometry. Primary differences in the two structures are that, in the C_s symmetry structure, the central H_3O^+ is more pyramidal and the O-H-O bond is slightly bent. The C_{2v} structure has a planar H_3O^+ core and a linear O-H-O bond.

The spectrum for $H_7O_3^+ \cdot H_2$ is shown in Fig. 4. The three features are located at 3587, 3642, and 3726 cm^{-1}. The band at 3642 cm^{-1}, assigned to the symmetric O-H stretch, is only 5 cm^{-1} shifted from that seen in $H_7O_3^+$. Similarly, the antisymmetric O-H stretch at 3726 cm^{-1} is

shifted by less than 5 cm^{-1} from $H_7O_3^+$. The third feature, however, has been shifted from 3667.0 to 3587 cm^{-1}, i.e. 80 cm^{-1}. This band corresponds to the O-H stretch of the unoccupied site of the H_3O^+ core. This shift leads us to conclude that the H_2 messenger is localized at this binding site.

Spectra taken of $H_7O_3^+$ by using neon as a messenger are presented in Fig. 7. The symmetric and antisymmetric O-H stretches are located at 3640.2 and 3722.3 cm^{-1}. The feature at 3640.2 cm^{-1} proves more interesting and was scanned more carefully as shown in Fig. 8. To the blue of the dominant feature at 3640.2 cm^{-1} are several shoulders. The first one, located at 3646.2 cm^{-1}, arises from leakage of $H_9O_4^+$ through the sector magnet. Even though the magnet has a very high resolution, there is generally more than two orders of magnitude more $H_9O_4^+$ than $H_7O_3^+ \cdot Ne$. Neon was chosen as a messenger because we expected neon to perturb the spectrum much less than H_2, since it would be bound much more weakly. However, precisely because it is bound so weakly, it is very difficult to make $H_7O_3^+ \cdot Ne$. Therefore, even though $H_7O_3^+ \cdot Ne$ and $H_9O_4^+$ are separated by two mass units, and even though the resolution of the sector magnet was $M/\Delta M \approx 150$, the fact that generally we had at least two orders of magnitude more $H_9O_4^+$ than $H_7O_3^+ \cdot Ne$ explains why several percent of the purported $H_7O_3^+ \cdot Ne$ beam was actually $H_9O_4^+$. The shoulder seen at 3646 cm^{-1} agrees

within experimental uncertainty with the frequency of the symmetric O-H stretch of $H_9O_4^+$ at 3645 cm^{-1} as presented below.

The next shoulder, at 3657.8 cm^{-1}, is assigned to the O-H stretch of the H_3O^+ with the neon localized at the free binding site. As expected, neon does prove to be a much more subtle messenger than H_2. The shift of the O-H stretch at this H_3O^+ site has been reduced from 80 cm^{-1} to 9 cm^{-1}.

A much smaller third shoulder is located at 3668.7 cm^{-1}. This is only 2 cm^{-1} away from the position of the O-H stretch of the unoccupied H_3O^+ site in $H_7O_3^+$. It is not possible that this feature originates from $H_7O_3^+$ itself since we initially select mass 75 and we detect at mass 55. When studying $H_7O_3^+$, we mass select 55 and detect at mass 37. So, even if some $H_7O_3^+ \cdot Ne$ were metastable and dissociated to $H_7O_3^+$ during the flight through the machine, we would not detect its spectroscopy as a peak since we're monitoring the $H_7O_3^+$ mass. Rather, if we had metastables, that would show up as a dip in the spectrum at the frequency at which $H_7O_3^+$ absorbs when detecting at mass 55. A previous ion source that used electron impact ionization after a supersonic expansion was much hotter than the corona discharge source used here, and metastables were sometimes seen when studying the weakly bound hydrogen cluster ions.[44] When metastables are present, a constant

background of fragment mass can be detected even when the laser is off. If the laser is on, the fragment mass count would decrease when the IR laser is tuned to a resonance of the fragment ion. This translates into a dip in the spectrum when monitoring the ion count at the fragment mass. It also is impossible that this shoulder arises from an $H_9O_4^+$ absorption, since $H_9O_4^+$ has no spectral features at this frequency. Assuming this feature is real, the most likely explanation seems to be that the neon can bind at a second site near one of the two outer water moieties. If this is the case, then the perturbations on the O-H stretch at the now unoccupied site of the H_3O^+ core would be extremely small. This shoulder, at 3669 cm^{-1}, is located within 2 cm^{-1} of that found in $H_7O_3^+$ and is tentatively assigned to the O-H stretch of the H_3O^+ of this second $H_7O_3^+ \cdot Ne$ structure.

Taking the above conjecture a step further, one might expect additional features from the inequivalent H_2O groups. The O-H stretches for the H_2O unit near which the neon messenger is located should be red shifted from the frequencies found for the case with no messenger. The frequencies for the O-H stretches for the other H_2O moiety should be essentially equal to that found for $H_7O_3^+$ through the IRMPD technique. Therefore, a feature shifted from 3640 cm^{-1} closer to 3637.4 cm^{-1}, where this mode was found for $H_7O_3^+$, is expected for the unperturbed H_2O unit, and a

feature further to the red is expected for the H_2O near which the neon is bound. In fact, our spectrum does show a partially resolved peak at 3637.5 cm^{-1}, which we tentatively assign to the free water moiety in this alternative structure for $H_7O_3^+ \cdot Ne$.

The spectra of $H_7O_3^+$ was taken by yet another method. Rather than using the cw F-center laser followed by MPD using a cw CO_2 laser or using a messenger, a pulsed Infrared Wavelength EXtender (IR-WEX) by Quanta Ray was used. This is the same laser as was used in the messenger study, but in this application, no messengers were used. The high peak powers generated by the pulsed IR laser made it possible for $H_7O_3^+$ to absorb more than one photon from this laser. The $H_5O_2^+$ fragment was again monitored as a function of the frequency of the IR-WEX laser. The spectrum obtained of $H_7O_3^+$ is shown in Fig. 9. The three bands are located at 3637.4, 3664.6, and 3721.6 cm^{-1} which is within experimental error of the positions found using the FCL and CO_2 laser method. The ratio of the intensities of the symmetric and antisymmetric O-H stretches is different, however, from the two color scheme. This may be due in part to the ion current, which decreased by 25% during this scan. To some extent this may also be due to a difficulty during analysis. The method of taking a few hundred cm^{-1} spectrum is to take several segments and splice them together. The splicing is done by normalizing

each segment with respect to the next to obtain a smooth curve with no abrupt changes in slope. This procedure generates a 10% uncertainty in the relative peak heights. Part of the difference in the intensity ratio may also be real. Because the second photon from the IR-WEX is nearly resonant, some frequency dependence in the signal could originate from the second photon. This means that the relative intensities from the two color FCL and CO_2 laser spectrum is probably more reliable than that from the one-color IR-WEX spectrum. A cautionary note is added because the density of vibrational states near the 3722 cm^{-1} band is higher than near the 3637 cm^{-1} band by between 2 and 25% (the range of values is due to the lumpiness of the vibrational distribution). Unless the transition is saturated, this difference in state density could skew the relative intensities in the two color spectrum. A higher resolution scan of the peak at 3721.6 cm^{-1} is shown in Fig. 10.

c. $H_9O_4^+$

The infrared spectrum of $H_9O_4^+$ is shown in Fig. 11. In $H_9O_4^+$, the first solvation shell around the H_3O^+ core has been filled. This leads to a three fold symmetry so that a high level of degeneracy exists in the spectrum. Only two fundamentals are observed. The lower frequency one at 3644.9 cm^{-1} is assigned to the symmetric O-H

stretch of the three outer H_2O groups. This is actually composed of a vibration of species A_1 and another of species E in point group C_{3v}, which are predicted to be separated by ~1 cm^{-1} with a relative intensity of 0.0 to 5.1 $D^2/(Å^2 \cdot amu)$, respectively.[40] The higher frequency mode at 3730.4 cm^{-1} is assigned to the antisymmetric O-H stretch of the outer water groups and is also comprised of an A_1 and E species vibration. The calculated splitting is again essentially zero with a relative intensity of 15.2 to 0.2 $D^2/(Å^2 \cdot amu)$, respectively.[40]

The spectrum of $H_9O_4^+ \cdot H_2$ is shown in Fig. 4. Each of the two features seen in $H_9O_4^+$ has been split into a doublet. In each doublet, there is roughly a two to one intensity ratio with the smaller intensity peak on the red side. Comparison with the frequencies observed in $H_9O_4^+$ shows that the higher intensity member of each pair in the messenger spectrum lies within 3 cm^{-1} of the corresponding peak in the IRMPD spectrum. This led to the conclusion described in Ref. 48 and 49 that the H_2 messenger is localized near one of the three outer H_2O groups causing the frequencies for that water group to be red shifted compared to the other two and have half the intensity of the unperturbed peaks.

An expansion of the 3730.4 cm^{-1} peak shows P, Q, R branches emerging (Fig. 12). This is characteristic of a parallel band transition in a symmetric top. $H_9O_4^+$ is

rigorously an oblate symmetric top with rotational constants from the calculated geometry of A = B = 0.0876 and C = 0.0453 cm^{-1}. The symmetry axis is perpendicular to the plane of the H_3O^+ core. This corresponds to having the antisymmetric stretch of the three H_2O groups in phase with each other for the A_1 species transition. The transition of species E, which would give rise to a perpendicular band, is calculated to have almost no intensity.

Also shown in Fig. 11 are the SCF calculated scaled frequencies for the D_{3h} and C_{3v} forms of $H_9O_4^+$, using a DZP basis set. The C_{3v} structure was calculated to be the lower energy geometry by 0.551 kcal/mole, and frequencies corresponding to this structure are shown by dashed lines. The predicted transitions for the higher energy D_{3h} structure are denoted by solid lines. The primary differences between the two geometries are that the C_{3v} geometry has a pyramidal H_3O^+ core and bent O-H-O bonds, whereas the D_{3h} geometry has a planar H_3O^+ core and linear O-H-O bonds. The calculated frequencies for the symmetric and antisymmetric O-H stretches of the H_2O moieties are practically the same for the D_{3h} and C_{3v} forms. Table I compares the predicted frequencies for both structures with the observed frequencies taken both with and without a messenger.

Two features at higher frequency were also observed. These are likely to be due to either combination bands of an O-H stretch and a low frequency mode or due to overtone bands of a high intensity mode near 2000 cm^{-1}, such as a bending mode. Calculations by Remington and Schaefer[40] do not predict a mode near 2000 cm^{-1}. If this is correct, then the two bands at 3795.6 and 3824.1 cm^{-1} could be combinations of the O-H symmetric stretch of the H_2O moieties at 3646 cm^{-1} with an intermolecular O-H-O stretch and an asymmetric wag of the H_2O's. These modes have predicted intensities of 19 and 12 $D^2/(Å^2.amu)$ and scaled frequencies of 281 and 251 cm^{-1}. Although the harmonic approach to calculating such large, floppy molecules is expected to have difficulty, especially with these low frequency modes, it is encouraging that the agreement between the frequencies of the observed bands and the calculated bands is quite good. It also may be significant that these two low frequency modes are expected to have such large intensities. These two bands were also observed in the $H_9O_4^+ \cdot H_2$ messenger spectrum.

A Doppler limited spectrum was also taken for $H_9O_4^+$ from 3722 to 3738 cm^{-1} and is presented in the next chapter.

IV. Discussion

A few remarks on the results presented in the previous section are in order. First, note that the frequencies of the symmetric and antisymmetric O-H stretches of the outer H_2O groups increase with cluster size. This trend is shown in Fig. 13. The red shift of the frequency of the antisymmetric O-H stretch has decreased from 72 cm^{-1} in $H_5O_2^+$ to 26 cm^{-1} in $H_9O_4^+$. The trend is also dramatic for the symmetric O-H stretch where the red shift decreased from 43 cm^{-1} in $H_5O_2^+$ to 7 cm^{-1} in $H_9O_4^+$. It would be interesting to pursue this work to the larger cluster ions such as $H_{11}O_5^+$ where the additional water group is added to the next solvation shell and compare the red shifts obtained then. We did the analogous experiment for the hydrogen cluster ions and found that the red shift in the H-H stretch decreased from 250 cm^{-1} in H_5^+ to 140 cm^{-1} in H_9^+ in which the first shell was filled.[43,44] As the cluster ion size was further increased from H_{11}^+ through H_{15}^+, the red shift in the H-H stretch remained within 30 cm^{-1} of that seen for H_9^+. Because the H_2 moiety depends on a perturbation from the H_3^+ core in order to exhibit an allowed transition, it is likely that the H_2 units in the second solvation shell may not be sufficiently perturbed to have a strong infrared intensity. Thus, the H-H stretch we observed for these larger hydrogen cluster ions almost certainly originated

from the inner solvation shell. In the case of the water cluster ions, the situation should be different. The O-H stretches in free water are infrared allowed and thus don't depend on the proximity of a perturbative force to be observed. Thus, it may be that two sets of O-H stretches could be found. One would correspond to the inner solvation shell and have frequencies close to that found in $H_9O_4^+$. The second would be shifted to the blue, closer to the frequencies found for free H_2O. Preliminary results on the ammoniated ammonium ions, $NH_4^+ \cdot (NH_3)_n$ (n = 1-10), show a shoulder, slightly shifted to the blue, emerging for $n \geq 5$ in the antisymmetric N-H stretch of the NH_3 moiety.[65] Work is in progress to ascertain whether this shoulder originates from the outer solvation shell.

As to the validity of the messenger technique, we can say the method shows potential to be useful in obtaining a low resolution scan of an otherwise unobservable ion. However, the choice of messenger is crucial in determining the degree of perturbation induced in the spectrum. For floppy molecules such as cluster ions, the shallowness of the potential makes these ions especially susceptible to significant structural and spectroscopic changes. In the case of $H_5O_2^+$, the hydrogen messenger stabilizes an H_3O^+ core changing the symmetry of the ion. This loss of symmetry leads to two new bands corresponding to one free O-H bond of the H_3O^+ core and one O-H bond also of the

H_3O^+ core to which the hydrogen messenger is loosely attached. For $H_7O_3^+$, the frequency of the O-H bond which is the site for the hydrogen messenger of the H_3O^+ core, is shifted by 80 cm^{-1} compared to the IRMPD spectrum. This shift is reduced to only 9 cm^{-1} when neon is used as the messenger. In $H_9O_4^+$, also, significant changes are seen in the spectra with and without the hydrogen messenger. The presence of the H_2 near one of the H_2O groups breaks the 3-fold symmetry and leads to a splitting of each of the bands with a 2:1 intensity ratio. The red shift of the lower frequency peak of each doublet is small (only 12 and 10 cm^{-1} for the symmetric and antisymmetric O-H stretches, respectively). Thus, it seems that the messenger technique would be more ideally suited to the study of rigid molecules that have deeper wells and higher barriers in the potential. Using a more inert messenger such as Ne or He would also minimize the perturbations introduced by the messenger. Since rigid molecules are more difficult to study using the IRMPD technique these two techniques are complementary. The ideal candidate for the IRMPD method is a floppy molecule, such as a cluster ion, with many low frequency modes so that the quasicontinuum occurs at relatively low energies. A paucity of low frequency modes might cause the beginning of the quasicontinuum to occur too high for the IRMPD technique to be feasible. This is the situation where using a

messenger may be the ideal solution to obtaining a rough approximation to the low resolution infrared spectrum.

ab initio theory predictions are also more reliable for rigid molecules with deep wells and high barriers in the potential. Cluster ions generally will be more floppy and have less well-defined structures. The structure calculated to be the lowest energy geometry may change as more sophisticated levels of theory are applied. This was seen in the case of $H_5O_2^+$ where the early SCF, DZP basis calculation found the asymmetric C_s geometry to be the lowest in energy.[40] When the better CISD, DZP basis results were obtained, the symmetric C_2 geometry had become the lowest in energy by slightly less than 0.2 kcal/mole. This is probably near the accuracy limit of these kinds of calculations. The larger cluster ions are not accessible at the CISD level. Thus, Remington and Schaefer were limited to using SCF to calculate $H_7O_3^+$ and $H_9O_4^+$. They calculate the C_s geometry of $H_7O_3^+$ to lie lowest in energy. Our experimental spectrum seems to indicate that the C_{2v} structure is actually the lower energy form. The energy difference calculated between the C_s and C_{2v} structures was only 0.5 kcal/mole. For $H_9O_4^+$, the calculated frequencies for the C_{3v} and D_{3h} structures are nearly identical. Therefore, the observed spectrum does not aid in determining which geometry is actually the lower energy form. From these comparisons, it seems that

ab initio theory has some difficulty in predicting relative energies for structures that are separated by only a few tenths of a kcal/mole as found in these cluster ions.

Besides the messenger technique and the two color IRMPD approach, a third approach was also tried to obtain the spectra. This was a one color multiphoton dissociation technique. Because $H_5O_2^+$ is bound most strongly, it would require three to four infrared photons to dissociate whereas both $H_7O_3^+$ and $H_9O_4^+$ only need two photons. We were not able to obtain the $H_5O_2^+$ spectrum in this way, but the spectra of $H_7O_3^+$ and $H_9O_4^+$ were successfully obtained. $H_5O_2^+$ is particularly difficult both because it has the strongest binding energy and because it is the smallest cluster ion and therefore has the fewest normal modes. Since the completion of this hydrated hydronium ion study, this technique has been successfully applied to study the ammoniated ammonium ions, $NH_4^+ \cdot (NH_3)_n$ (n = 3-10).[65] Once again, this approach is limited to the larger size cluster ions. For n = 1 and 2, the two color technique using a CO_2 laser is necessary in order to obtain the infrared spectra.

V. Future Work

As discussed above, one logical extension of this work is to study the larger hydrated hydronium ions.

Observing absorptions from both the inner and outer solvation shells would be exciting. Another objective would be to find the size of the second solvation shell and see if any unexpected structural changes occur.

The two color IRMPD experiment was done using the F-center laser. This laser is not capable of scanning below about 3000 cm^{-1}. Using the IR-WEX laser, the scanning range can be extended by almost 800 cm^{-1} to the red, as was done for the earlier messenger work. It would be useful to do this for the hydrated hydronium ions, both to corroborate the results obtained using the hydrogen messenger and to improve the signal to noise of the features found. For $H_9O_4^+ \cdot H_2$, a broad band was observed at 2670 cm^{-1},[47-49] in agreement with the low resolution spectra obtained by Schwarz,[25] but in disagreement with theoretical predictions.[40] This mode was assigned to the hydrogen-bonded O-H stretch of the H_3O^+ core and thus was considered to be relatively free from perturbations due to the H_2 messenger which was located outside of the first solvation shell. In $H_7O_3^+ \cdot H_2$, a broad low intensity band appeared to peak at or beyond the red limit of the IR-WEX laser. Due to the low laser power and low $H_7O_3^+ \cdot H_2$ ion count, the peak of the band was impossible to determine.[47-49] Questions such as these could be answered by studying the spectroscopy of the hydrated hydronium ions between 2200 and 3000 cm^{-1}.

A very different type of experiment would be to use the two color approach to determine infrared lifetimes. By systematically varying the delay time between a 5 msec F-center laser pump beam and a CO_2 probe beam, it seems that the lifetimes can be pinned down within 5 msec for the stronger transitions. By changing to a pulsed laser system, the vibrational lifetimes should be amenable to a more accurate determination, but careful attenuation of the pump beam would need to be done in order to prevent multiphoton processes from this beam.

VI. Conclusion

The study of the infrared spectroscopy of cluster ions is a challenge, both experimentally and theoretically. Experimentally, the difficulty is caused largely by the very low ion densities obtained. In order to overcome this limitation, we have used "consequence" spectroscopy where the consequence of absorbing an infrared photon is an observable event. The consequence which was utilized in these experiments was dissociation. The tandem mass spectrometer is an ideal instrument to detect dissociation products. Not only is there little to no background at the fragment ion mass, but also, every fragment ion can be detected with nearly perfect detection efficiency. Three dissociation schemes have been described: messenger studies using hydrogen and neon, two

color infrared multiphoton dissociation, and one color infrared dissociation. Results using these three techniques have been compared for the hydrated hydronium ions, $H_3O^+ \cdot (H_2O)_n$ (n = 1, 2, 3).

Theoretically, the difficulty is caused by the shallowness of the potential wells and barriers found in cluster ions. This makes the relative energies of the different geometries highly dependent on the level of theory. This means that clusters present a double whammy for theorists. By definition, clusters have more electrons than their respective monomers, often forcing theorists to use smaller basis sets and less sophisticated calculation methods. However, it is especially for many clusters that higher levels of theory must be used in order to have reliable results due to the sensitivity of the results to the method employed.

REFERENCES

1. For recent reviews, see: C. I. Ratcliffe and D. E. Irish, in Water Science Reviews 2, F. Franks, ed. (Cambridge University Press, Cambridge, 1986) p. 149; and C. I Ratcliffe and D. E. Irish, in Water Science Reviews 3, F. Franks, ed. (Cambridge University Press, Cambridge, in press).

2. R. S. Narcisi and A. D. Bailey, J. Geophys. Res. **70**, 3687 (1965).

3. E. E. Ferguson, F. C. Fehsenfeld, and D. L. Albritton, in Gas Phase Ion Chemistry, Vol. 1, M. T. Bowers, ed. (Academic Press, New York, 1979) p. 45.

4. I. Olovsson, J. Chem. Phys. **49**, 1063 (1968).

5. J.-O. Lundgren and I. Olovsson, J. Chem. Phys. **49**, 1068 (1968).

6. J.-O. Lundgren and I. Olovsson, in The Hydrogen Bond: II. Structure and Spectroscopy, P. Schuster, G. Zundel, and C. Sandorfy, eds. (North-Holland, Amsterdam, 1976), Chap 10.

7. R. Attig and J. M. Williams, Angew. Chem., Int. Ed. Engl. **15**, 491 (1976).

8. J. Roziere and J. M. Williams, Inorg. Chem. **15**, 1174 (1976).

9. A. Nakahara, Y. Saito, and H. Kuroya, Bull. Chem. Soc. Jap. **25**, 331 (1952).

10. R. D. Gillard and G. Wilkinson, J. Chem. Soc., 1640 (1964).

11. J. Rudolph and H. Zimmermann, Z. Phys. Chem. (Frankfurt) **43**, 311 (1964).

12. J. Roziere and J. Potier, J. Mol. Struct. **13**, 91 (1972).

13. A. S. Gilbert and N. Sheppard, J. Chem. Soc., Faraday Trans. II **69**, 1628 (1973).

14. J. M. Williams, in The Hydrogen Bond: II. Structure and Spectroscopy, P. Schuster, G. Zundel, and C. Sandorfy, eds. (North-Holland, Amsterdam, 1976), Chap. 14.

15. D. Schioberg and G. Zundel, Can. J. Chem. **54**, 2193 (1976).

16. N. B. Librovich, V. P. Sakun, and N. D. Sokolov, Chem. Phys. **39**, 351 (1979).

17. G. J. Kearley, A. N. Fitch, and B. E. F. Fender, J. Mol. Struct. **125**, 229 (1984).

18. J. Q. Searcy and J. B. Fenn, J. Chem. Phys. **61**, 5282 (1974).

19. G. M. Lancaster, F. Honda, Y. Fukuda, and J. W. Rabalais, Int. J. Mass Spectrom. Ion Phys. **29**, 199 (1979).

20. R. J. Beuhler and L. Friedman, J. Chem. Phys. **77**, 2549 (1982).

21. P. Kebarle, S. K. Searles, A. Zolla, J. Scarborough, and M. Arshadi, J. Am. Chem. Soc. **89**, 6393 (1967).

22. A. J. Cunningham, J. D. Payzant, and P. Kebarle, J. Am. Chem. Soc. **94**, 7627 (1972).

23. Y. K. Lau, S. Ikuta, and P. Kebarle, J. Am. Chem. Soc. **104**, 1462 (1982).

24. M. Meot-Ner and F. H. Field, J. Am. Chem. Soc. **99**, 998 (1977).

25. H. A. Schwarz, J. Chem. Phys. **67**, 5525 (1977).

26. M. H. Begemann, C. S. Gudeman, J. Pfaff, and R. J. Saykally, Phys. Rev. Lett. **51**, 554 (1983).

27. M. H. Begemann and R. J. Saykally, J. Chem. Phys. **82**, 3570 (1985).

28. N. H. Haese and T. Oka, J. Chem. Phys. **80**, 572 (1984).

29. D.-J. Liu and T. Oka, Phys. Rev. Lett. **54**, 1787 (1985).

30. D.-J. Liu, N. H. Haese, and T. Oka, J. Chem. Phys. **82**, 5368 (1985).

31. D.-J. Liu, T. Oka, and T. J. Sears, J. Chem. Phys. **84**, 1312 (1986).

32. V. Spirko and P. R. Bunker, J. Mol. Spectrosc. **95**, 226 (1982).

33. M. E. Colvin, G. P. Raine, H. F. Schaefer III, and M. Dupuis, J. Chem. Phys. **79**, 1551 (1983).

34. P. R. Bunker, W. P. Kraemer, V. Spirko, J. Mol. Spectrosc. **101**, 180 (1983).

35. P. R. Bunker, T. Amano, V. Spirko, J. Mol. Spectrosc. **107**, 208 (1984).

36. M. D. Newton and S. Ehrenson, J. Am. Chem. Soc. **93**, 4971 (1971).

37. M. D. Newton, J. Chem. Phys. **67**, 5535 (1977).

38. G. V. Yukhnevich, E. G. Kokhanova, A. I. Pavlyuchko, and V. V. Volkov, J. Mol. Struct. **122**, 1 (1985).

39. A. Potier, J. M. Leclercq, and M. Allavena, J. Phys. Chem. **88**, 1125 (1984).

40. R. Remington and H. F. Schaefer, unpublished results.

41. R. J. Saykally and C. S. Gudeman, Annu. Rev. Phys. Chem. **35**, 387 (1984).

42. Recently this has been achieved for a few small stable ions. See: J. Coe and R. J. Saykally, in Spectroscopy and Structures of Molecular Clusters and Molecular Ions, John Myer, ed. (Elsevier Science Publishers, Amsterdam, 1988), to be published.

43. M. Okumura, L. I. Yeh, and Y. T. Lee, J. Chem. Phys. **83**, 3705 (1985).

44. M. Okumura, L. I. Yeh, and Y. T. Lee, J. Chem. Phys. **88**, 79 (1988).

45. D. F. Coker, R. E. Miller, and R. O. Watts, J. Chem. Phys. **82**, 3554 (1985).

46. M. F. Vernon, D. J. Krajnovich, H. S. Kwok, J. M. Lisy, Y. R. Shen, and Y. T. Lee, J. Chem. Phys. **77**, 47 (1982).

47. M. Okumura, L. I. Yeh, J. D. Myers, and Y. T. Lee, J. Chem. Phys. **85**, 2328 (1986).

48. M. Okumura, Ph.D. Thesis, University of California, Berkeley, 1986.

49. M. Okumura, L. I. Yeh, J. D. Myers, and Y. T. Lee, to be published.

50. L. I. Yeh, M. Okumura, J. D. Myers, J. M. Price, and Y. T. Lee, to be published.

51. V. J. Caldecourt, D. Zakett, and J. C. Tou, Int. J. Mass Spectrom. Ion Phys. **49**, 233 (1983).

52. R. J. Beuhler and L. Friedman, J. Chem. Phys. **77**, 2549 (1982).

53. H. A. Enge, Rev. Sci. Instrum. **30**, 248 (1959)

54. C. F. Giese, Rev. Sci. Instrum. **30**, 260 (1959).

55. C.-S. Lu and H. E. Carr, Rev. Sci. Instrum. **33**, 823 (1962).

56. S. Taya, I. Kanomata, H. Hirose, T. Noda, and H. Matsuda, Int. J. Mass Spectrom. Ion Phys. **26**, 237 (1978).

57. H. D. Zeman, Rev. Sci. Instrum. **48**, 1079 (1977).

58. Further details on the machine can be found in: S. W. Bustamente, Ph.D. Thesis, University of California, Berkeley, 1983; and S. W. Bustamente, M. Okumura, D. Gerlich, H. S. Kwok, L. R. Carlson, and Y. T. Lee, J. Chem. Phys. **86**, 508 (1987).

59. P. J. Robinson and K. A. Holbrook, Unimolecular Reactions (Wiley-Interscience, New York, 1972).

60. H.-J. Werner, P. Rosmus, and E.-A. Reinsch, J. Chem. Phys. **79**, 905 (1983).

61. N. R. Daly, Rev. Sci. Instrum. **31**, 264 (1960).

62. G. Herzberg, Molecular Spectra and Molecular Structure: II. Infrared and Raman Spectra of Polyatomic Molecules (Van Nostrand Reinhold Company Inc., New York, 1945).

63. H. C. Allen, Jr. and P. C. Cross, Molecular Vib-Rotors (John Wiley and Sons, Inc., New York, 1963).

64. W. Demtroder, Laser Spectroscopy: Basic Concepts and Instrumentation (Springer-Verlag, New York, 1982) p. 87.

65. J. M. Price and M. W. Crofton, private communication.

TABLE I. Experimental and theoretical frequencies for the hydrated hydronium ions. Experimental frequencies were found using the IRMPD technique and the messenger technique. Units are cm^{-1}.

		Messenger		Theory[a]		
	IRMPD	H_2	Neon	Lower[b]	Higher[c]	Assignment
$H_5O_2^+$		3528			3549	H_3O^+ sym stretch with H_2 attached
	3608.8	3617		3624	3594	H_2O sym stretch
		3662			3633	H_3O^+ asym stretch
	3684.4	3693		3710	3678	H_2O asym stretch
$H_7O_3^+$	3637.4	3642	3640 3638	3619	3617	H_2O sym stretch
	3667.0	3587	3658 3669	3627	3662	H_3O^+ O-H stretch
	3721.6	3726	3722	3702	3703	H_2O asym stretch
$H_9O_4^+$		3636				
	3644.9	3648		3628	3630	H_2O sym stretch, out-of-phase
		3723				
	3730.4	3733		3714	3715	H_2O asym stretch, in-phase

a. All of the calculations were done at the self consistent field level except for the C_2 geometry for $H_5O_2^+$. A DZP basis set was used.

b. This column gives the scaled frequencies for the lowest energy calculated structure, i.e. $H_5O_2^+$: C_2, $H_7O_3^+$: C_s, and $H_9O_4^+$: C_{3v}.

c. This column gives the scaled frequencies for the structure calculated to be second lowest in energy, i.e. $H_5O_2^+$: C_s, $H_7O_3^+$: C_{2v}, and $H_9O_4^+$: D_{3h}.

FIGURE CAPTIONS

Fig. 1 Lowest energy structures calculated for $H_5O_2^+$, $H_7O_3^+$, and $H_9O_4^+$ by Remington and Schaefer. See text for details.

Fig. 2 Schematic of the corona discharge ion source.

Fig. 3 Schematic of the tandem mass spectrometer.

Fig. 4 Infrared spectra of the messenger ions, $H_5O_2^+ \cdot H_2$, $H_7O_3^+ \cdot H_2$, and $H_9O_4^+ \cdot H_2$. In the top panel, the dashed lines correspond to the frequencies and intensities calculated in Ref. 40 for the C_s geometry of $H_5O_2^+$. The arrows point to the locations of the symmetric and antisymmetric O-H stretches in H_2O. The dashed lines in the middle and lowest panels correspond to the frequencies for the lowest energy calculated structures for $H_7O_3^+$ and $H_9O_4^+$, respectively. The dashed curve in the bottom panel shows the low resolution spectrum for $H_9O_4^+$ obtained by Schwarz.

Fig. 5 Infrared spectrum of $H_5O_2^+$ obtained using the two color IRMPD technique. The dashed lines

correspond to the frequencies and intensities calculated in Ref. 40 for the C_2 symmetry structure.

Fig. 6 Infrared spectrum of $H_7O_3^+$ obtained using the IRMPD method. Dashed lines correspond to the lowest energy C_s structure and solid lines to the C_{2v} structure.

Fig. 7 Infrared spectrum of $H_7O_3^+ \cdot Ne$.

Fig. 8 Detail of the 3640 cm^{-1} feature in the neon messenger spectrum of $H_7O_3^+$.

Fig. 9 Infrared spectrum of $H_7O_3^+$ taken with the one color IR-WEX scheme.

Fig. 10 Detail of the 3722 cm^{-1} feature in the IR-WEX $H_7O_3^+$ spectrum.

Fig. 11 Infrared spectrum of $H_9O_4^+$ obtained using the two color IRMPD approach. The dashed lines correspond to the lowest energy C_{3v} structure and the solid lines to the D_{3h} structure.

Fig. 12 Detail of the 3730 cm^{-1} feature in the IRMPD $H_9O_4^+$ spectrum.

Fig. 13 Position of the antisymmetric (top) and symmetric (bottom) O-H stretches as a function of cluster size. The horizontal dashed lines are the locations of the respective O-H stretches in H_2O.

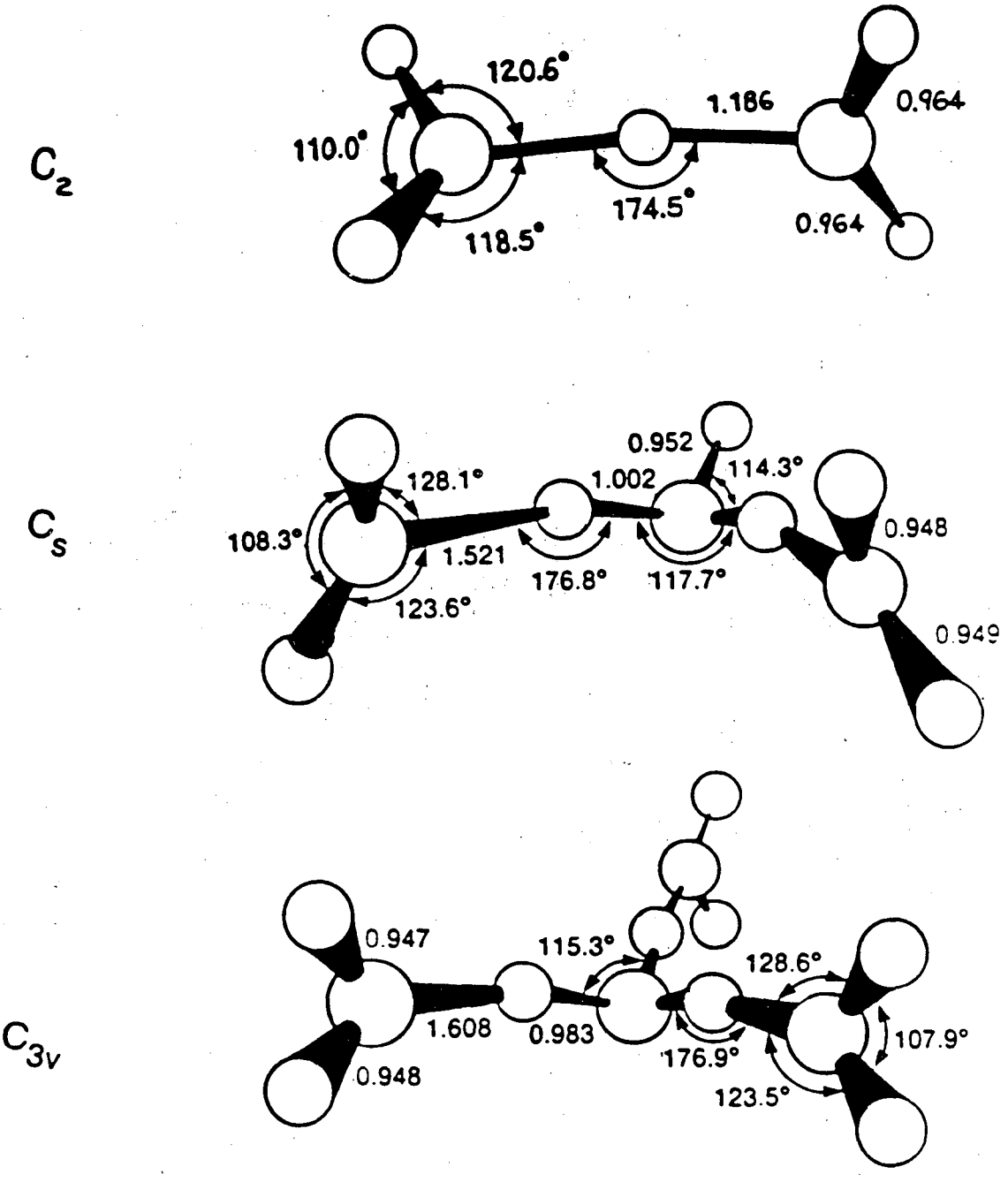

Figure 1

XBL 8811-3843

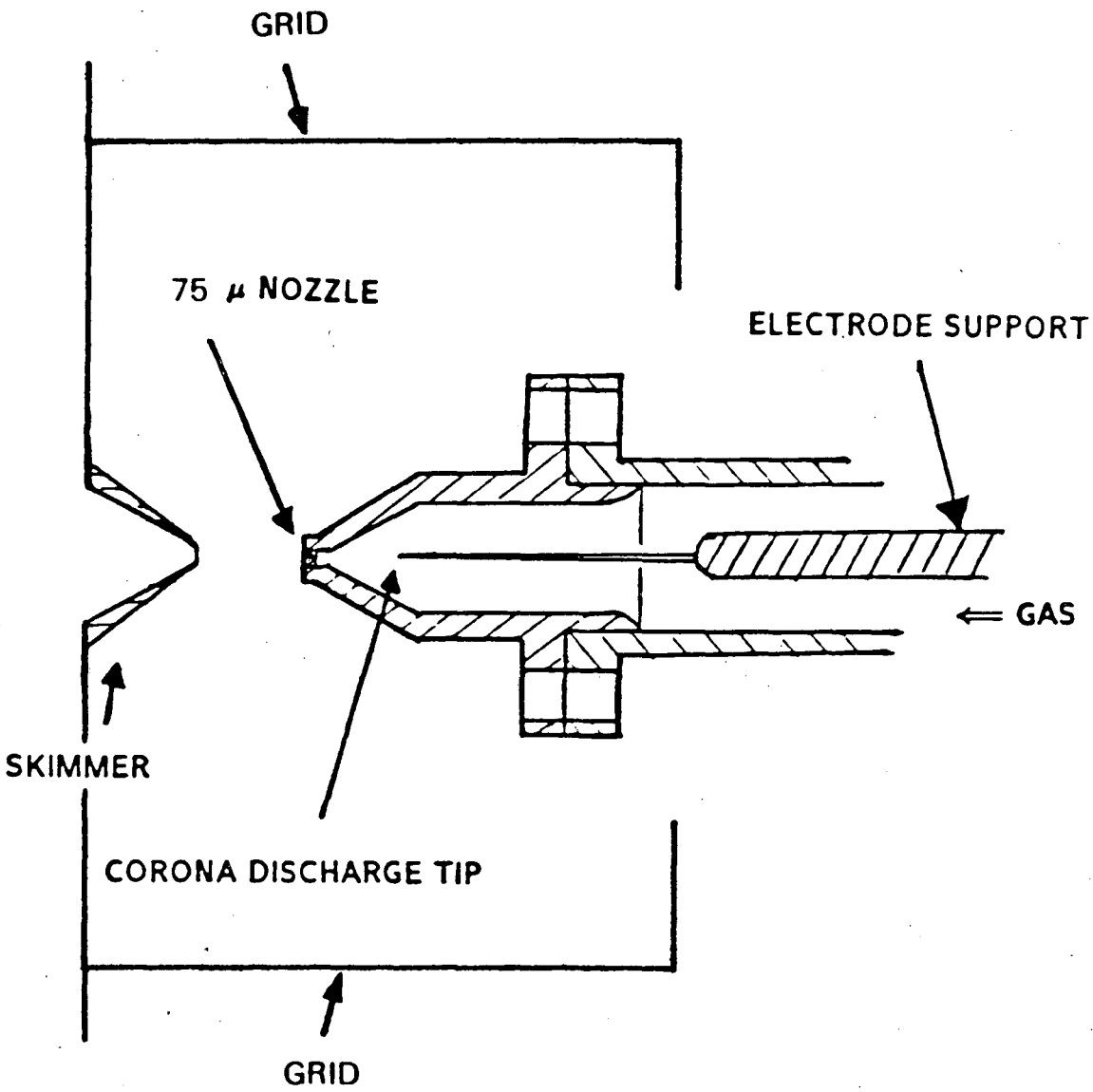

XBL 8711-4636 A

Figure 2

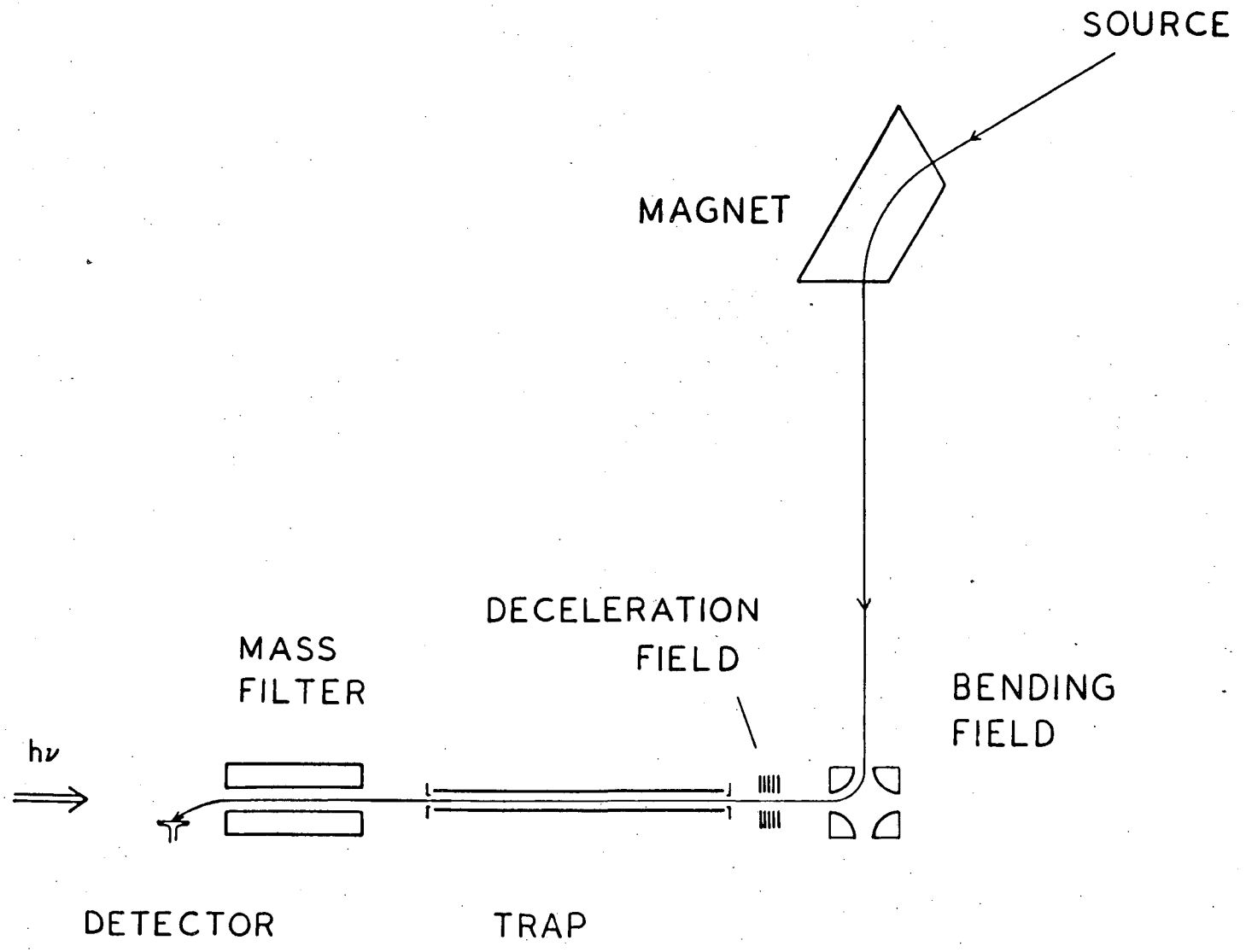

XBL 857-3143

Figure 3

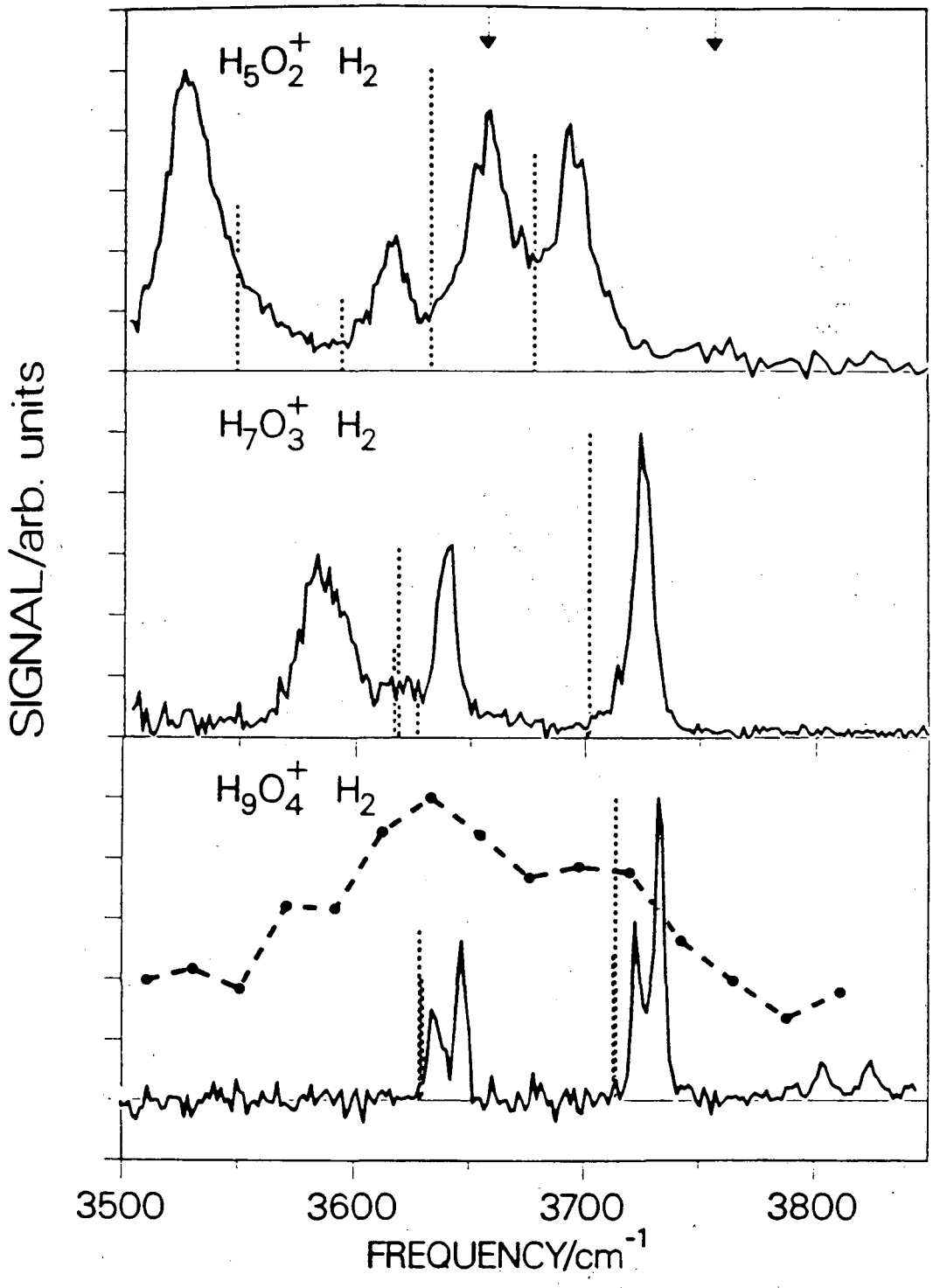

Figure 4 XBL 8811-3842

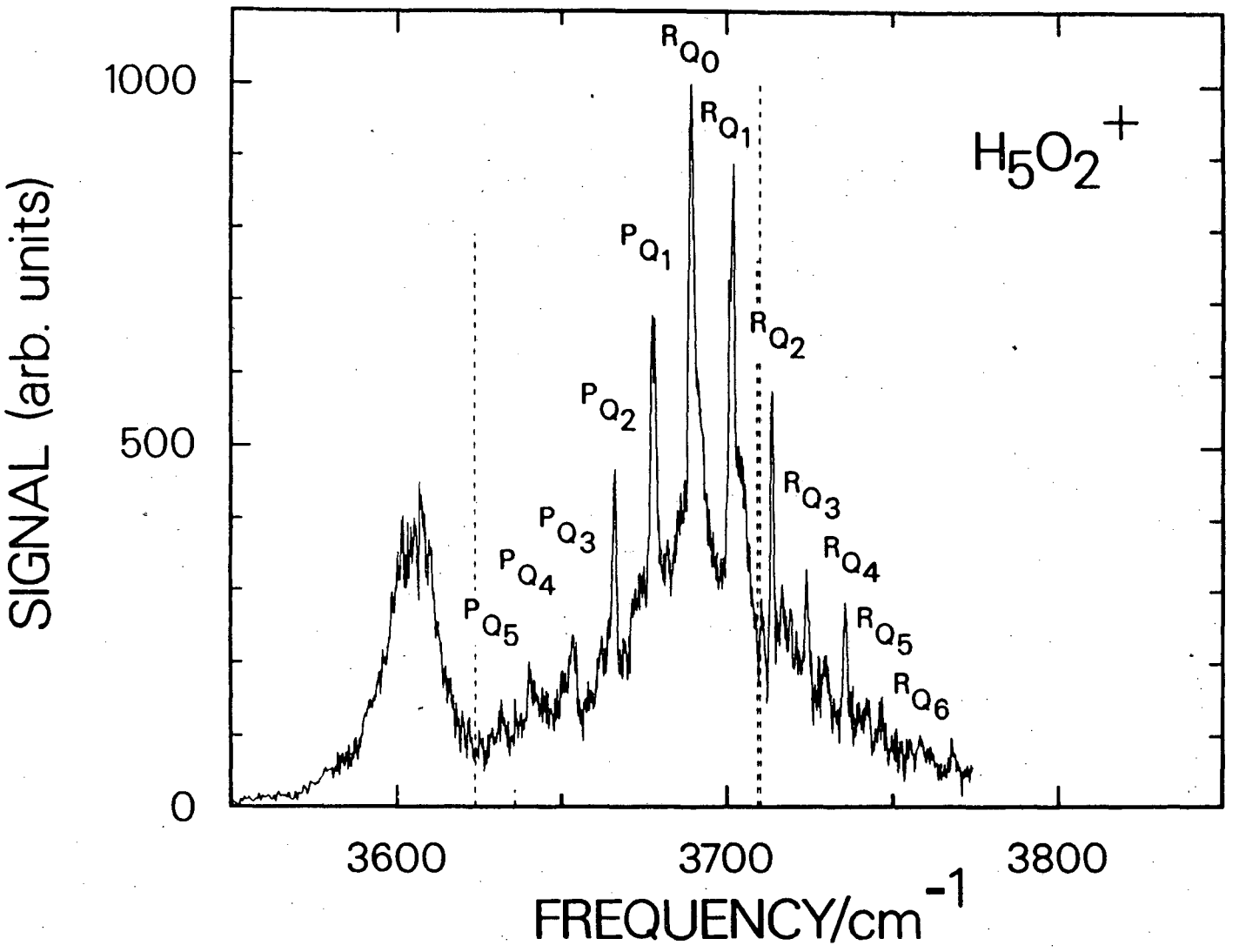

Figure 5

XBL 888-2873 A

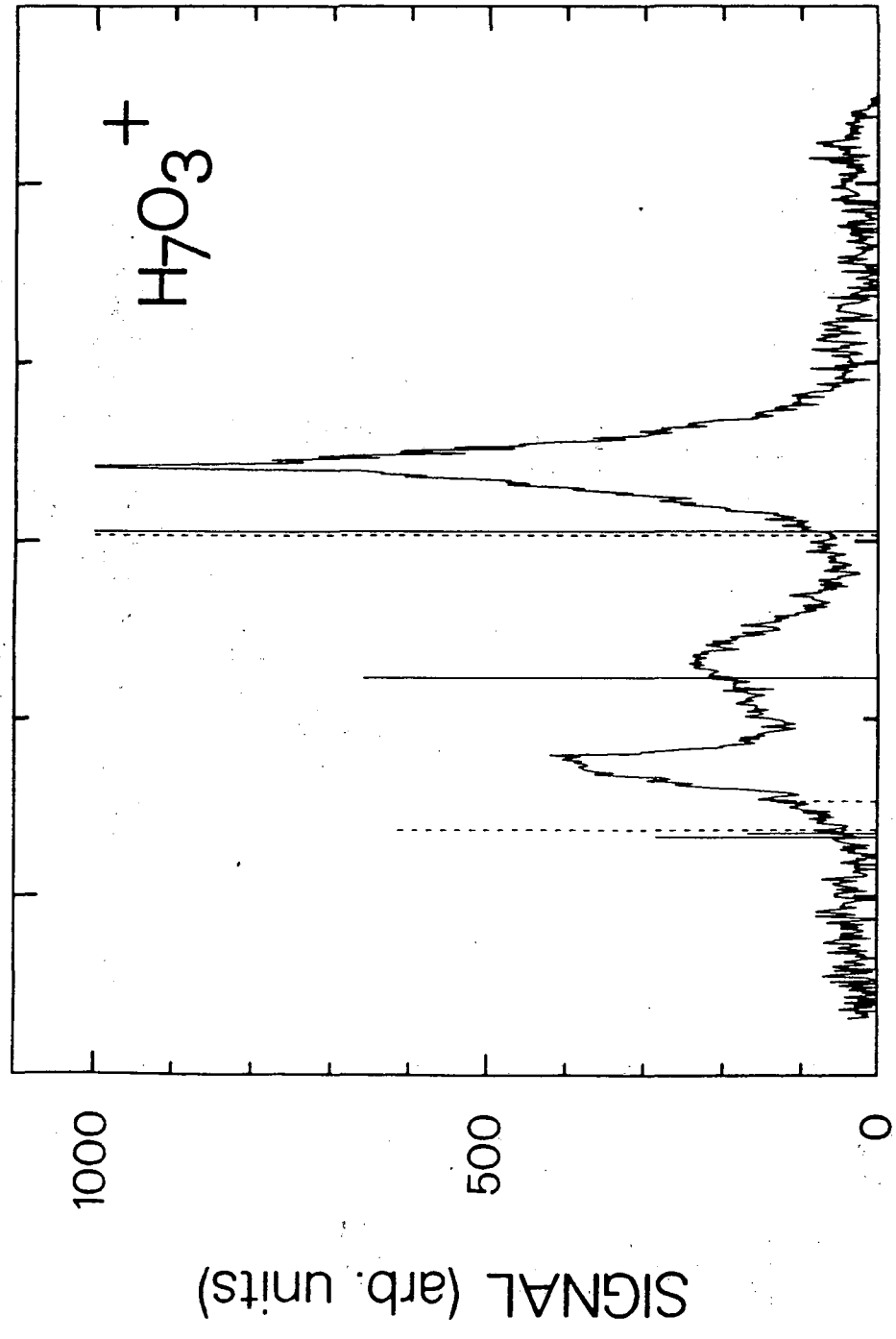

XBL 888-2874

Figure 6

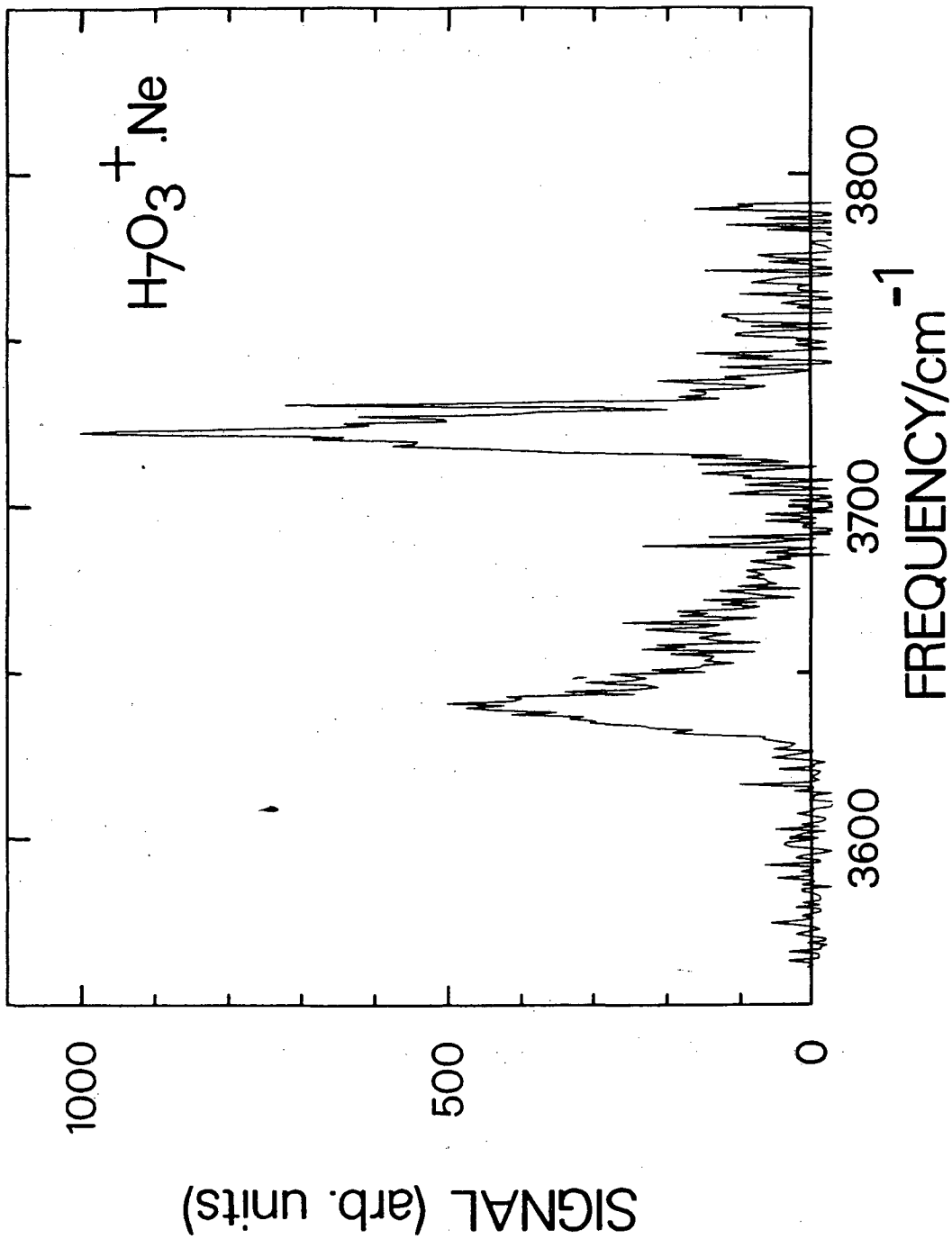

XBL 888-2877

Figure 7

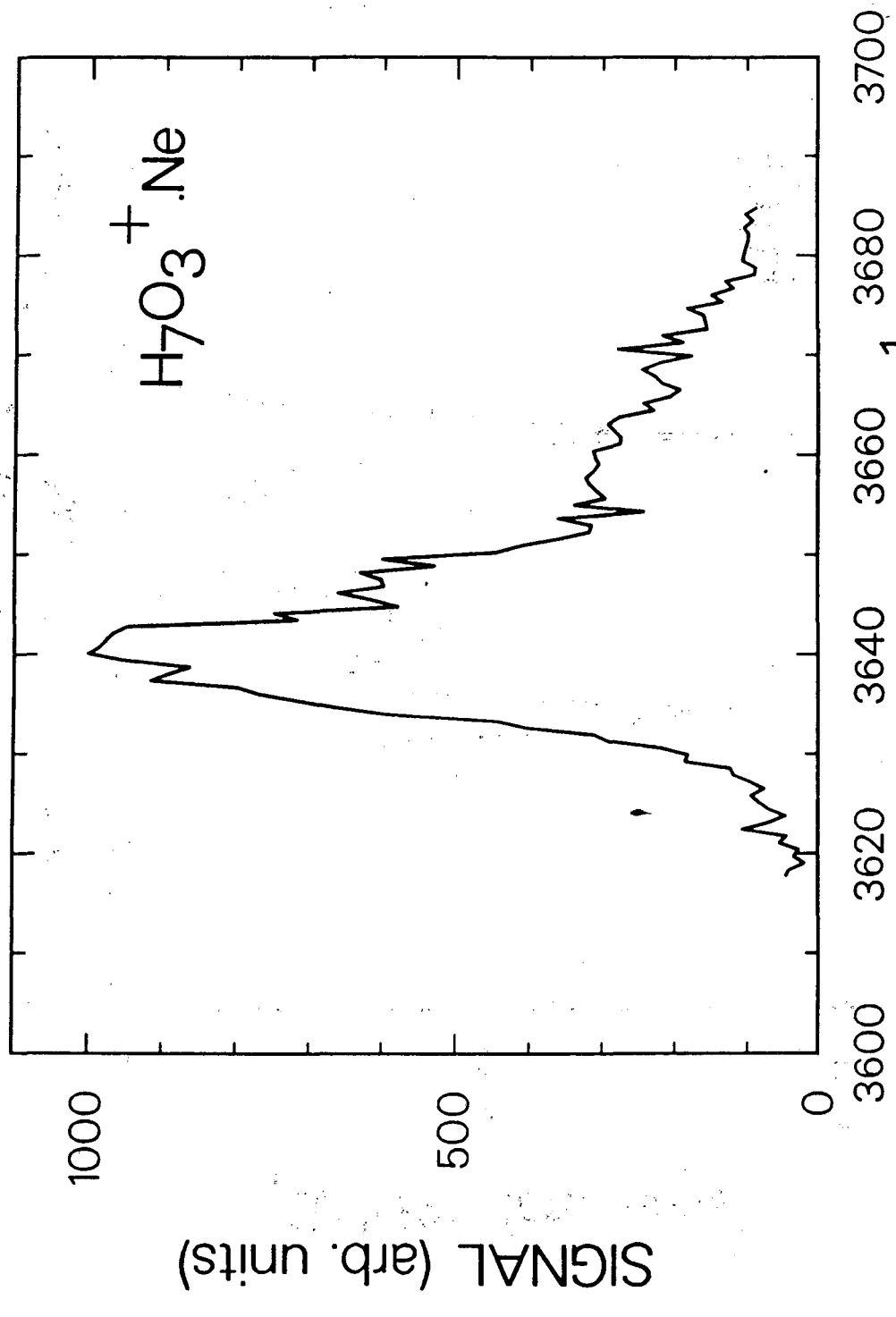

XBL 888-2878

Figure 8

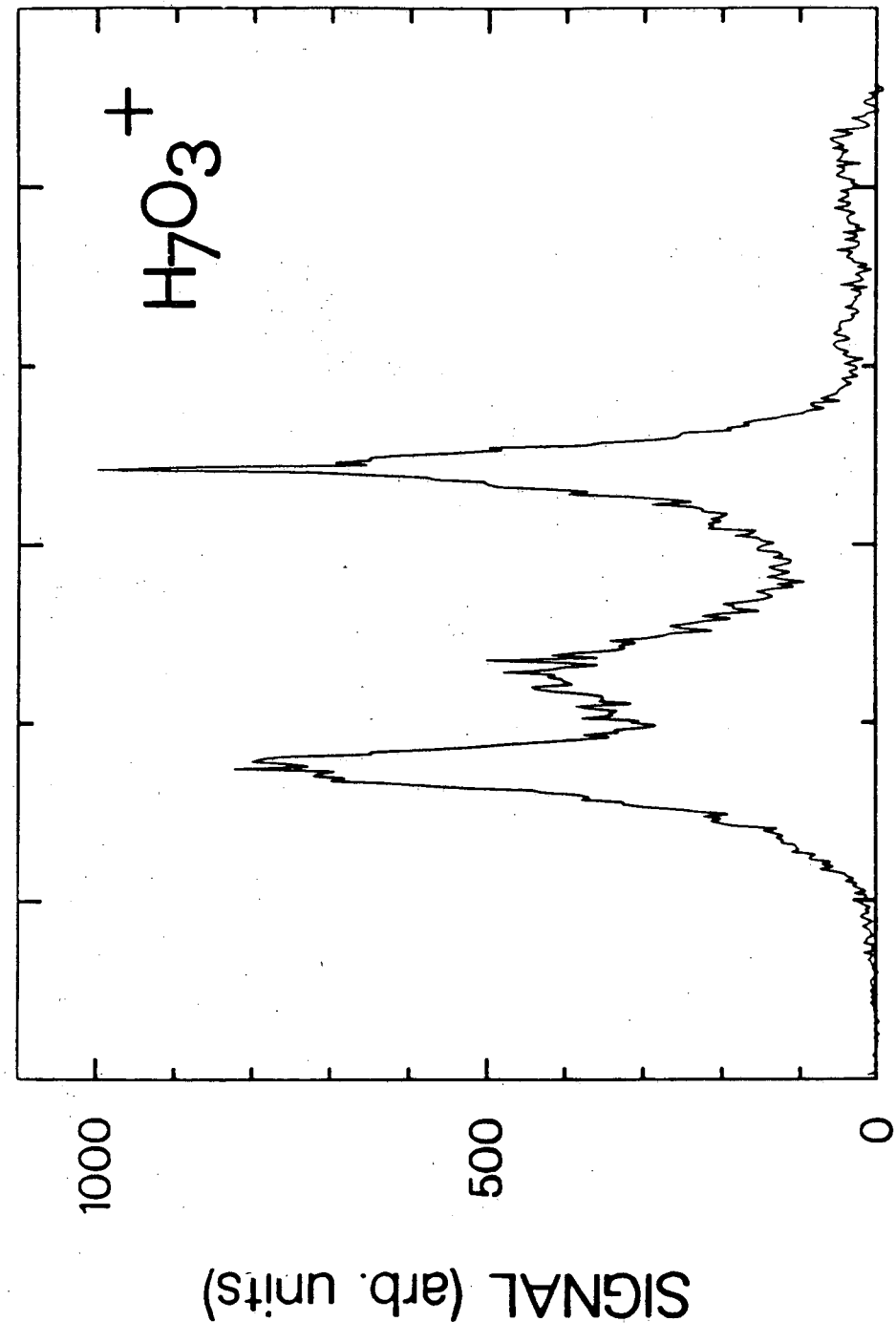

XBL 888-2867

Figure 9

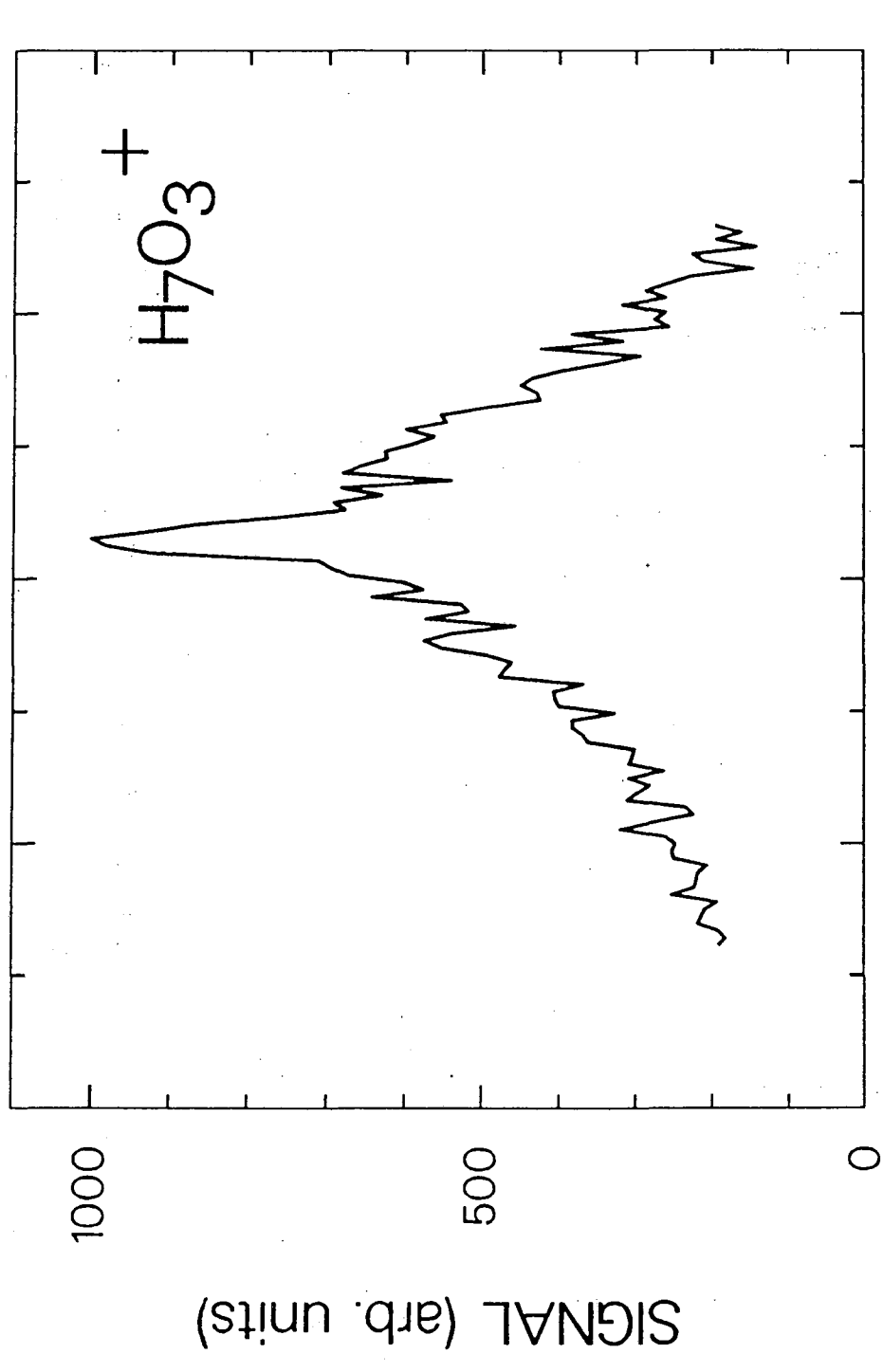

XBL 888-2872

Figure 10

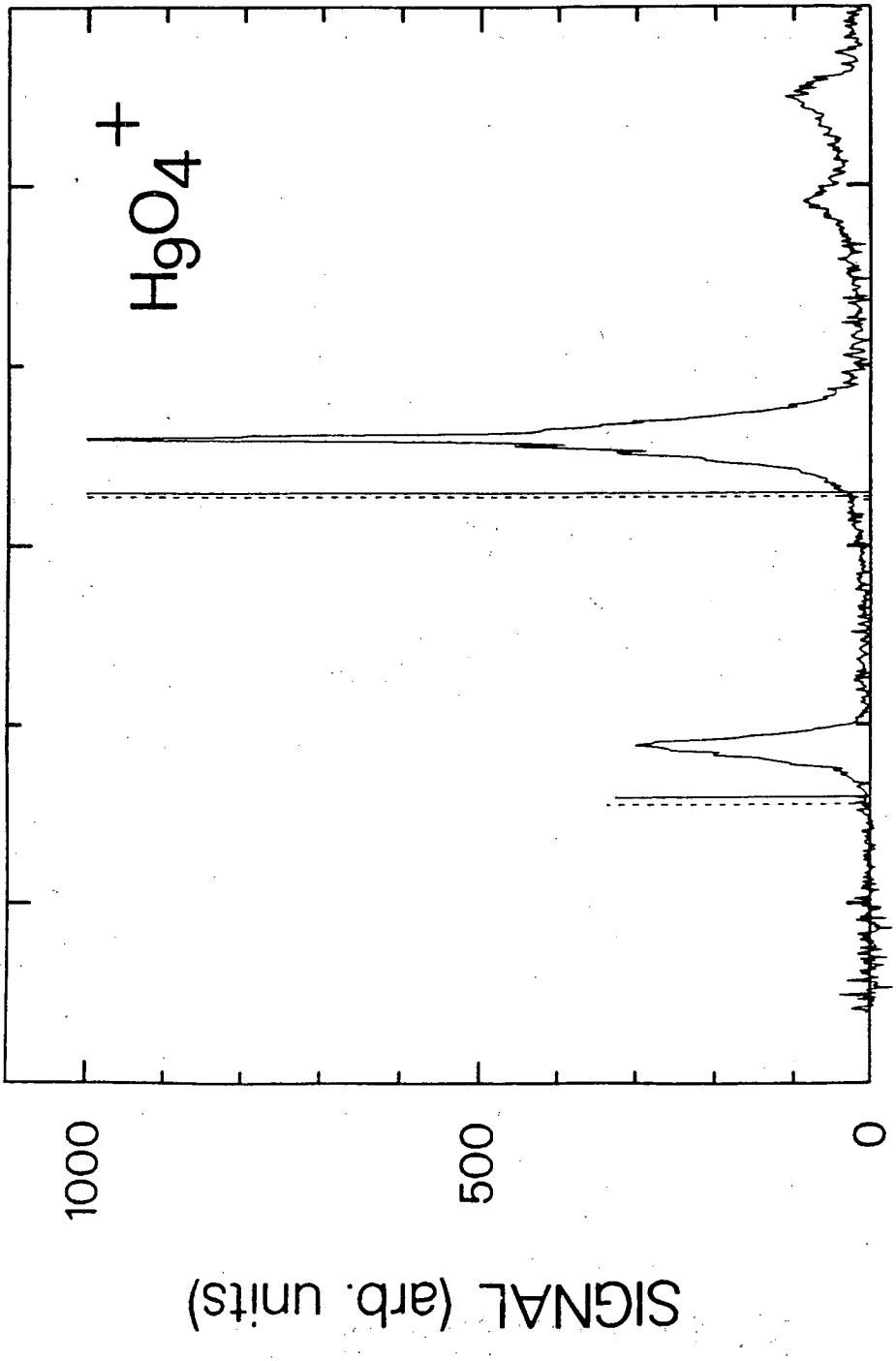

XBL 888-2875

Figure 11

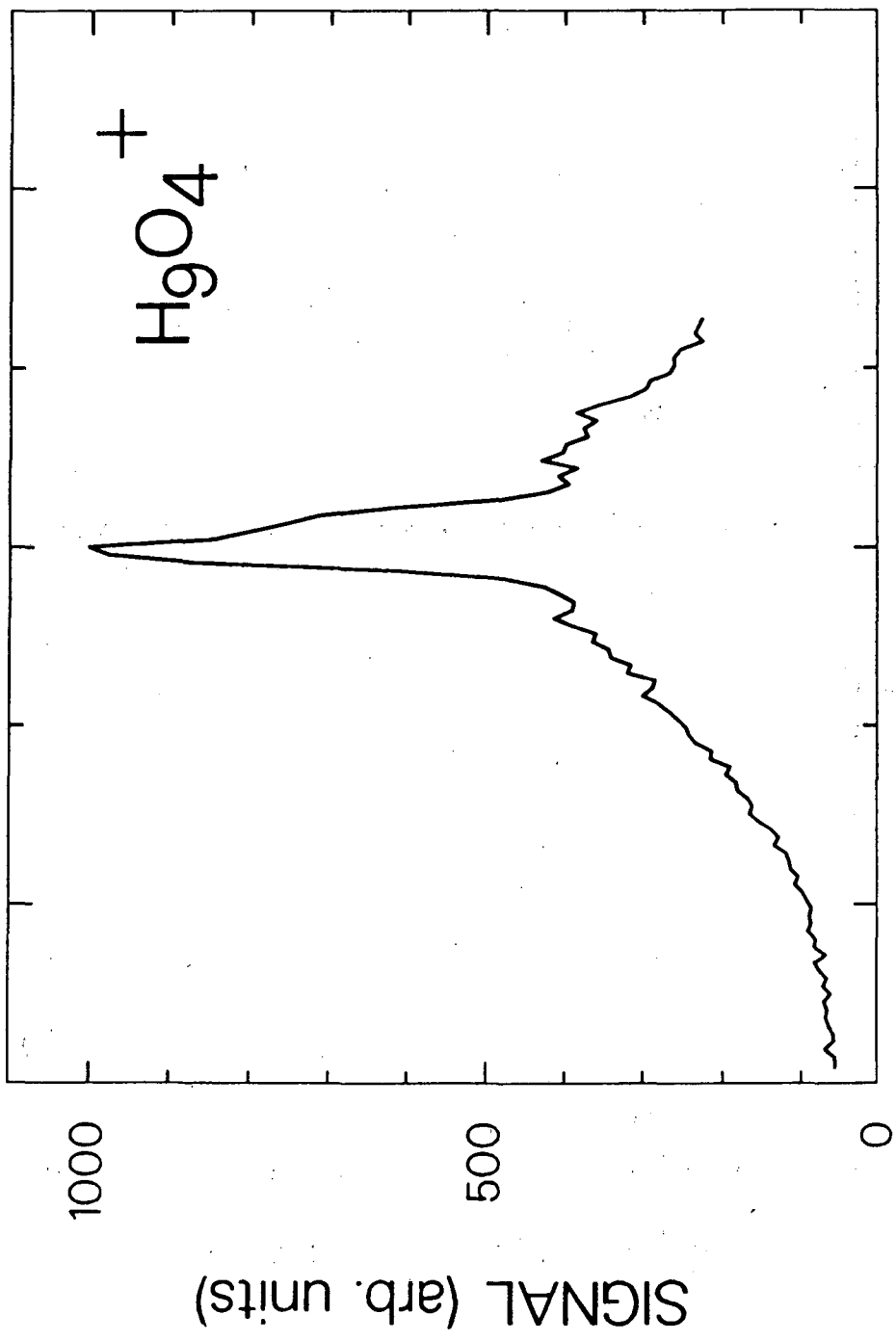

XBL 888-2876

Figure 12

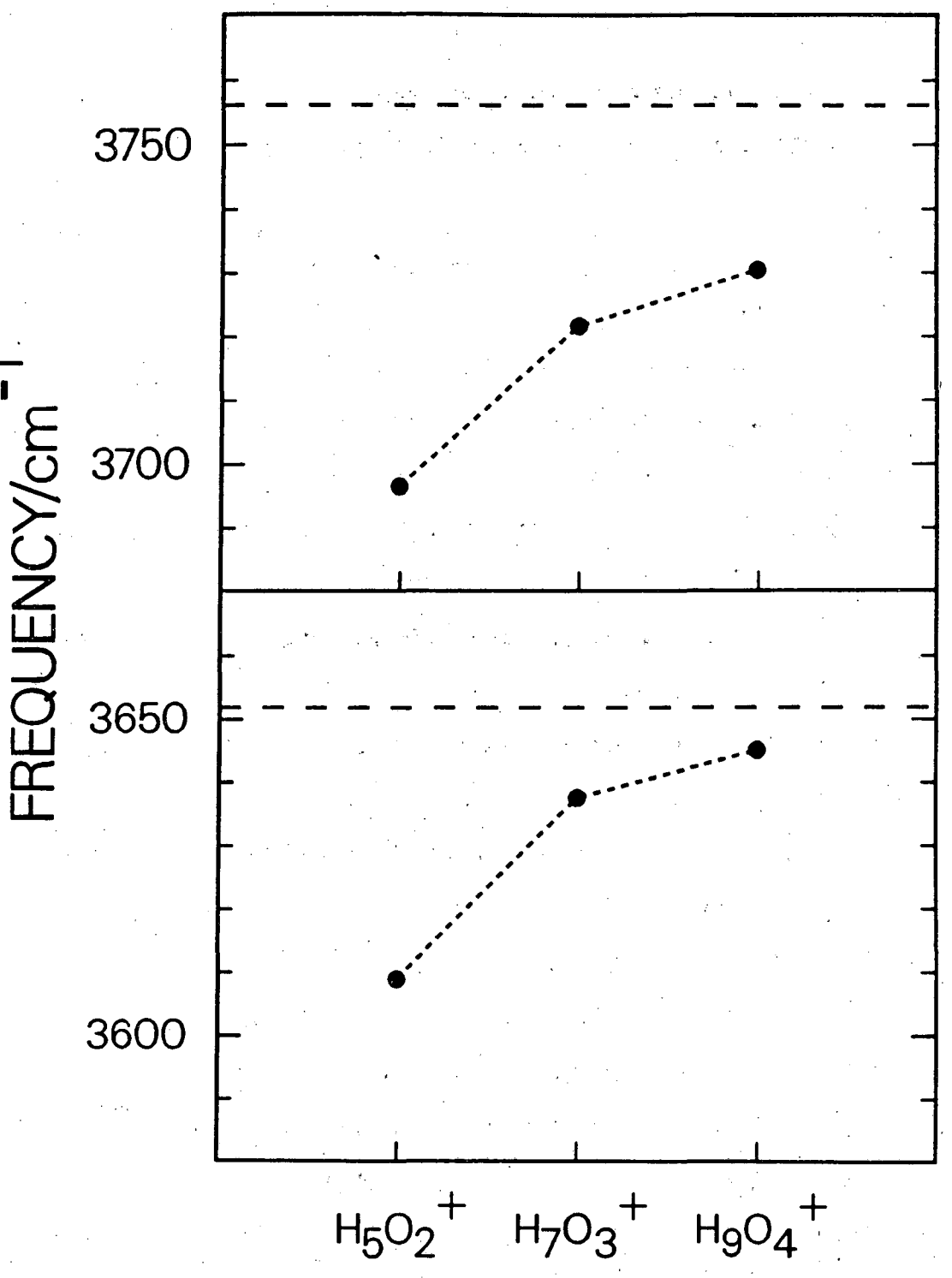

XBL 888-2880

Figure 13

Chapter III

High Resolution Spectroscopy of the Hydrated Hydronium Ions $H_5O_2^+$ and $H_9O_4^+$

I. Introduction

The spectroscopic study of cluster ions is a rapidly developing field. In just a few years, low resolution infrared spectra have been obtained of the hydrogen cluster ions (H_n^+),[1,2] the hydrated hydronium ions $(H_3O^+ \cdot (H_2O)_n)$,[3,4] the ammoniated ammonium ions $(NH_4^+ \cdot (NH_3)_n)$,[5] and some mixed cluster species. Efforts to obtain rotational resolution in the smallest hydrogen cluster ion, H_5^+, have been unsuccessful to date. Limited success was obtained in the mixed cluster $H_3O^+ \cdot H_2$ which showed partially resolved rotational structure.[6,7] Our first true high resolution spectra were obtained on the cluster ions $H_3O^+ \cdot (H_2O)_n$ (n = 1, 3). These spectra were Doppler limited to a resolution of 0.01-0.02 cm^{-1}.

Recently, M. Bogey et al. reported on the high resolution millimeter and submillimeter wave spectra of ArH_3^+, $ArHD_2^+$, ArH_2D^+, and ArD_3^+.[8,9] They conclude that these isotopomers are planar with the Ar lying near the apex of the H_3^+ (or substituted moiety). The Ar-H_3^+ centroid distance was found to be 2.38 Å with a binding

energy of 6.6 kcal/mole. Because the Ar is held so weakly, the internal rotation of the H_3^+ in the plane is expected to occur. In fact, Bogey et al. observed tunneling splittings and used these to obtain a barrier height for the internal rotation of H_3^+ or D_3^+ of 1700 cm^{-1} using a semirigid model or 1000 cm^{-1} using a flexible model.

The presence of tunneling splittings is expected to be a characteristic of the high resolution spectra of cluster ions that are weakly bound. This potentially leads to extremely complicated spectra that are impossible to assign using a rigid molecule Hamiltonian. The traditional point group approach also becomes too constrained, and an alternative theory must be used. One such alternative theory, called permutation inversion group theory, utilizes molecular symmetry groups and was first developed by Longuet-Higgins[10] and Hougen.[11,12] Since then, it has been successfully applied to a number of floppy molecules such as $(H_2O)_2$,[13-17] N_2H_4,[18-21] C_2H_6,[22-24] and ArH_3^+.[8,9] We will use permutation-inversion group theory in our discussion of the $H_5O_2^+$ high resolution spectrum.

At this point, it is appropriate to summarize the results presented in the previous chapter. $H_9O_4^+$ can be viewed as an H_3O^+ core which has been solvated by three water groups. The low resolution scan between 3570-3800

cm^{-1} shows two fundamentals. The band at 3730.4 cm^{-1} is the antisymmetric stretch of an outer H_2O moiety, and the band at 3644.9 cm^{-1} is the symmetric stretch of an outer H_2O moiety. These features have been red shifted by 25.4 and 6.8 cm^{-1}, respectively, from free H_2O. The band at 3730.4 cm^{-1} shows a partially resolved P, Q, R branch structure, implying a parallel transition.

$H_5O_2^+$ can most properly be viewed as two H_2O units equally sharing a proton. The low resolution spectrum corroborates this picture. Two features are seen, centered at 3684.4 and 3608.8 cm^{-1}. Calculations by Remington and Schaefer[25] show that the symmetric C_2 point group structure would have two dominant features in this frequency range, and the asymmetric C_s point group structure, which is predicted to be <0.2 kcal/mole higher in energy, would have four bands. In fact, the spectrum of $H_5O_2^+ \cdot H_2$ consists of four peaks, strongly suggesting that the presence of the weakly bound H_2 modifies the structure of $H_5O_2^+$ by stabilizing an H_3O^+ core. Those results are presented elsewhere.[4,6,7] The feature in the $H_5O_2^+$ spectrum centered near 3684.4 cm^{-1} corresponds to the antisymmetric stretch of an H_2O unit, and the band at 3608.8 cm^{-1} is assigned to a symmetric stretch of an H_2O moiety. The low resolution scan reveals a progression of Q branches in the higher frequency feature which indicates

a perpendicular type transition. This will be discussed more fully below.

II. Experimental Details

The experimental apparatus will only be briefly described here.[26] A schematic is shown in Fig. 1. The cluster ions are produced in a corona discharge ion source. Typical discharge conditions behind the nozzle are 1.2 kV from cathode to anode, 20-40 μA discharge current, and 200 torr of H_2 gas containing trace amounts of H_2O. The copper wall of the source serves as the cathode and is located 0.150 ± 0.003 in. away from the anode, which is a nickel plated iron needle. The beam is expanded supersonically through a 75 μm nozzle and then skimmed by a 1.5 mm diameter skimmer. The potential difference between the nozzle and skimmer is kept less than 1 V in order to maintain a weak field which allows drifting of the ions toward the skimmer but minimized collisional heating precesses. A grid surrounding the nozzle/skimmer area is used to keep this region relatively field free.

Downstream of the skimmer, the ions are focussed and mass selected using a 60° sector magnet. This allows unambiguous identification of the ion being studied. The interaction region is a radio-frequency octopole ion trap under ultra-high vacuum. The ion trap consists of eight

molybdenum rods of 0.32 cm diameter evenly spaced on a 1.25 cm diameter circle. An rf of 7.4 MHz, 200-300 V peak-to-peak is applied with opposite phases on adjacent rods. While the ions are trapped, they are probed spectroscopically with infrared lasers.

Two lasers were used in the pumping scheme. The first is a tunable IR laser used for spectroscopic interrogation and the second is a line tunable CO_2 laser used for detecting the vibrationally excited molecules by the IRMPD method. The tunable IR laser is a Burleigh cw F-center laser containing an intracavity etalon which gives a linewidth of 3×10^{-5} cm^{-1}. The FCL is frequency scanned by simultaneously ramping the voltage applied to the etalon and turning a grating causing the laser to hop cavity modes which are spaced by 0.0095 cm^{-1}. Because we expected the Doppler width of the ions moving back and forth in the trap to be on the order of, or slightly larger than, the cavity mode spacing, we chose the mode-hopping approach over scanning the cavity length. The frequency of the FCL is scanned near the center of the band assigned to the antisymmetric O-H stretch of the H_2O moieties (3700 cm^{-1} for $H_5O_2^+$ and 3730 cm^{-1} for $H_9O_4^+$).

The second laser in the pumping scheme is an MPB Technologies Inc. cw CO_2 laser. This laser is used to dissociate the vibrationally excited $H_5O_2^+$ or $H_9O_4^+$ ion through a multiphoton process. The frequency and inten-

sity of the CO_2 laser is determined by trying to reach the ideal situation where none of the ground state $H_3O^+ \cdot (H_2O)_n$ ions absorb enough photons to dissociate, but those in v = 1 do dissociate into $H_3O^+ \cdot (H_2O)_{n-1}$ and H_2O. This ideal situation is different for $H_5O_2^+$ and $H_9O_4^+$ as has been extensively described in the previous chapter. Briefly, two factors make it much more difficult for $H_5O_2^+$ to undergo multiphoton dissociation from the vibrationally excited state. The first factor is that the energy for dissociation in $H_5O_2^+$ is about 12 kcal/mole greater than in $H_9O_4^+$. This means that $H_5O_2^+$ has to absorb roughly four more CO_2 photons than does $H_9O_4^+$. The second factor is that the density of states at v = 1 is about 10^6 times greater for $H_9O_4^+$.[27] So, not only do the $H_5O_2^+$ vibrationally excited ions need to absorb more photons, but absorption is also more difficult. Therefore, the CO_2 laser is run with no attenuation (8 W out of the laser) on R(24) of the $00^0 1\text{-}02^0 0$ transition when studying $H_5O_2^+$. In addition to the CO_2 frequency and power, the length of time the ions are trapped in the octopole trap is also used to optimize the signal level. When studying $H_5O_2^+$, 100 msec was used. Typical ion counts were 2500 cps at a sampling rate of 8 times per second giving about 300 ions in the trap at a time. Both the FCL and CO_2 lasers were run cw into the trap. In the case of $H_9O_4^+$, the CO_2 laser was run on R(20) of the $00^0 1\text{-}10^0 0$ transition, and the

intensity was attenuated to 1.5 W using a gas cell containing ethylene. A trapping time of 57.5 msec was used yielding ion count rates of 30,000-40,000 cps at a sampling rate of 14 times per second. The FCL and CO_2 beams were resolved temporally with a chopper to control the sequence of photons absorbed. This was not necessary in the case of $H_5O_2^+$ because the ground state ions absorb CO_2 photons only minimally. After the interaction with the lasers, the cluster ions dissociate. A quadrupole mass filter is used with a Daly detector to count the fragment ions produced.

III. Results

The spectra of $H_5O_2^+$ and $H_9O_4^+$ taken at 0.5 cm^{-1} resolution are reproduced in Figs. 2 and 3. Both spectra show two bands assigned to the antisymmetric and symmetric O-H stretches of an H_2O moiety. An enlargement of the antisymmetric stretch for $H_9O_4^+$ is shown in Fig. 4.

A. $H_5O_2^+$

$H_5O_2^+$ is a near symmetric top with rotational constants from the ab initio C_2 structure of A = 6.120, B = 0.2936, and C = 0.2923 cm^{-1}.[25] This gives 1.1 x 10^{-4} for the b asymmetry parameter.[28] Because our Doppler width is estimated to be 0.01-0.02 cm^{-1}, we do not expect to resolve K splittings except for very high J states.

Working within the symmetric rotor approximation, we would expect to see a perpendicular band, or a parallel band, or a hybrid thereof. The progression seen is characteristic of a perpendicular band progression, and Fig. 2 shows the assignment of the Q branches to the different sub-bands. The spacing between the Q branches gives 2(A'-B') = 11.6 cm^{-1}.[29]

High resolution spectra were obtained under the $^{R}Q_{0}$ and $^{R}Q_{1}$ peaks and are shown in Figs. 5 and 6, respectively. Careful examination of Fig. 6 reveals what appears to be the $^{R}Q_{1}$ branch and a progression of peaks in the $^{R}R_{1}$ branch as would be expected at the rigid rotor level. Closer examination reveals several peaks for every level predicted using the simplistic rigid rotor approximation. These cannot be explained using a rigid molecular model. This should not be surprising since $H_5O_2^+$ is considered to be a floppy molecule and is expected to have low barriers to internal motions. Therefore, a theory that incorporates large amplitude motions must be employed. This is the topic of the section on permutation-inversion group theory.

B. $H_9O_4^+$

$H_9O_4^+$ is rigorously an oblate symmetric top with rotational constants from the calculated geometry of A = B = 0.0876 and C = 0.0453 cm^{-1}.[25] The vibration of species

A_1 consists of three antisymmetric stretches of the H_2O groups in phase and would give rise to a parallel band. In the species E vibration, the three antisymmetric stretches are not in phase and a perpendicular band would result. According to the intensity predictions of Remington and Schaefer, the intensity of the A_1 transition is almost two orders of magnitude larger than that of the E band.

The low resolution $H_9O_4^+$ spectrum does, in fact, imply a parallel band transition. The high resolution spectrum shown in Fig. 7 does not suggest such a simple picture. Instead of a single sharp central Q-branch, four central features are seen. To the red and blue sides are seen what resembles a ripple of peaks separated by 0.17 cm^{-1}. In fact, the spacing in the P and R branches of a parallel band should be 2B which, for $H_9O_4^+$, equals 0.175 cm^{-1}.[29] Again, the surplus of peaks is probably attributable to tunneling splittings.

IV. Permutation-Inversion Group Theory

The hydrated hydronium ion, $H_5O_2^+$, is nonrigid, and therefore the possibility of observing tunneling splittings through several different barriers is high. To use permutation-inversion group theory[30] to treat this problem, one starts by constructing the complete nuclear permutation inversion (CNPI) group. We label the hydro-

gens 1 through 5 and the oxygens a and b as shown below. Permutations consist of exchange of identical nuclei.

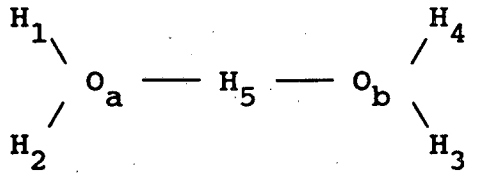

The notation for exchanging hydrogens 1 and 2 is (12). Three nuclei can also be interchanged and this is denoted by (123) which means the laboratory-fixed coordinates of hydrogen 1 are replaced by the coordinates of 2, the coordinates of 2 are replaced by those of 3, and the coordinates of 3 are replaced by those of 1.[18] A cyclic permutation of 4 and 5 nuclei is also included in the nuclear permutation group and is denoted by (1234) and (12345). The combination of a pair of nuclei exchanging and a cyclic permutation of three nuclei is represented by (12)(345). The last possibility is inversion of all nuclei through the center of the molecule and this is denoted by E^*. If a permutation is accompanied by an inversion, it is represented, for example, by $(123)^*$. The identity is called E. To construct the complete nuclear permutation inversion group, one takes all possible combinations of the above elements. These are indicated in Table I. The size of the CNPI group is determined simply by taking the direct product of the complete nuclear permutation group, which consists of 5! x 2! = 240

elements, and the inversion group, which consists of 2 elements. (In the CNP group, the 5 originates from having 5 hydrogen nuclei and the 2 from 2 oxygen nuclei.) Therefore the CNPI group consists of 480 elements. The next step is to decide which elements of the CNPI group represent feasible motions and which correspond to tunneling motions with barriers too high to observe tunneling through. Using the labels in the diagram above, (12) and also (34) correspond to internal rotation about the C_2 axis of an H_2O monomer which is expected to have a low enough barrier to be considered a feasible motion. On the other hand, (13) is not a feasible motion. Exchange with the central proton, (15), will be considered as an unfeasible motion in this discussion. Its barrier is expected to be an order of magnitude larger than the barriers for the motions considered as feasible in this treatment. Another feasible motion is $(ab)(1324)^*$ which corresponds to inversion of one $H_2O - H^+$ group and $(ab)(1423)^*$ which is inversion of the opposite $H_2O - H^+$ group. Inversion of both $H_2O - H^+$ groups simultaneously is described by the element (12)(34) and is expected to have a higher barrier than inversion of a single side. Basically, all the motions which keep hydrogens 1 and 2 on oxygen a, keep hydrogens 3 and 4 on oxygen b, and keep hydrogen 5 in the center will be considered as feasible elements and all others will be considered unfeasible.

The feasible elements, which are listed in Table II, comprise the molecular symmetry (MS) group.

Only 16 elements remain in the MS group from the original 480 elements in the CNPI group. This gives a G_{16} group. Because $H_5O_2^+$ has C_2 symmetry, pairs of the above elements yield identical frameworks. Therefore, there are only eight nonsuperimposable equilibrium frameworks. These are shown in Fig. 8 sighting down the O-H-O axis. Oxygen a is above the plane of the paper and oxygen b is below for all eight frameworks.

A complication arises in molecules that exhibit a large torsional amplitude such as H_2CCH_2, H_2NNH_2, and $H_2OHOH_2^+$. When both H_2 groups increase their torsional angle, γ, by π and when the Euler angle χ is incremented by π, the spatial configuration of the atoms is unchanged.[31] This means the coordinate system is double-valued since any configuration can be expressed by two sets of coordinates: $(\varphi,\theta,\chi,\gamma)$ and $(\varphi,\theta,\chi+\pi,\gamma+\pi)$. In order to keep the overall wavefunction single-valued, each element in the G_{16} molecular symmetry group corresponds to two coordinate transformations. The symmetry group becomes twice as large and is called $G_{16}^{(2)}$, the double group of G_{16}.

The character table of $G_{16}^{(2)}$ as given in Merer and Watson[31] is reproduced in Table III. From this we can easily generate the reverse correlation table as shown in

Table IV between $G_{16}^{(2)}$ and the C_2 point group. Briefly, the letters a through e at the top of Table III denote the generating operations of $G_{16}^{(2)}$. The operation b corresponds to the permutation inversion element (ab)(14)(23) which is equivalent to the C_2 operation in the C_2 point group. Because C_2 is the only symmetry element in the C_2 point group, the correlation of the $G_{16}^{(2)}$ species with the A and B species in the C_2 point group, can be immediately deduced by looking under the column labeled b in the $G_{16}^{(2)}$ character table. The generating operation a corresponds to the permutation-inversion element $(ab)(1324)^*$ when using Hougen's notation[18] and $(ab)(1423)^*$ when using Merer and Watson's notation[31]. The generating operation c corresponds to the inversion element, E^*. The generating operation d corresponds to the permutation inversion identity, E, when $(\varphi,\theta,\chi,\gamma) = (\varphi,\theta,\chi+\pi,\gamma+\pi)$. The generating operation e is the identity.

Also included in Table IV are the nuclear spin statistical weights. The five hydrogens give $2^5 = 32$ nuclear spin wavefunctions. The reducible representation obtained from these nuclear spin functions is given in Table III in the row labeled Γ_{ns}. Γ_{ns} reduces to $12A_{1g}^+ \oplus 2B_{1g}^+ \oplus 6B_{2u}^+ \oplus 6E^+$. The species of the total internal wavefunction must be B_{1g}^+ for positive parity and A_{1u}^- for negative parity. Therefore the product of the species for rotation-vibration-electronic, Γ_{rve}, times the species for

Γ_{ns} must equal either B_{1g}^{+} or A_{1u}^{-}. Working this through gives the nuclear spin statistical weights shown in Table IV for the rotational levels with the indicated symmetry species.

At this point, it is helpful to compare $H_2OH^{+}OH_2$ with H_2NNH_2. Both molecules use the $G_{16}^{(2)}$ double group and have C_2 symmetry in a rigid frame. The feasible operations lead to the same eight nonsuperimposable equilibrium frameworks shown in Fig. 8 through the same tunneling paths. Therefore, the quantum mechanical treatment will lead to the same Hamiltonian matrix and eigenvectors so that the eigenvalues for $H_5O_2^{+}$ will be expressed by the same formulas derived for N_2H_4. The reader is referred to Ref. 18 for details on this derivation. These results are rederived in Ref. 20 and summarized in Ref. 21.

The starting point in the determination of the energy levels will be the rigid rotor energy levels labeled by the quantum numbers J and K_a. Higher order effects such as centrifugal distortion can shift these energy levels, but not create additional levels. Permutation-inversion group theory tells us that since there are eight equilibrium frameworks, each level described by the quantum numbers J,K_a can split into at most eight energy levels. The size of the splitting of each of these eight levels from the original energy is determined by the tunneling barrier from framework 1 to each of the seven other

frameworks. The procedure is first to estimate the size of the tunneling barriers. By comparing with other molecules whose tunneling properties have been studied, one then guesses at an appropriate tunneling splitting. These values are then used in the formulas below with some phase factors dependent on the K value and some higher order terms dependent on both J and K. For this initial treatment, these higher order terms will be neglected. By comparing the calculated splitting patterns and predicted spectrum with the experimental spectrum, one then modifies the initially chosen values for the tunneling splittings to try to produce a match using an iterative procedure.

We will now estimate the size of the barriers between framework 1 and the other seven in order to obtain approximations to the tunneling splittings. The motion used to change from framework 1 to framework 5 or 6 is the umbrella inversion motion of an $H_2O - H^+$ unit. Remington and Schaefer have calculated energies for several geometries of $H_5O_2^+$.[25] Their C_s geometry approximates the geometry at the top of the barrier to inversion. One $H_2O - H^+$ unit is pyramidal, and the other is planar. The difference between their C_s geometry and the geometry at the barrier to inversion is the degree to which the central proton is shifted closer to the pyramidal side. This is not expected to change the energy significantly. The energy of their C_s structure is less than 0.2

kcal/mole higher in energy than their lowest energy C_2 structure. The table below gives other known barrier heights and inversion splittings. In addition to the

Molecule	Barrier height	Inversion splitting	Ref
NH_3	5.9 kcal/mole	0.79 cm^{-1}	32
PH_3	17	5×10^{-6}	32
N_2H_4		0.54	21
NH_2CH_3	1.9	0.2	34
H_3O^+	2.0	55	33
$H_5O_2^+$	0.2		25
$H_9O_4^+$	0.6		25

barrier height, another factor to consider is that the inversion motion in $H_5O_2^+$ is accompanied by an internal torsion of about 20°. This would decrease the inversion splitting from the otherwise expected quantity. An inversion splitting on the order of 0.5 cm^{-1} seems reasonable. Ultimately, the accuracy of the value is determined by how well the predicted and experimental spectra match.

Tunneling between frameworks 1 and 2 corresponds to inversion of both ends of the molecule. This barrier is expected to be significantly higher, and calculations of Remington and Schaefer show that the geometry with both end moieties planar is about 0.7 kcal/mole higher in

energy than the C_2 structure.[25] The tunneling splitting should then be significantly smaller than that for inversion of a single $H_2O - H^+$ group.

Tunneling between frameworks 1 and 3 corresponds to torsional rotation. There will be different barrier heights through the trans barrier and through the cis barrier. The table below lists barrier heights and torsional splittings for other molecules. Because the

Molecule	Barrier height		Torsional splitting	Ref
HOOH	trans	1.1 kcal/mole	11.4 cm^{-1}	35
	cis	7.0	<0.002	
H_2NNH_2	trans	6.0	0.00019	21
HNCNH	trans	7.96	<0.02	36,37
	cis	7.93	<0.02	
H_3CCH_3		2.9	0.006	24
H_3CCCCH_3		<0.03	1-5	38
$H_5O_2^+$	trans	0.7		25

oxygens in $H_5O_2^+$ are separated by the proton in the center, the cis and trans barriers are expected to be closer in energy than molecules where the torsion occurs along a shorter axis. Birk and Winnewisser have reported that the trans and cis barriers in HNCNH are quite similar.[36,37] From the structures calculated by Remington and Schaefer, an estimate for the trans barrier height in $H_5O_2^+$ is 0.7 kcal/mole.[25]

Going from framework 1 to 4 is a complex motion and requires simultaneous tunneling motions. In this initial treatment, this motion was considered to have a high enough barrier that the tunneling splitting would not be observed.

Finally, the motion from framework 1 to 7 or 8 corresponds to a rotation of one H_2O group around the C_2 axis of that moiety. An example of this is in water dimer which has been studied rather extensively. The tunneling splitting in $(H_2O)_2$ is about 6 cm^{-1} with a calculated barrier of 0.4 kcal/mole.[15] Water dimer is bound much less strongly than $H_5O_2^+$ so one needs to exercise caution in extrapolating the value from water dimer. In addition, there is some uncertainty whether the tunneling path consists primarily of the C_2 motion or an inversion combined with internal rotation.[15,39] Both motions produce the same final framework in water dimer.

Once the initial guesses to the tunneling splittings have been made, the next step is to try them out in the energy formulas below.[18,21]

$$W(A_{1g}^{+}) = (\alpha_1 + \alpha_2) + (\alpha_3 + \alpha_4) + 2\alpha_5 + 2\alpha_7$$
$$W(A_{1u}^{-}) = (\alpha_1 + \alpha_2) - (\alpha_3 + \alpha_4) + 2\alpha_5 - 2\alpha_7$$
$$W(B_{1g}^{+}) = (\alpha_1 + \alpha_2) + (\alpha_3 + \alpha_4) - 2\alpha_5 - 2\alpha_7$$
$$W(B_{1u}^{-}) = (\alpha_1 + \alpha_2) - (\alpha_3 + \alpha_4) - 2\alpha_5 + 2\alpha_7$$

$$W(A_{2g}^{-}) = (\beta_1 + \beta_2) + (\beta_3 + \beta_4) + 2\beta_5 + 2\beta_7$$

$$W(A_{2u}^{+}) = (\beta_1 + \beta_2) - (\beta_3 + \beta_4) + 2\beta_5 - 2\beta_7$$

$$W(B_{2g}^{-}) = (\beta_1 + \beta_2) + (\beta_3 + \beta_4) - 2\beta_5 - 2\beta_7$$

$$W(B_{2u}^{+}) = (\beta_1 + \beta_2) - (\beta_3 + \beta_4) - 2\beta_5 + 2\beta_7$$

$$W(E^{+}) = [(\alpha_1 - \alpha_2) - (\alpha_3 - \alpha_4) + (\beta_1 - \beta_2) + (\beta_3 - \beta_4)]/2 + \{0.25[(\alpha_1 - \alpha_2) - (\alpha_3 - \alpha_4) - (\beta_1 - \beta_2) - (\beta_3 - \beta_4)]^2 + (2\gamma_5 + 2\gamma_7)^2\}^{0.5}$$

$$W(E^{-}) = [(\alpha_1 - \alpha_2) + (\alpha_3 - \alpha_4) + (\beta_1 - \beta_2) - (\beta_3 - \beta_4)]/2 + \{0.25[(\alpha_1 - \alpha_2) + (\alpha_3 - \alpha_4) - (\beta_1 - \beta_2) + (\beta_3 - \beta_4)]^2 + (-2\gamma_5 + 2\gamma_7)^2\}^{0.5}$$

$$W(E^{+}) = [(\alpha_1 - \alpha_2) - (\alpha_3 - \alpha_4) + (\beta_1 - \beta_2) + (\beta_3 - \beta_4)]/2 - \{0.25[(\alpha_1 - \alpha_2) - (\alpha_3 - \alpha_4) - (\beta_1 - \beta_2) - (\beta_3 - \beta_4)]^2 + (2\gamma_5 + 2\gamma_7)^2\}^{0.5}$$

$$W(E^{-}) = [(\alpha_1 - \alpha_2) + (\alpha_3 - \alpha_4) + (\beta_1 - \beta_2) - (\beta_3 - \beta_4)]/2 - \{0.25[(\alpha_1 - \alpha_2) + (\alpha_3 - \alpha_4) - (\beta_1 - \beta_2) + (\beta_3 - \beta_4)]^2 + (-2\gamma_5 + 2\gamma_7)^2\}^{0.5}$$

Notice that there are 12 components for each original rotational level with a given J,K quantum number, but there are only eight frameworks. This means that some of the components will be degenerate. The α's, β's, and γ's represent tunneling matrix elements between framework 1 and the framework indicated by the index. That is, α_n = <1A|H|nA>, β_n = <1B|H|nB>, and γ_n = <1A|H|nB> where n = 1, 2, 3, 5, and 7. The symbols A and B indicate the symmetry species of the wavefunction in the C_2 point group. The

values of α_1 and β_1 are the ordinary single framework near symmetric rotor energies of the A and B rotational levels. The other quantities depend on the J and K quantum numbers as given below.

$$\alpha_2 = (-1)^K[h_{2v} + h_{2k}K^2] + \delta_{1,K}(-1)^J f_2 J(J+1)$$

$$\beta_2 = (-1)^K[h_{2v} + h_{2k}K^2] - \delta_{1,K}(-1)^J f_2 J(J+1)$$

$$\alpha_3 = \beta_3 = h_{3v}^t + (-1)^K h_{3v}^c + h_{3k}^t K^2$$

$$\alpha_4 = (-1)^K[h_{4v} + h_{4k}K^2] + \delta_{1,K}(-1)^J f_4 J(J+1)$$

$$\beta_4 = (-1)^K[h_{4v} + h_{4k}K^2] - \delta_{1,K}(-1)^J f_4 J(J+1)$$

$$\alpha_5 = \beta_5 = (i)^K[h_{5v} + h_{5j}J(J+1) + h_{5k}K^2] \quad \text{for K = even}$$

$$\alpha_5 = +\delta_{K,1}(-1)^J g_5 J(J+1) + (i)^{K+1}[q_5 + q_{5j}J(J+1) + q_{5k}K^2]K \quad \text{for K = odd}$$

$$\beta_5 = -\delta_{K,1}(-1)^J g_5 J(J+1) + (i)^{K+1}[q_5 + q_{5j}J(J+1) + q_{5k}K^2]K \quad \text{for K = odd}$$

$$\gamma_5 = (i)^K[q_5 + q_{5j}J(J+1) + q_{5k}K^2]K \quad \text{for K = even}$$

$$\gamma_5 = (i)^{K-1}[h_{5v} + h_{5j}J(J+1) + h_{5k}K^2] \quad \text{for K = odd}$$

$$\alpha_7 = \beta_7 = (i)^K[h_{7v} + h_{7j}J(J+1) + h_{7k}K^2] \quad \text{for K = even}$$

$$\alpha_7 = +\delta_{K,1}(-1)^J g_7 J(J+1) + (i)^{K+1}[q_7 + q_{7j}J(J+1) + q_{7k}K^2]K \quad \text{for K = odd}$$

$$\beta_7 = -\delta_{K,1}(-1)^J g_7 J(J+1) + (i)^{K+1}[q_7 + q_{7j}J(J+1) + q_{7k}K^2]K \quad \text{for K = odd}$$

$$\gamma_7 = 0 \quad \text{for K = even}$$

$$\gamma_7 = -\delta_{1,K}(-1)^J f_7 J(J+1) \quad \text{for K = odd}$$

In this preliminary treatment, only the first order terms will be kept. Higher order terms will be set to zero. A more sophisticated analysis is in progress.

Using the above equations, energy levels can be predicted assuming various tunneling splittings. As an illustration, we will consider three sources of tunneling splittings separately, and then consider a situation with three splittings combined. The largest splitting in $H_5O_2^+$ is expected to be due to tunneling through the inversion barrier. Suppose $2h_{5v} = 0.55\ cm^{-1}$. Ignoring the higher order terms, we obtain $\alpha_2 = \beta_2 = (-1)^K(0.55)$. Putting these values into the energy formulas, we obtain the splitting patterns shown in Fig. 9. Notice that the E levels are in the middle for even K and on the outside of the fork for odd K. Also, the states on the top in the fork with K = 0 are on the bottom for K = 2 and vice-versa. For $K \geq 1$, each J,K level consists of an unresolved doublet of C_2 symmetry species A and B, so all $G_{16}^{(2)}$ species are allowed for each level. On the other hand, for K = 0 even J levels belong to species A and odd J levels have species B in the C_2 point group. Therefore, the reverse correlation table (Table IV) must be used to determine the allowed symmetry species for each J level in $G_{16}^{(2)}$. Determining which E states correlate to even and odd J levels is more subtle. From Ref. 18, Table VI and VIII, the following formulas are obtained for K = 0:

$$A: \quad W(E^+) = (\alpha_1 - \alpha_2) - (\alpha_3 - \alpha_4)$$

$$B: \quad W(E^+) = (\beta_1 - \beta_2) + (\beta_3 - \beta_4)$$

$$A: \quad W(E^-) = (\alpha_1 - \alpha_2) + (\alpha_3 - \alpha_4)$$

$$B: \quad W(E^-) = (\beta_1 - \beta_2) - (\beta_3 - \beta_4).$$

A second source of tunneling splitting is that due to torsion by rotation through the trans and cis barriers. If the trans splitting is $h_{3v}^t = 0.05$ and $h_{3v}^c = 0.03$, we notice that each level splits into two separated by the sum or difference of h_{3v}^t and h_{3v}^c depending on whether K is even or odd, respectively. This is shown in Fig. 10. A third source of tunneling splitting is due to tunneling from framework 1 to framework 7. This can be achieved by either rotation of an H_2O moiety about its C_2 axis or by inversion followed by torsion. If the path resembles the latter, then the tunneling splitting parameter $2h_{7v}$ should be smaller than either $2h_{5v}$ (corresponding to inversion) or h_{3v}^t (corresponding to torsion). If the former path is chosen, the value of $2h_{7v}$ could be larger. As an example, a value of $2h_{7v} = 0.02$ cm^{-1} is chosen. The splitting patterns are shown in Fig. 11. The levels with even K are split into forks, but the level with K = 1 shows no splitting. Combining all three of these tunneling paths in one diagram and assuming that $2h_{5v} = 0.55$, $h_{3v}^t = 0.05$, $h_{3v}^c = 0.03$, and $2h_{7v} = 0.02$ cm^{-1}, Fig. 12 is obtained.

Note that the effect of h_{7v} is only to shift the levels; no additional splitting is obtained.

To calculate transition frequencies and thus obtain spectral patterns, a few more points need to be addressed. The first is the selection rule for dipole allowed transitions. The space fixed dipole moment operator belongs to the symmetry species B_{1u}^-. Therefore the product of the species of the lower and upper state must give B_{1u}^- (from the fact that $\langle \Psi'_{rve} | \mu | \Psi''_{rve} \rangle$ must be totally symmetric). The symmetry selection rules are $B_{1g}^+ <-> A_{1u}^-$, $B_{2g}^- <-> A_{2u}^+$, $A_{1g}^+ <-> B_{1u}^-$, $A_{2g}^- <-> B_{2u}^+$, and $E^+ <-> E^-$. Since there are two E^+ states and two E^- states, there is some ambiguity to which E^- state a given E^+ state can undergo a transition. It is expected that one transition will dominate over the other. Both transitions will be included in the spectral patterns as dotted lines when there is some ambiguity as to which are the allowed transitions. Another question to be answered is what is the effect of vibrational excitation. If we define r_{nm} as the distance between H_n and O_m, the two vibrations which have the possibility of being excited can be called q_s and q_d. They are defined as follows:

$$q_s = (r_{1a} - r_{2a}) - (r_{3b} - r_{4b})$$

$$q_d = (r_{1a} - r_{2a}) + (r_{3b} - r_{4b})$$

Using Table II from Ref. 18, it is seen that q_s is of symmetry species A in the C_2 point group and q_d is of species B. Remington and Schaefer have calculated the relative intensities of the transitions of A and B symmetry to be 8.6 to 6.5.[25] Using Eq. 7 from Ref. 21 one can calculate the overlap integral between framework 1 and framework n in both the ground and vibrationally excited state. In this situation where the primary interest is in determining how the sign of h_{nv} changes with vibrational excitation, the integration is greatly simplified. As an example, suppose the excitation is from v = 0 to v = 1 in q_s and one is interested in determining how the sign of h_{2v} is affected by this vibrational excitation. We then have:

$$\frac{h'_{2v}}{h''_{2v}} = \frac{\langle \Psi'_{1s}\Psi'_{1d}\Psi'_{1x}|V|\Psi'_{2s}\Psi'_{2d}\Psi'_{2x}\rangle}{\langle \Psi''_{1s}\Psi''_{1d}\Psi''_{1x}|V|\Psi''_{2s}\Psi''_{2d}\Psi''_{2x}\rangle}$$

where Ψ'_{1s} is the wavefunction in the q_s coordinate in the upper state in framework 1, Ψ'_{1d} is the wavefunction for q_d in framework 1, and Ψ'_{1x} is the wavefunction in the remainder of the coordinates in framework 1 in the upper state. Ψ'_{2s}, Ψ'_{2d}, and Ψ'_{2x} are the corresponding wavefunctions in framework 2 and the double primed functions correspond to the lower state. In this example, only $\Psi'_{1s} \neq \Psi''_{1s}$ and $\Psi'_{2s} \neq \Psi''_{2s}$. The other single primes can be

replaced by double primes. A ground state wavefunction is positive everywhere; the vibrationally excited wavefunction has the form $q_s \cdot \exp(-q_s^2)$. Using the above statements and recalling that the interest is in determining the sign, the problem can be simplified to determining the sign of $\langle \Psi'_{1s} | \Psi'_{2s} \rangle$ in a first order approximation. Tunneling from framework 1 to 2 corresponds to the Merer and Watson (MW) generating operation a^2.[31] Therefore,

$$
\begin{aligned}
\langle \Psi'_{1s} | \Psi'_{2s} \rangle &\approx \langle \Psi'_{1s} | a^2 \Psi'_{1s} \rangle \\
&\approx \langle q_s \cdot \exp(-q_s^2) | a^2 q_s \cdot \exp(-q_s^2) \rangle \\
&\approx \langle q_s \cdot \exp(-q_s^2) | a^2 [(r_{1a} - r_{2a}) - (r_{3b} - r_{4b})] \\
&\qquad \cdot a^2 \exp(-q_s^2) \rangle \\
&\approx \langle q_s \cdot \exp(-q_s^2) | a [(r_{3b} - r_{4b}) - (r_{2a} - r_{1a})] \\
&\qquad \cdot a^2 \exp(-q_s^2) \rangle \\
&\approx \langle q_s \cdot \exp(-q_s^2) | [(r_{2a} - r_{1a}) - (r_{4b} - r_{3b})] \\
&\qquad \cdot a^2 \exp(-q_s^2) \rangle \\
&\approx \langle q_s \cdot \exp(-q_s^2) | -q_s \cdot \exp(-q_s^2) \\
&\approx -\langle \Psi'_{1s} | \Psi'_{1s} \rangle
\end{aligned}
$$

This indicates that the sign of h_{2v} changes upon vibrational excitation. Table V summarizes the sign changes in this simple approximation for vibrational excitation. Unfortunately, this approach is not able to give us the effect of tunneling to frameworks 5-8 because the overlap

integral is zero. A more sophisticated treatment awaits further theoretical developments.

We are finally ready to calculate transition frequencies and spectral patterns. Two examples will be worked out. The first is $2h_{5v} = 0.55\ cm^{-1}$. This is shown in Fig. 13. Because we do not know how the sign of h_{5v} changes with vibrational excitation, we have assumed it does not change. Notice that the predicted intensities differ for the $^{R}R_{0}$ and $^{R}R_{1}$ branches. In the $^{R}R_{1}$ branch, the pattern repeats every $0.5\ cm^{-1}$ (assuming $2B \approx 0.5\ cm^{-1}$) whereas in the $^{R}R_{0}$ branch even J values have higher intensity than odd J values. The Q branch in this simplified treatment would consist of a doublet split by $1.10\ cm^{-1}$.

In the second example, the assumption is that $2h_{5v} = 0.60$, $h_{3v}^{t} = 0.04$, $h_{3v}^{c} = 0.03$, and $2h_{7v} = 0.01\ cm^{-1}$. The allowed transitions and spectral patterns are shown in Fig. 14. The basic patterns obtained with $2h_{5v} = 0.55\ cm^{-1}$ are retained with some additional splitting from torsional tunneling. The predicted patterns can be compared with the experimental spectrum shown in Figs. 5 and 6. Although additional analysis and fits are in progress, at this early stage it is encouraging to note the similarity between the predicted and experimental spectra. In Fig. 6 the broad peak centered at $3702.4\ cm^{-1}$ is tentatively assigned to the higher frequency component

of the $^{R}Q_1$ branch. The progression toward higher frequency contains both components of the $^{R}R_1$ branch and is dominated by pairs of lines separated by 2B. The complexity of Fig. 5 is explained by postulating that the spectrum is dominated by a quartet of lines separated by 2B with alternating quartets having slightly greater intensity.

One obvious question is why the pair of Q-branches, predicted by the description above, was not observed experimentally. In both the K = 0 -> 1 and K = 1 -> 2 sub-bands, a gap in the F-center laser coverage at high resolution happens to coincide with the most probable locations of the second Q-branches. However, in the low resolution spectrum there is a suggestion of a doubling of the Q-branches. This is seen most clearly in the $^{R}Q_1$ branch where a splitting of 0.95 cm^{-1} was consistently seen. Initially this was interpreted as likely due to a power dip. Later analysis seems to indicate this doubling of the $^{R}Q_1$ branch is real.

V. Future Work

The existing data are in the process of analysis. Although the noise level is fairly high and the frequency range is limited, there seems to be the potential to obtain a relatively solid first guess for some rotational constants and tunneling splittings. Further theoretical

work also needs to be done as pointed out in the text to determine, for example, the effect of vibrational excitation on the parameter h_{5v}.

Obviously, additional experimental data would be useful. In the infrared region, it would be worthwhile to pursue the effort to locate the missing Q-branches. Two approaches suggest themselves. One is another attempt with the F-center laser being careful to rid the system of as much water as possible. Another possibility to try if the first is unsuccessful is using the IR-Wavelength Extender (IR-WEX) pumped by a Nd:YAG containing an intracavity etalon. This would give less complete resolution of the structure, but should have no difficulty in separating out two Q-branches if they are split by nearly 1 cm^{-1}. This is similar to the resolution needed to resolve individual J transitions in $C_2H_7^+$. In $C_2H_7^+$, 2B = 1.10 cm^{-1} and the IR-WEX was able to resolve partially the different rotational levels in the R branch. This is presented in the next chapter. Additionally, any experimental spectra, be it in the microwave, far infrared, or infrared would be useful. As in $(H_2O)_2$, where many laboratories contributed to the current pool of knowledge, an understanding of $H_5O_2^+$ will need contributions from many sources, both experimental and theoretical.

VI. Conclusions

The high resolution spectra of $H_5O_2^+$ and $H_9O_4^+$ have been presented. Although the analysis is continuing, the theory being used to interpret the $H_5O_2^+$ spectrum has been explained. Permutation-inversion group theory is necessary to account for the tunneling splittings observed. The treatment here is only the first step in understanding the high resolution spectrum of $H_5O_2^+$. Much additional work is necessary in order to gain a deeper understanding of the tunneling paths in both the ground state and vibrationally excited states.

REFERENCES

1. M. Okumura, L. I. Yeh, and Y. T. Lee, J. Chem. Phys. **83**, 3705 (1985).

2. M. Okumura, L. I. Yeh, and Y. T. Lee, J. Chem. Phys. **88**, 79 (1988).

3. M. Okumura, L. I. Yeh, J. D. Myers, and Y. T. Lee, J. Chem. Phys. **85**, 2328 (1986).

4. L. I. Yeh, M. Okumura, J. D. Myers, J. M. Price, and Y. T. Lee, to be published.

5. J. M. Price, M. W. Crofton, and Y. T. Lee, to be published.

6. M. Okumura, Ph.D. Thesis, University of California, Berkeley, 1986.

7. M. Okumura, L. I. Yeh, J. D. Myers, and Y. T. Lee, to be published.

8. M. Bogey, H. Bolvin, C. Demuynck, and J. L. Destombes, Phys. Rev. Lett. **58**, 988 (1987).

9. M. Bogey, H. Bolvin, C. Demuynck, J. L. Destombes, and B. P. van Eijck, J. Chem. Phys. **88**, 4120 (1988).

10. H. C. Longuet-Higgins, Mol. Phys. **6**, 445 (1963).

11. J. T. Hougen, J. Chem. Phys. **37**, 1433 (1962).

12. J. T. Hougen, J. Chem. Phys. **39**, 358 (1963).

13. T. R. Dyke, J. Chem. Phys. **66**, 492 (1977).

14. J. T. Hougen, J. Mol. Spectrosc. **114**, 395 (1985).

15. L. H. Coudert and J. T. Hougen, J. Mol. Spectrosc. **130**, 86 (1988).

16. Z. S. Huang and R. E. Miller, J. Chem. Phys. **88**, 8008 (1988).

17. K. L. Busarow, R. C. Cohen, G. A. Blake, K. B. Laughlin, Y. T. Lee, and R. J. Saykally, J. Chem. Phys. (submitted).

18. J. T. Hougen, J. Mol. Spectrosc. **89**, 296 (1981).

19. S. Tsunekawa, T. Kojina, and J. T. Hougen, J. Mol. Spectrosc. **95**, 133 (1982).

20. N. Ohashi and J. T. Hougen, J. Mol. Spectrosc. **112**, 384 (1985).

21. N. Ohashi, W. J. Lafferty, and W. B. Olson, J. Mol. Spectrosc. **117**, 119 (1986).

22. J. T. Hougen, J. Mol. Spectrosc. **82**, 92 (1980).

23. L. Henry, A. Valentin, W. J. Lafferty, J. T. Hougen, V. M. Devi, P. P. Das, and K. N. Rao, J. Mol. Spectrosc. **100**, 260 (1983).

24. R. Fantoni, K. van Helvoort, W. Knippers, and J. Reuss, Chem. Phys. **110**, 1 (1986).

25. R. Remington and H. F. Schaefer, unpublished results.

26. Additional details on the machine can be found in the previous chapter. See also: S. W. Bustamente, Ph.D. Thesis, University of California, Berkeley, 1983; and S. W. Bustamente, M. Okumura, D. Gerlich, H. S. Kwok, L. R. Carlson, and Y. T. Lee, J. Chem. Phys. **86**, 508 (1987).

27. P. J. Robinson and K. A. Holbrook, Unimolecular Reactions (Wiley-Interscience, New York, 1972).

28. H. C. Allen, Jr. and P. C. Cross, Molecular Vib-Rotors (John Wiley and Sons, Inc., New York, 1963).

29. G. Herzber, Molecular Spectra and Molecular Structure: II. Infrared and Raman Spectra of Polyatomic Molecules (Van Nostrand Reinhold Company Inc., New York, 1945).

30. P. R. Bunker, Molecular Symmetry and Spectroscopy (Academic Press, Inc., London, 1979).

31. A. J. Merer and J. K. G. Watson, J. Mol. Spectrosc. **47**, 499 (1973).

32. C. H. Townes and A. L. Schawlow, Microwave Spectroscopy (Dover Publications, Inc., New York, 1975).

33. D.-J. Liu, T. Oka, and T. J. Sears, J. Chem. Phys. **84**, 1312 (1986).

34. K. Shimoda, T. Nishikawa, and T. Itoh, J. Phys. Soc. Jap. **9**, 974 (1954).

35. R. H. Hunt, R. A. Leacock, C. W. Peters, and K. T. Hecht, J. Chem. Phys. **42**, 1931 (1965).

36. M. Birk, M. Winnewisser, E. A. Cohen, G. McRae, and J. Farhoomand, presented at the Tenth Colloquium on High Resolution Molecular Spectroscopy, Dijon, 1987.

37. M. T. Nguyen, N. V. Riggs, L. Radom, M. Winnewisser, B. P. Winnewisser, and M. Birk, Chem. Phys. **122**, 305 (1988).

38. P. R. Bunker and H. C. Longuet-Higgins, Proc. Roy. Soc. (London), Ser. A **280**, 340 (1964).

39. D. F. Coker and R. O. Watts, J. Phys. Chem. **91**, 2513 (1987).

TABLE I. Elements of the permutation group of the 5 hydrogen nuclei in $H_5O_2^+$. The complete nuclear permutation group of $H_5O_2^+$ is four times larger and can be obtained by taking the direct product of the elements given below with E, (ab), E^*, and $(ab)^*$.

Type E = 1 element

Type (jk) = 10 elements

(12)	(13)	(14)	(15)
	(23)	(24)	(45)
		(34)	(35)
			(45)

Type (jkl) = 20 elements

(123)	(124)	(125)	(134)	(135)	(145)
(132)	(142)	(152)	(143)	(153)	(154)
(234)	(235)	(245)	(345)		
(243)	(253)	(254)	(354)		

Type (jklm) = 30 elements

(1234)	(1235)	(1245)	(1345)	(2345)
(1243)	(1253)	(1254)	(1354)	(2354)
(1324)	(1325)	(1425)	(1435)	(2435)
(1342)	(1352)	(1452)	(1453)	(2453)
(1423)	(1523)	(1524)	(1534)	(2534)
(1432)	(1532)	(1542)	(1543)	(2543)

Type (jklmn) = 24 elements

(12345)	(13245)	(14235)	(15234)
(12354)	(13254)	(14253)	(15243)
(12435)	(13425)	(14325)	(15324)
(12453)	(13452)	(14352)	(15342)
(12534)	(13524)	(14523)	(15423)
(12543)	(13542)	(14532)	(15432)

Type (jk)(lm) = 15 elements

(12)(34)	(13)(24)	(14)(23)	(15)(23)	(23)(45)
(12)(35)	(13)(25)	(14)(25)	(15)(24)	(24)(35)
(12)(45)	(13)(45)	(14)(35)	(15)(34)	(25)(34)

Type (jk)(lmn) = 20 elements

(12)(345)	(13)(245)	(14)(235)	(15)(234)
(12)(354)	(13)(254)	(14)(253)	(15)(243)
	(23)(145)	(24)(135)	(25)(134)
	(23)(154)	(24)(153)	(25)(143)
		(34)(125)	(35)(124)
		(34)(152)	(35)(142)
			(45)(123)
			(45)(132)

TABLE II. Feasible elements of the complete nuclear permutation inversion group of $H_5O_2^+$.

E	E^*
(12)	$(12)^*$
(34)	$(34)^*$
(12)(34)	$(12)(34)^*$
(ab)(1423)	$(ab)(1423)^*$
(ab)(1324)	$(ab)(1324)^*$
(ab)(14)(23)	$(ab)(14)(23)^*$
(ab)(13)(24)	$(ab)(13)(24)^*$

TABLE III. Character table for the double group $G_{16}^{(2)}$ from Merer and Watson (Ref. 31). The letters at the top are the generating operations and are described in the text. The last row corresponds to the reducible representation of the nuclear spin functions.

	e	d	a^2	a^2d	c cd	a^2c a^2cd	b a^2b	bd a^2bd	bc a^2bcd	a^2bc bcd	a a^3 ad a^3d	ac a^3c acd a^3cd	ab a^3b abd a^3bd	abc a^3bc abcd a^3bcd
A_{1g}^+	1	1	1	1	1	1	1	1	1	1	1	1	1	1
A_{2u}^-	1	1	1	1	1	1	-1	-1	-1	-1	1	1	-1	-1
A_{1u}^-	1	1	1	1	-1	-1	1	1	-1	-1	1	-1	1	-1
A_{2g}	1	1	1	1	-1	-1	-1	-1	1	1	1	-1	-1	1
B_{1g}^+	1	1	1	1	1	1	1	1	1	1	-1	-1	-1	-1
B_{2u}^-	1	1	1	1	1	1	-1	-1	-1	-1	-1	-1	1	1
B_{1u}^-	1	1	1	1	-1	-1	1	1	-1	-1	-1	1	-1	1
B_{2g}	1	1	1	1	-1	-1	-1	-1	1	1	-1	1	1	-1
E^+	2	2	-2	-2	2	-2	0	0	0	0	0	0	0	0
E^-	2	2	-2	-2	-2	2	0	0	0	0	0	0	0	0
E_1	2	-2	2	-2	0	0	2	-2	0	0	0	0	0	0
E_2	2	-2	2	-2	0	0	-2	2	0	0	0	0	0	0
E_g	2	-2	-2	2	0	0	0	0	2	-2	0	0	0	0
E_u	2	-2	-2	2	0	0	0	0	-2	2	0	0	0	0
Γ_{ns}	32	32	8	8	32	8	8	8	8	8	4	4	16	16

TABLE IV. Reverse correlation table between the C_2 point group and the $G_{16}^{(2)}$ double group for $H_5O_2^+$. The numbers in parentheses are the nuclear spin statistical weights.

C_2 point group	$G_{16}^{(2)}$ double group
A(52)	$A_{1g}^{+}(2) \oplus A_{1u}^{-}(12) \oplus B_{1g}^{+}(12) \oplus B_{1u}^{-}(2) \oplus E^{+}(6) \oplus E^{-}(6)$
B(36)	$A_{2g}^{-}(0) \oplus A_{2u}^{+}(6) \oplus B_{2g}^{-}(6) \oplus B_{2u}^{+}(0) \oplus E^{+}(6) \oplus E^{-}(6)$

TABLE V. Summary of sign changes in the h_{nv} constants expected in the case of vibrational excitation. For framework 1 of Fig. 8, the C_2 point group operation is equivalent to the (ab)(14)(23) molecular symmetry group operation. Therefore, q_s as defined below is of symmetry species A in the C_2 point group, and q_d is of species B. The zeros in the table below indicate that the sign change cannot be predicted for that framework using the simple treatment taken here.

$$q_s = r_{1a} - r_{2a} - r_{3b} + r_{4b}$$

$$q_d = r_{1a} - r_{2a} + r_{3b} - r_{4b}$$

Framework	2	3	4	5	6	7	8
MW operation	a^2	bc	a^2bc	a	a^3	abc	a^3bc
q_s	$-q_s$	$-q_s$	q_s	q_d	$-q_d$	$-q_d$	q_d
q_d	$-q_d$	q_d	$-q_d$	$-q_s$	q_s	$-q_s$	q_s
Sign change for:							
$v(q_s) = 1$	-1	-1	1	0	0	0	0
$v(q_d) = 1$	-1	1	-1	0	0	0	0

FIGURE CAPTIONS

Fig. 1 Schematic of the tandem mass spectrometer with rf ion trap.

Fig. 2 Low resolution ($\Delta\nu \approx 0.5$ cm^{-1}) infrared spectrum of $H_5O_2^+$ taken using the F-center laser and CO_2 laser. The higher frequency band, centered at 3684.4 cm^{-1}, is a perpendicular band progression and is assigned to the antisymmetric O-H stretch of an H_2O moiety. The lower band, at 3608.8 cm^{-1}, is the symmetric O-H stretch of an H_2O unit. The dashed lines correspond to the frequencies and intensities calculated in Ref. 25 for the C_2 symmetry structure.

Fig. 3 Low resolution infrared spectrum of $H_9O_4^+$ taken with the F-center laser and CO_2 laser. The antisymmetric O-H stretch of an outer H_2O unit is located at 3730.4 cm^{-1} and the symmetric stretch at 3644.9 cm^{-1}.

Fig. 4 Expansion of the antisymmetric O-H stretch of an H_2O moiety in $H_9O_4^+$ revealing a P, Q, R branch structure. The spectrum was taken at 0.5 cm^{-1}

resolution with the F-center laser and CO_2 laser.

Fig. 5 High resolution scan of $H_5O_2^+$ in the region under the $^RQ_0$ sub-band. The resolution, which is Doppler limited, is estimated to be 0.01 cm^{-1}. The spectrum was obtained by mode hopping the F-center laser. The modes are separated by 0.010 cm^{-1}.

Fig. 6 High resolution scan of $H_5O_2^+$ in the region under the $^RQ_1$ sub-band. The feature at 3702.4 cm^{-1} is probably the upper component of the Q branch which has been split by tunneling. The lower component, which was seen in the low resolution scans around 3701.4 cm^{-1}, lies in a region of low F-center laser power at high resolution.

Fig. 7 High resolution scan of $H_9O_4^+$ exciting the antisymmetric stretch of an outer H_2O moiety. The ripples on either side of the central features are separated by 2B. The central features are likely Q-branches which have been split by tunneling motions such as the umbrella inversion mode of the H_3O^+ core.

Fig. 8 $H_5O_2^+$ has eight nonsuperimposable equilibrium frameworks. The perspective is an end on view, sighting down the O-H-O axis. Oxygen a, which is attached to hydrogens 1 and 2, is located above the plane of the paper. Under the framework number, the Merer and Watson generating operations are indicated (see Ref. 31). The permutation-inversion operations which will generate each of the frameworks from framework 1 is also indicated.

Fig. 9 Splitting patterns obtained for K = 0, 1, and 2 assuming $2h_{5v} = 0.55$ cm^{-1}. The numbers in parenthesis are the nuclear spin statistical weights. Inversion of an $H_2O - H^+$ unit is likely to lead to the largest tunneling splitting.

Fig. 10 Splitting patterns obtained for K = 0, 1, and 2 assuming $h_{3v}^t = 0.05$ and $h_{3v}^c = 0.03$ cm^{-1}. This corresponds to torsion along the O-H-O axis. Note that for even K the splitting goes as the sum of h_{3v}^t and h_{3v}^c, whereas for odd K the splitting goes as the difference.

Fig. 11 Splitting patterns obtained for K = 0, 1, and 2 assuming $2h_{7v} = 0.02\ cm^{-1}$. At the level of approximation used in this treatment, the K = 1 state shows no splitting.

Fig. 12 Splitting patterns obtained combining the previous three figures. The constants used were $2h_{5v} = 0.55$, $h_{3v}^{t} = 0.05$, $h_{3v}^{c} = 0.03$, and $2h_{7v} = 0.02\ cm^{-1}$.

Fig. 13 Allowed transitions and spectrum obtained using $2h_{5v} = 0.55\ cm^{-1}$ and $2B = 0.5\ cm^{-1}$. The lower three forks correspond to v = 0 and the upper three forks correspond to $v(q_s) = 1$. The levels and the separation of the forks are not drawn to scale. The separation of the tick marks on the frequency scale is $0.2\ cm^{-1}$.

Fig. 14 Allowed transitions and spectrum obtained using $2h_{5v} = 0.60$, $h_{3v}^{t} = 0.04$, $h_{3v}^{c} = 0.03$, and $2h_{7v} = 0.01\ cm^{-1}$. The lower three forks correspond to v = 0 and the upper three forks to $v(q_s) = 1$. Due to the uncertainty over which transitions involving the E symmetry species levels will dominate the spectrum, the transitions have been drawn in using a dashed line. The levels and

the separation of the splitting patterns are not drawn to scale. The separation of the tick marks on the frequency scale is 0.2 cm^{-1}.

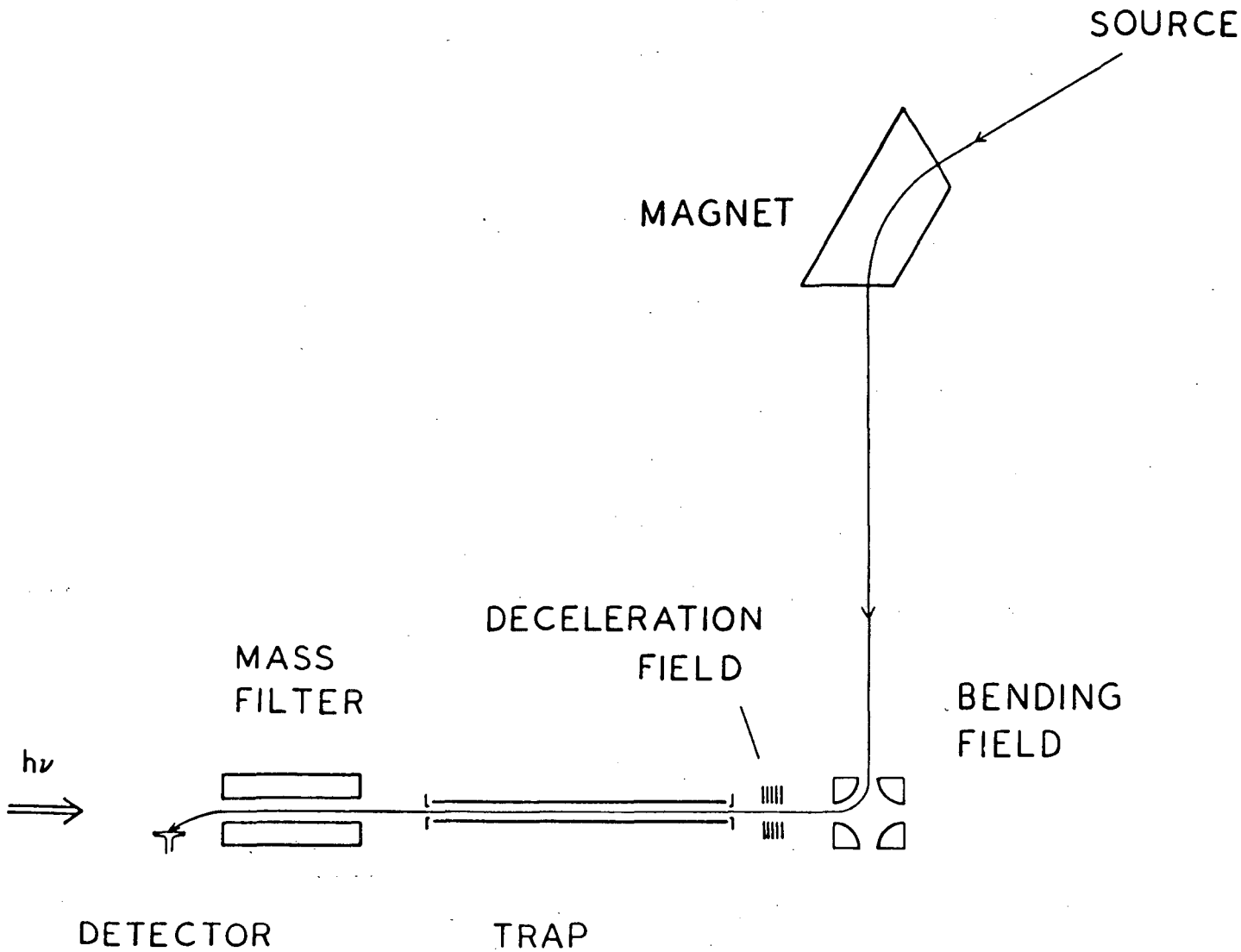

Figure 1

XBL 857-3143

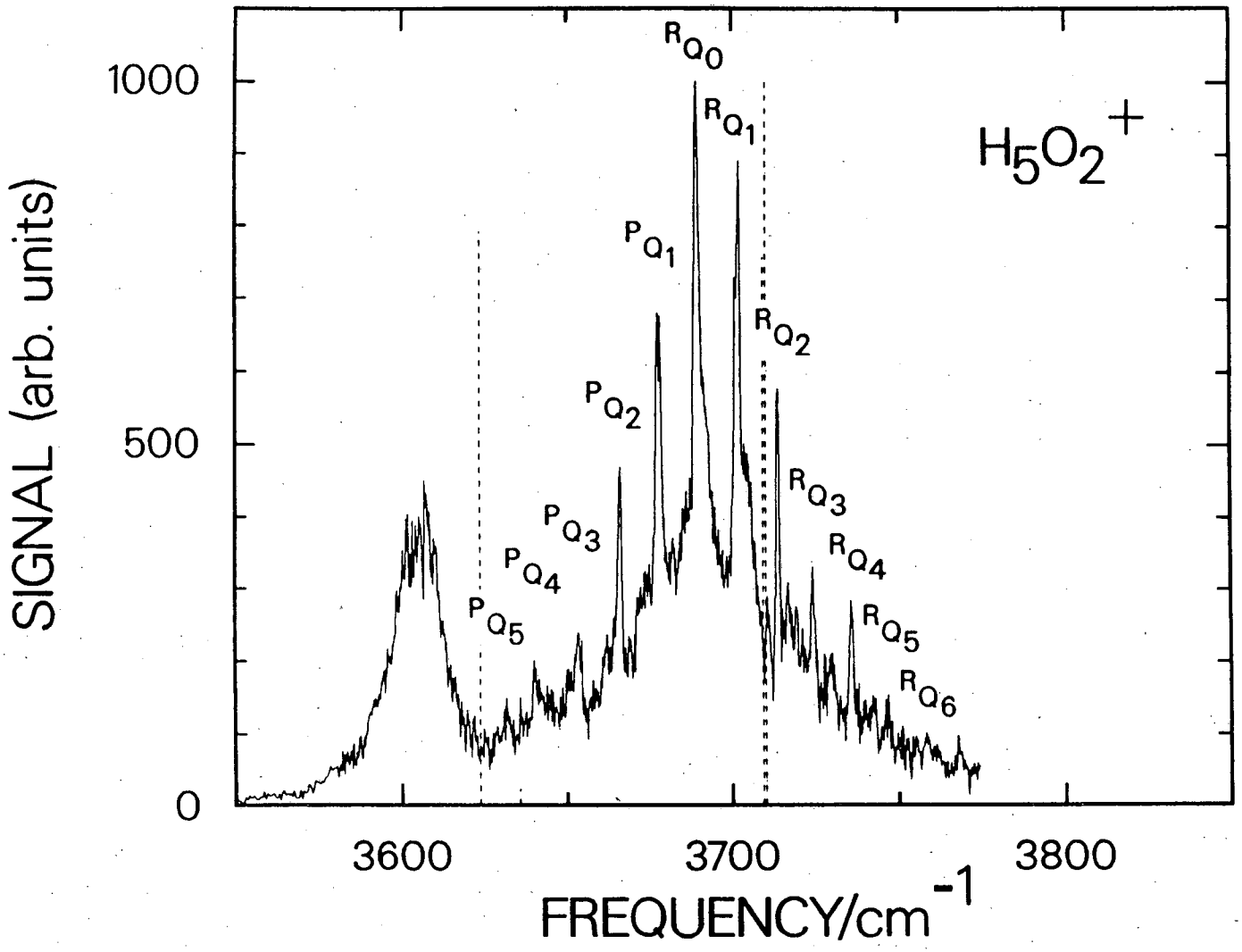

Figure 2

XBL 888-2873 A

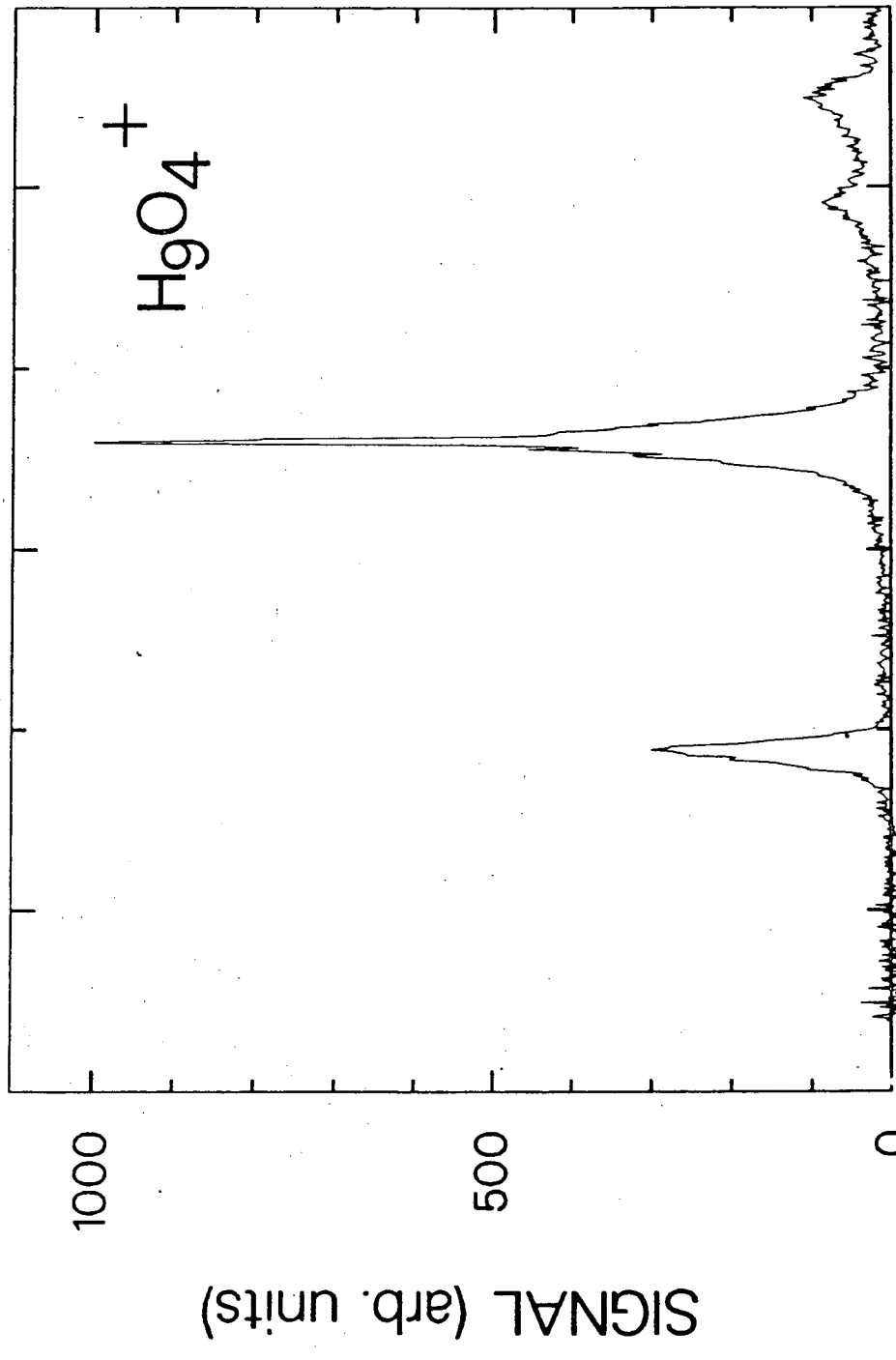

XBL 888-2763

Figure 3

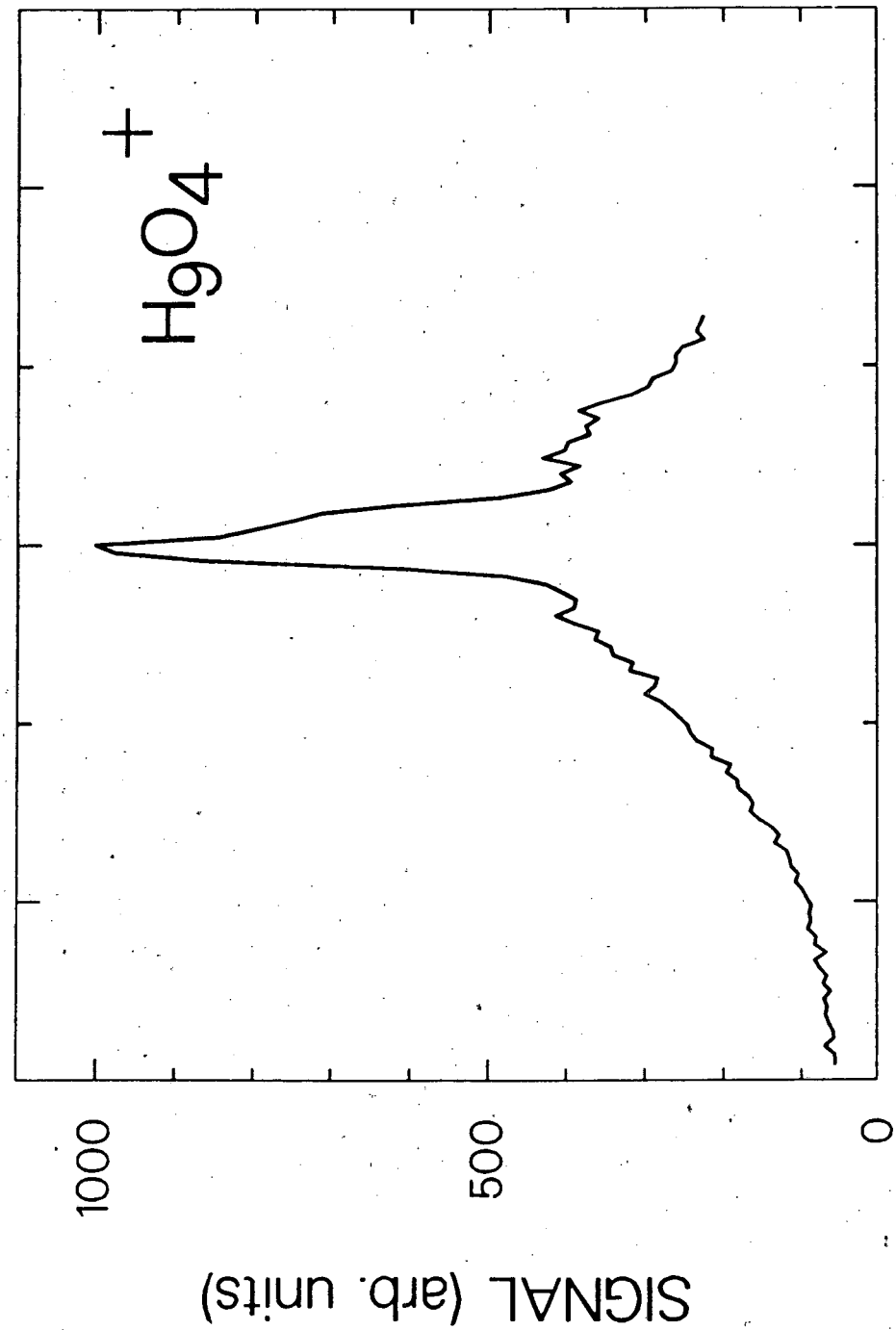

XBL 888-2876

Figure 4

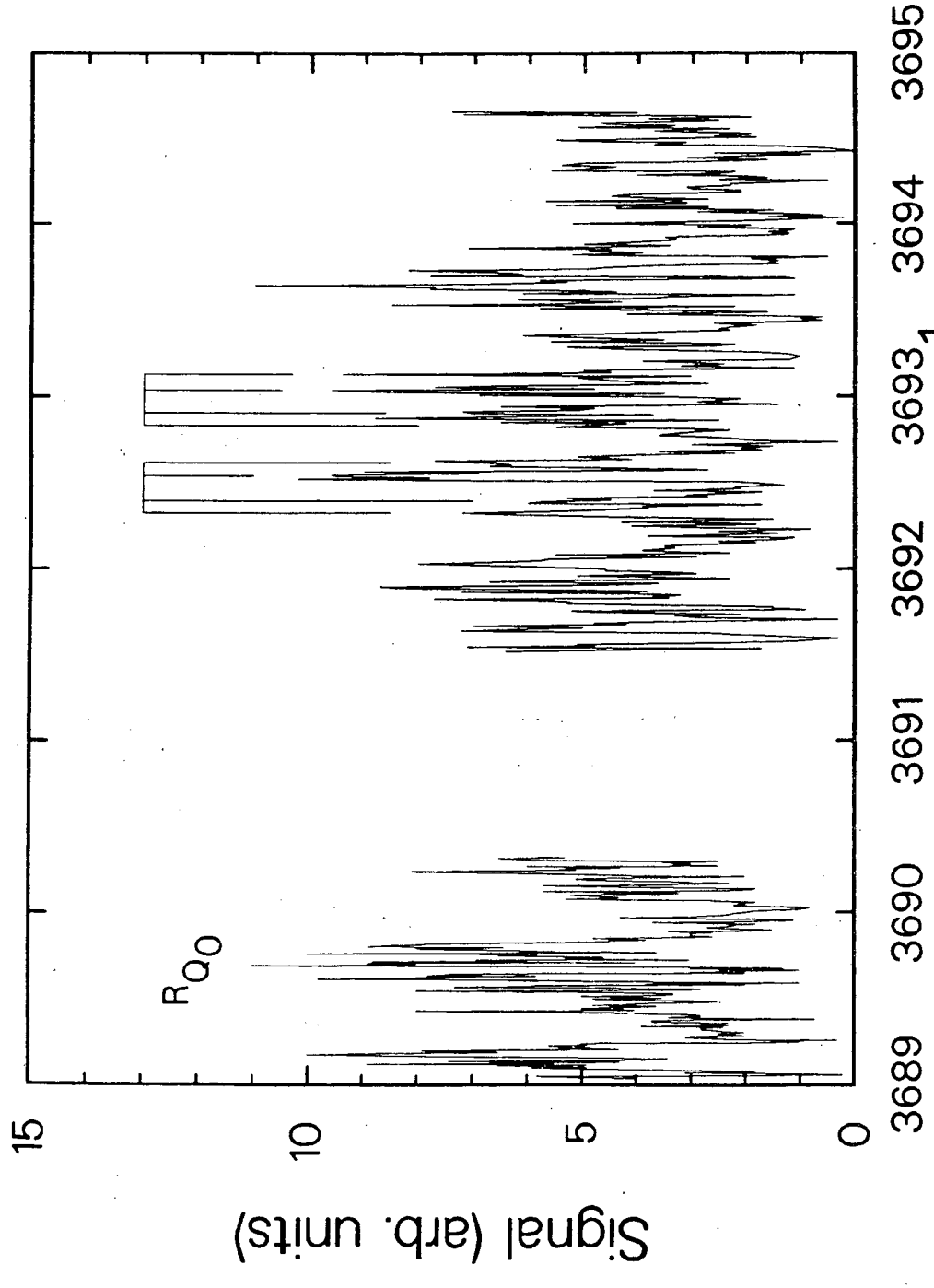

XBL 8811-3924

Figure 5

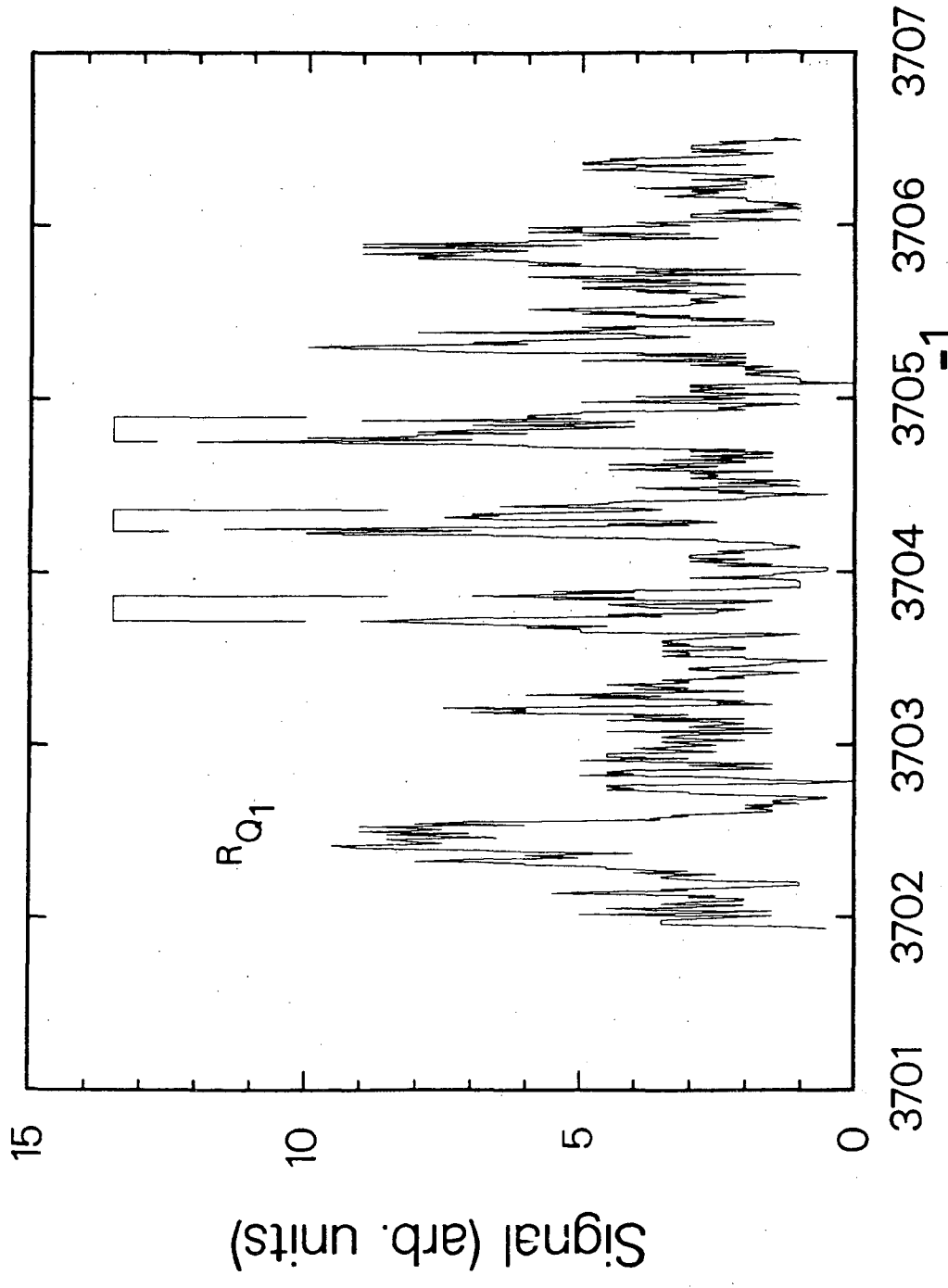

XBL 8811-3925

Figure 6

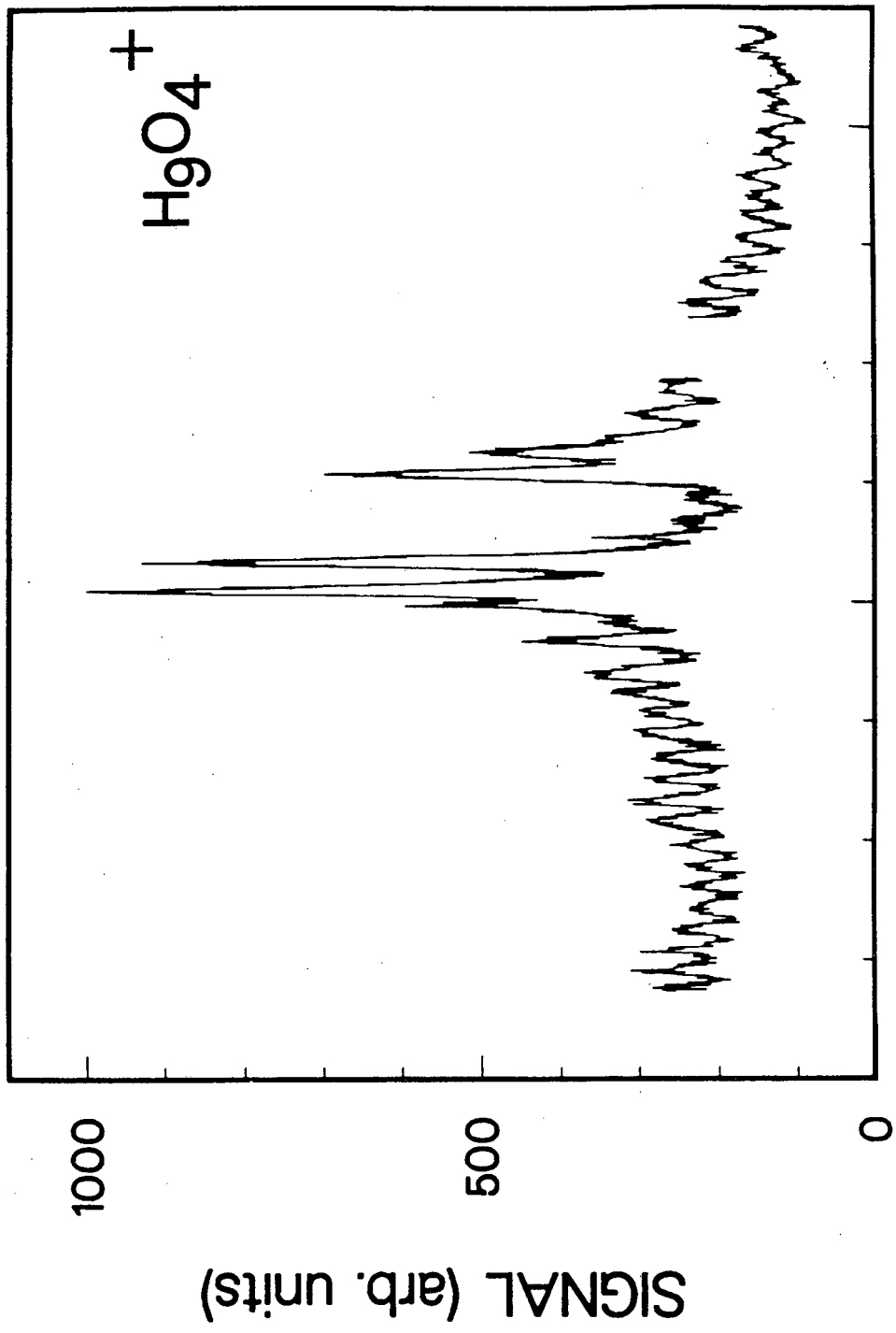

XBL 8811-3918

Figure 7

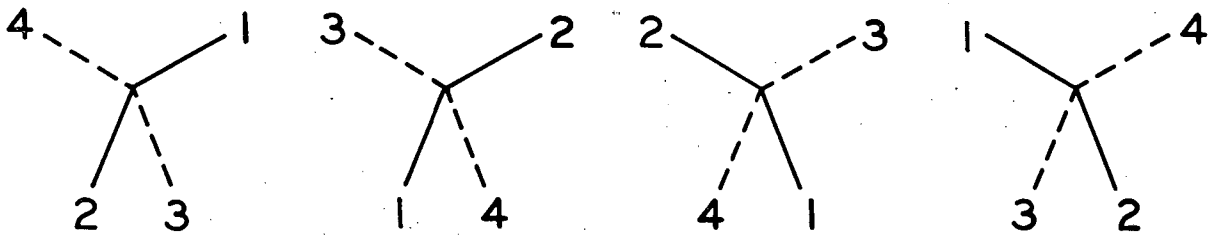

FRAMEWORK	1	2	3	4
MW operation	e	a^2	bc	a^2bc
PI operation	E	(12)(34)	(ab)(13)(24)*	(ab)(14)(23)*

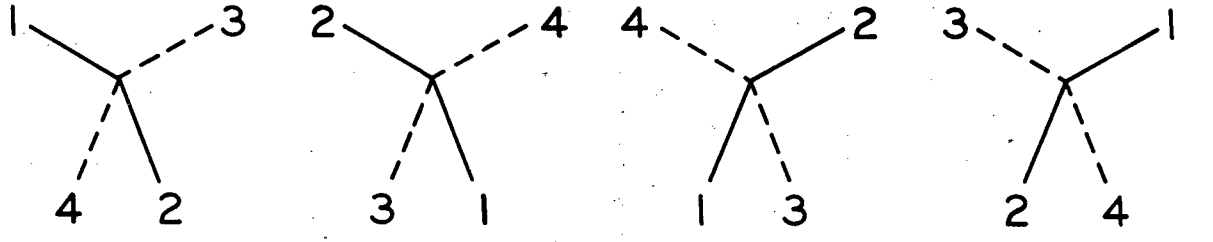

FRAMEWORK	5	6	7	8
MW operation	a	a^3	abc	a^3bc
PI operation	(ab)(1324)*	(ab)(1423)*	(12)	(34)

XBL 8811-3919

Figure 8

$2h_{5v} = 0.55\ cm^{-1}$

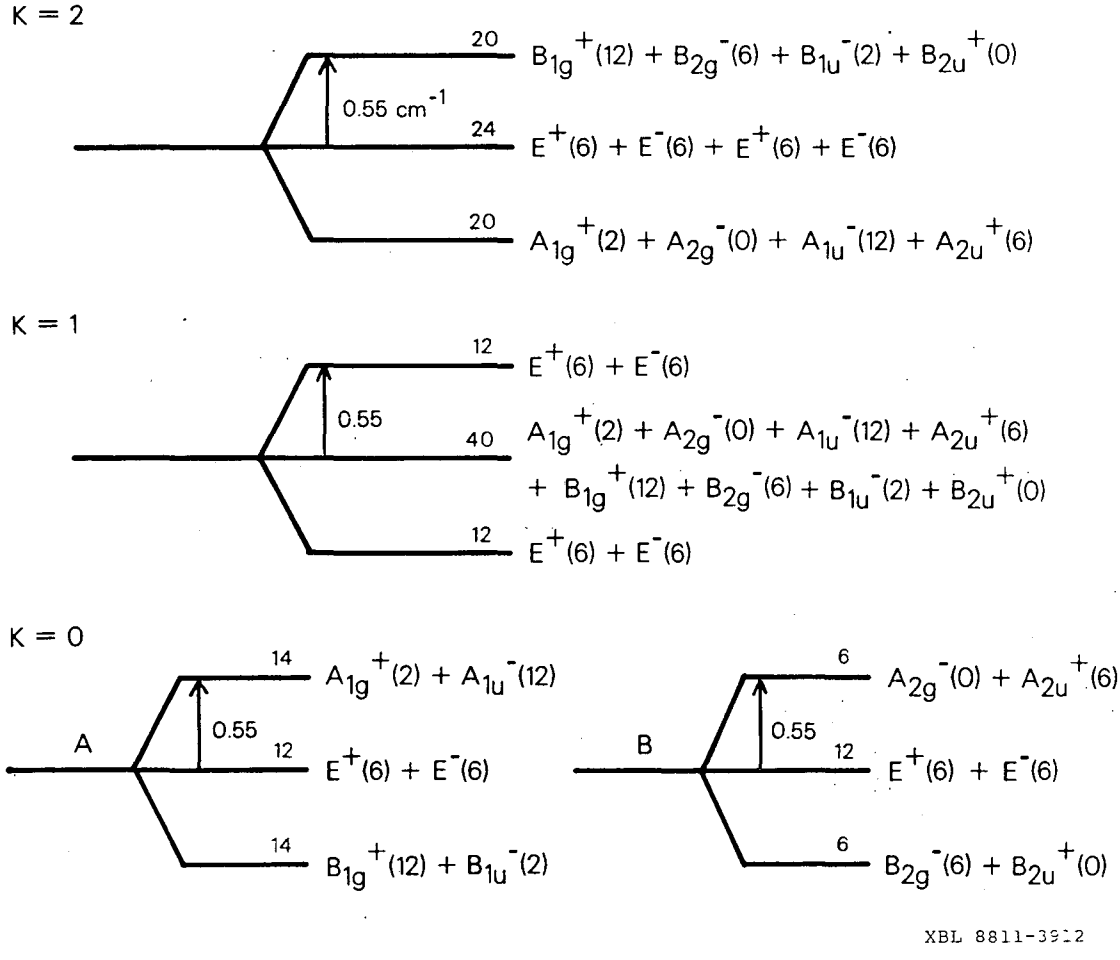

Figure 9

$$h_{3v}{}^{t} = 0.05\ cm^{-1}$$
$$h_{3v}{}^{c} = 0.03\ cm^{-1}$$

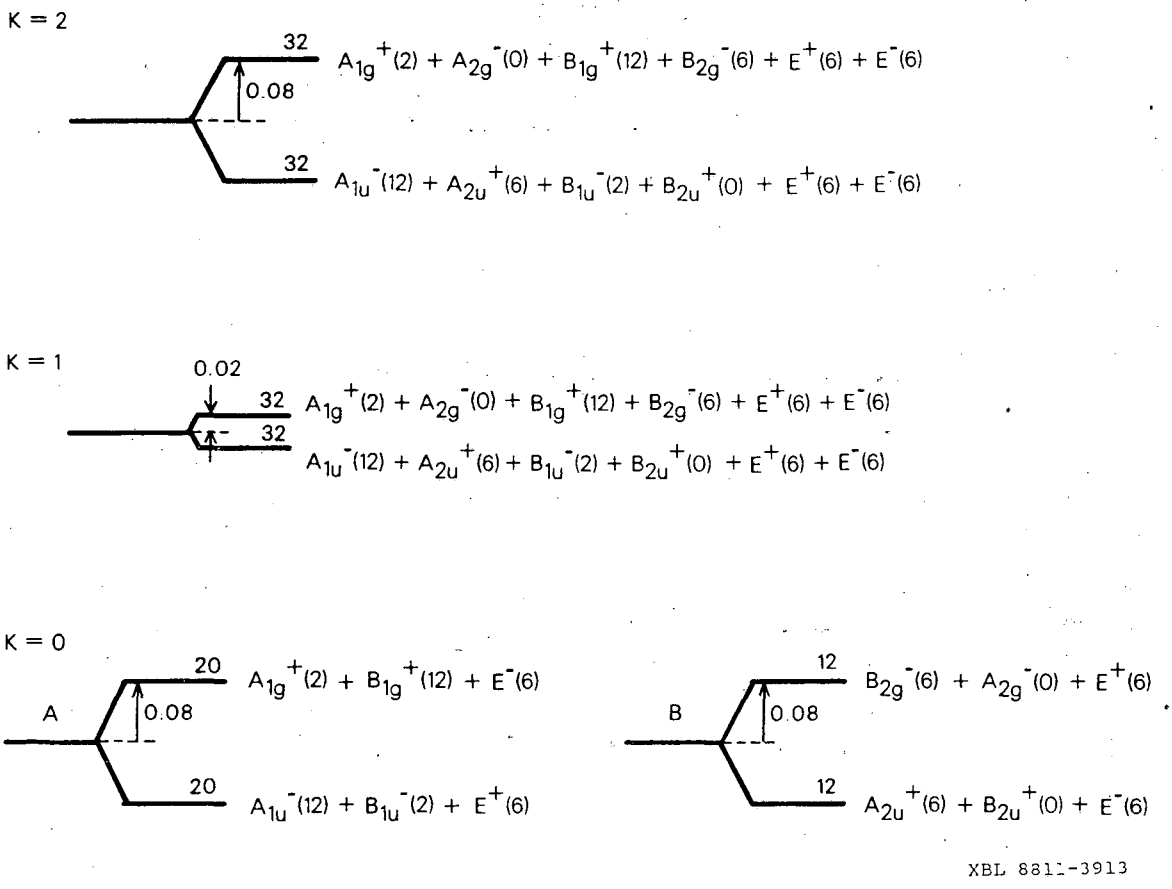

Figure 10

$2h_{7v} = 0.02\ cm^{-1}$

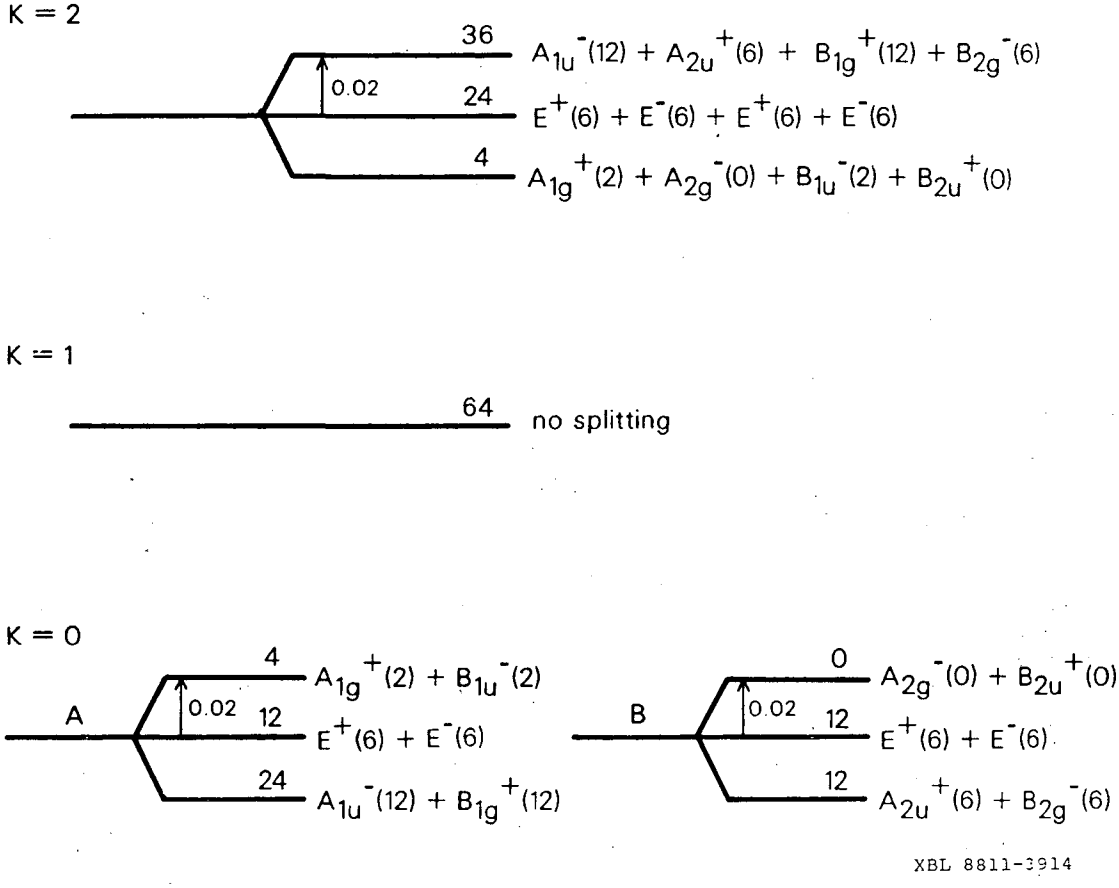

Figure 11

$2h_{5v} = 0.55\ cm^{-1}$

$h_{3v}^{t} = 0.05\ cm^{-1}$ $\quad h_{3v}^{c} = 0.03\ cm^{-1}$

$2h_{7v} = 0.02\ cm^{-1}$

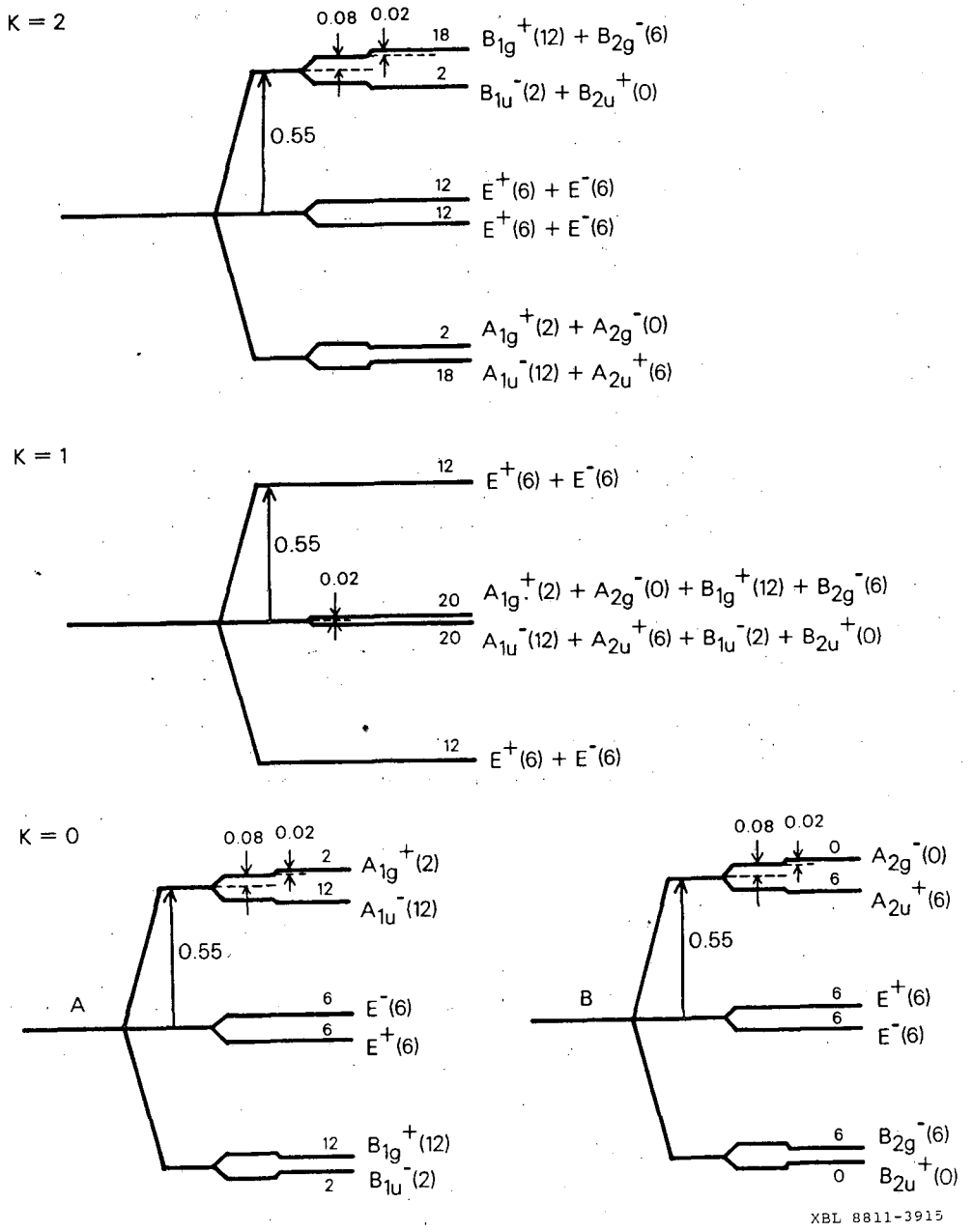

Figure 12

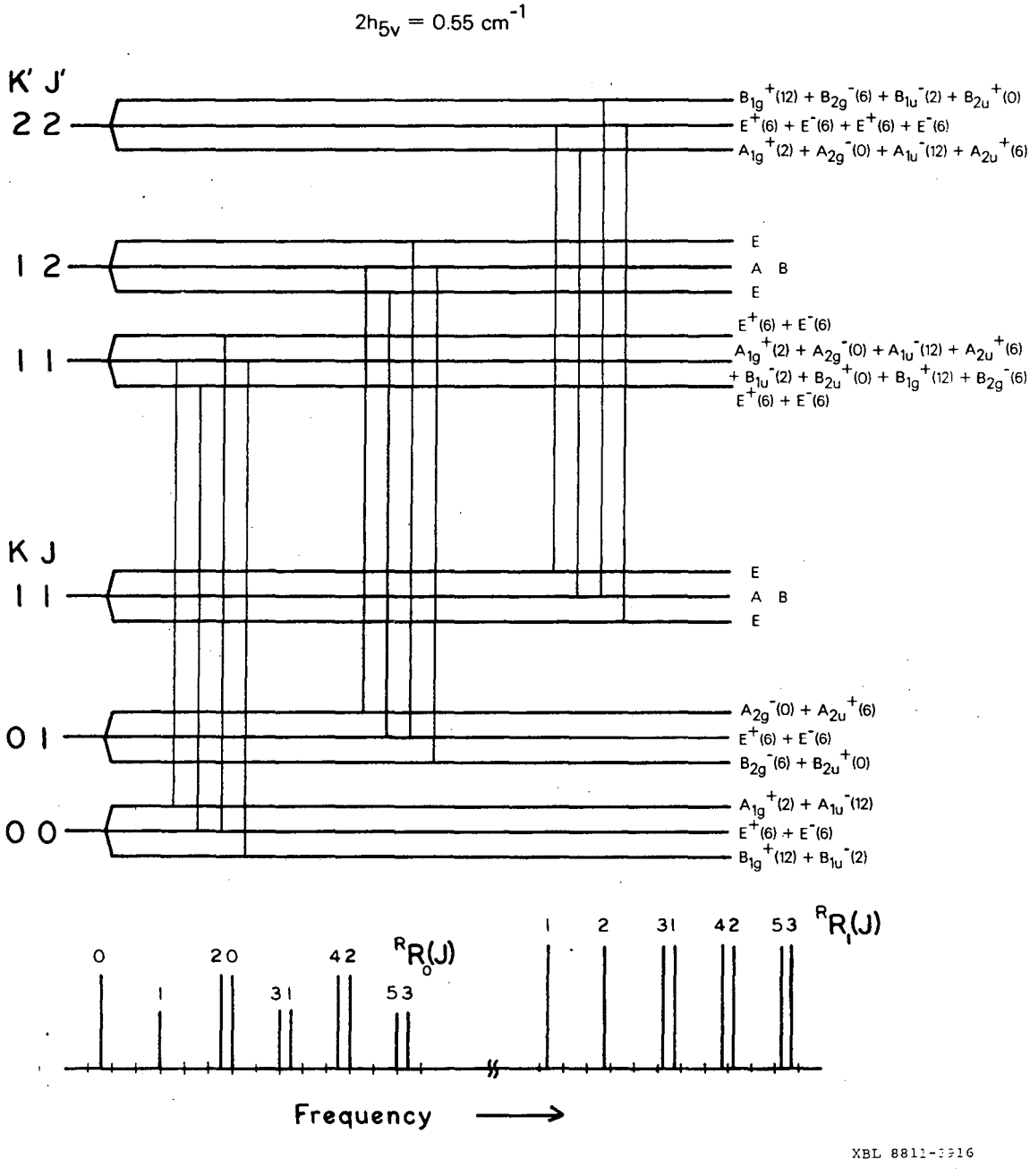
$2h_{5v} = 0.55\ cm^{-1}$
K' J'
2 2
1 2
1 1
K J
1 1
0 1
0 0
$B_{1g}^{+}(12) + B_{2g}^{-}(6) + B_{1u}^{-}(2) + B_{2u}^{+}(0)$
$E^{+}(6) + E^{-}(6) + E^{+}(6) + E^{-}(6)$
$A_{1g}^{+}(2) + A_{2g}^{-}(0) + A_{1u}^{-}(12) + A_{2u}^{+}(6)$
E
A B
E
$E^{+}(6) + E^{-}(6)$
$A_{1g}^{+}(2) + A_{2g}^{-}(0) + A_{1u}^{-}(12) + A_{2u}^{+}(6)$
$+ B_{1u}^{-}(2) + B_{2u}^{+}(0) + B_{1g}^{+}(12) + B_{2g}^{-}(6)$
$E^{+}(6) + E^{-}(6)$
E
A B
E
$A_{2g}^{-}(0) + A_{2u}^{+}(6)$
$E^{+}(6) + E^{-}(6)$
$B_{2g}^{-}(6) + B_{2u}^{+}(0)$
$A_{1g}^{+}(2) + A_{1u}^{-}(12)$
$E^{+}(6) + E^{-}(6)$
$B_{1g}^{+}(12) + B_{1u}^{-}(2)$
0
1
20
31
42
53
$^{R}R_{0}(J)$
1
2
31
42
53
$^{R}R_{1}(J)$
Frequency
XBL 8811-9916

Figure 13

$2h_{5v} = 0.60,$

$h_{3v}{}^{t} = 0.04,\ h_{3v}{}^{c} = 0.03,$

$2h_{7v} = 0.01\ cm^{-1}$

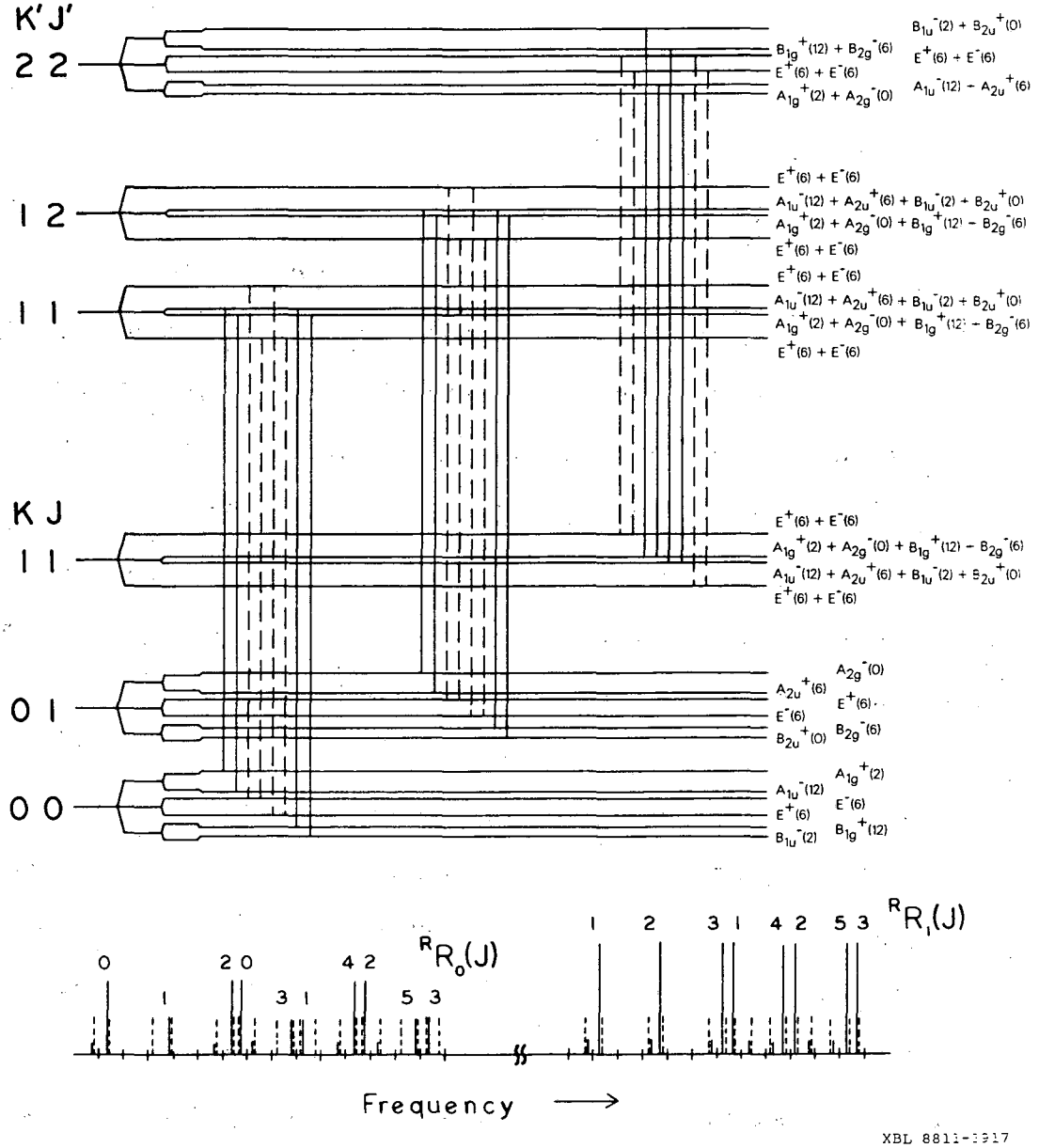

Figure 14

Chapter IV

Infrared Spectroscopy of the Pentacoordinated Carbonium Ion $C_2H_7^+$

I. Introduction

Gas-phase ion spectroscopy, though still a relatively young field, can now be used to probe molecular ions of increasing complexity by making use of improved technology and novel approaches. One of these new methods, recently developed in our laboratory,[1] uses a two color laser scheme. The first laser is a tunable infrared laser that is used to probe the vibrations of the molecular ion of interest. The second laser is a CO_2 laser that is used to dissociate the vibrationally excited parent ion. We utilize the very high detection sensitivity of ions by monitoring formation of fragment ions as a function of the frequency of the tunable laser in order to obtain the infrared spectrum. This technique has allowed us to study the pentacoordinated carbonium ion $C_2H_7^+$. A great deal of effort has been expended to study electron deficient carbonium ions. The early work focused on elucidating the structure of these reactive carbonium ions. Other work concentrated on their kinetics, energetics, and thermochemistry. More recently, much has been learned about the

spectroscopy of the simpler of these carbonium ions. Following is a brief history of this work.

A. History

In the early work, a need arose to explain rearrangement of carbonium ions, such as norbornyl cation in solution. Hydrogen migration to form a σ-bonded intermediate was proposed. This intermediate, which contains a 2-electron 3-center bond, was given the name "nonclassical" ion. A pioneer is these studies was S. Winstein. In 1952, he reported a solvolysis study of endo- and exo-norbornyl arylsulfonates.[2,3] Acetolysis yields the exo-norbornyl acetate, independent of whether the starting diastereomer was of the endo- or exo- configuration as shown in Fig. 1a. In a complementary experiment, solvolysis of optically active exo-norbornyl p-bromobenzenesulfonate gave a racemic product mixture which was shown by the loss of optical activity (Fig. 1b).[3] A third observation was the enhanced rate of reaction of the exo-isomer over the endo-isomer.[3] All of these anomalies could be explained by a bridged structure for the norbornyl cation containing a pentavalent carbon. Bridged structures such as this, that have delocalized bonding σ-electrons, are now known as nonclassical ions.[4]

This concept of nonclassical ions was generally accepted when applied to the norbornyl and many other

systems until 1962, when H. C. Brown strongly objected.[4,5] He claimed that scientific scrutiny had been bypassed in the general labeling of many ions as nonclassical. Other theories could also explain the anomalous behavior, so the nonclassical interpretation did not need to hold for every case. Strong supporting evidence should be found for each system before a nonclassical carbonium ion structure could be definitively concluded.

Brown proposed alternative explanations for the controversial experimental observations.[5] One possibility was that two interchanging asymmetric classical structures go through a nonclassical structure momentarily. This indeed seemed to be possible for a number of systems where an asymmetric product is obtained from an isotopically tagged reactant with negligible scrambling of the tag.[6] This test is only suggestive, not conclusive, and will only be informative when the equilibration of the two distinctly tagged structures is not more rapid than the identification process chosen. Another possibility was that the bridged form was a transition state with a very low barrier allowing facile rearrangement.[5] Brown also believed a clarification needed to be made between σ-bridging and hyperconjugation. G. Olah has also emphasized this point.[7] In both σ-bridging and hyperconjugation a σ-bond orbital and p orbital overlap to allow electron delocalization involving that σ bond. When there

is little or no rearrangement of the nuclei, this is called hyperconjugation. When there is extensive nuclear reorganization, this is called bridging.[7]

In 1975, G. Olah[7] proclaimed that he had proven the existence of the nonclassical norbornyl cation using NMR techniques and settled the question once and for all.

> "Study of the long-lived norbornyl cation has resulted in indisputable proof for the σ-bridged, nonclassical structure... Nonclassical carbonium ions containing two-electron, three-center bonded carbocation centers are now firmly proven to exist...The 'classical-nonclassical ion controversy' is brought to conclusion not only by overwhelming chemical and structural evidence, but also by consideration of our present day understanding of chemical bonding and charge delocalization. Simply, there is no such thing as a completely 'classical' type of carbocation. Charge is always delocalized to a significant degree whenever an electron-deficient center is formed in a molecule. Whether this happens through π-, n-, or σ-electron-pair interactions and to what a degree is dependent of the specific system, but not of principle. The norbornyl cation is only one of the many carbocations showing C-C σ-bond delocalization, and will be remembered in years to come as an interesting but by no means unique member of a substantial class of compounds."[7]

Thus it has been shown that nonclassical structures do exist. The question then becomes which carbonium ions have this nonclassical structure? Candidates include the pentacoordinated carbonium ion protonated ethane, and non-saturated alkanes such as protonated acetylene and protonated ethylene. The rest of this history will concentrate on these three systems. Classical and bridged structures for these three carbonium ions are shown schematically in Fig. 2.

$C_2H_7^+$ was seen in the 1960's with a discharge of methane and/or ethane in mass spectrometric studies.[8-11] It appears that in methane, $C_2H_7^+$ was formed through a second order process and needed to undergo collisional stabilization to survive. It was clear that $C_2H_7^+$ easily dissociated to give $C_2H_5^+ + H_2$ products. Olah et al.[12] observed pentacoordinated carbon cations in acid solution using NMR. This pointed out the importance of carbonium ions in solution chemistry. Blair et al.[13] observed $C_2H_7^+$ in an ion trap using a continuous electron beam to trap the ions through negative space charge. The quantity of $C_2H_7^+$ increased with trapping time.

In the early 1970's, Lathan, Hehre, and Pople[14] calculated the relative energies of bridged and classical forms of $C_2H_3^+$, $C_2H_5^+$, and $C_2H_7^+$. In his earliest paper, Pople used Molecular Orbital-Self Consistent Field (MO-SCF) theory with small (STO-3G, 4-31G) basis sets and calculated that the classical structure of $C_2H_3^+$ was more stable by far compared to the bridged conformer. The classical form of $C_2H_5^+$ was also more stable than the bridged form (by 7 kcal/mole). However, calculations on $C_2H_7^+$ showed the bridged structure to be more stable by almost 10 kcal/mole. In a second paper, Hariharan, Lathan, and Pople[15] found a preferential stabilizing effect of polarization functions on the bridged form over the classical. For $C_2H_3^+$, the classical structure was

still found to be more stable, but by only 5.7 kcal/mole. In the case of $C_2H_5^+$, however, the bridged structure became the more stable conformer by ~1 kcal/mole when d-functions were included on C and p-functions on H.

Meanwhile, Chong and Franklin[16] caused a stir when they claimed that $C_2H_7^+$ was less stable than $C_2H_5^+ + H_2$ and invoked an activation barrier to explain observation of $C_2H_7^+$. This led to a paper by Bohme et al.[17] in disagreement contending that $C_2H_7^+$ was more stable than $C_2H_5^+ + H_2$. They used CO and C_2H_4 to bracket the proton affinity of ethane between 136 and 159 kcal/mole.

By this time, the controversy over whether $C_2H_3^+$, $C_2H_5^+$, and $C_2H_7^+$ have classical or nonclassical forms had generated a large amount of theoretical interest. Zurawski, Alrichs, and Kutzelnigg[18] produced a landmark paper when the effects of electron correlation were studied using the independent-electron-pair approximation based on the direct calculations of pair-natural orbitals (IEPA PNO). Polarization functions were again found to be very important to stabilize the bridged structure, and electron correlation further preferentially stabilized the nonclassical form by an equally substantial amount. They found the bridged structure to be more stable than the classical for both $C_2H_3^+$ and $C_2H_5^+$ (by 7 and 9 kcal/mole, respectively). The IEPA method was also used to calculate the relative energies of the C_s and C_{2v} geometries in CH_5^+

by Dyczmons and Kutzelnigg.[19] Whereas at the SCF level the C_s structure was more stable, including electron correlation energy led to equal stabilities of the two. Semi-empirical methods were used in 1975 by Bischof and Dewar[20] to calculate the relative stabilities of $C_2H_7^+$. They found the classical form more stable by 15 kcal/mole. This is clearly at odds with ab initio calculations. Nevertheless, Bischof and Dewar came out in strong defense of the MINDO/3 method. This led to work by Kohler and Lischka[21] comparing SCF, Coupled Electron Pair Approximation (CEPA) PNO, and MINDO/3 calculations on the $C_2H_7^+$ ion. At the SCF and CEPA PNO levels, the bridged structures were more stable by 8.5 and 6.3 kcal/mole, respectively. However, at the MINDO/3 level, the classical $C_2H_7^+$ structure was more stable than the bridged form by 11 kcal/mole. This shows the inadequacy of the MINDO/3 method in calculating relative energies for protonated ethane. The fact that their calculations at the SCF and CEPA levels with their larger basis set found the MINDO/3 classical geometry with a CHH three-center bond to be lower in energy than the ab initio STO-3G structure with a loose intermolecular complex between H_2 and $C_2H_5^+$ casts doubt on their results. The fact that their SCF calculations led to a larger relative stability of the bridged structure than at the CEPA PNO level also is surprising in light of previous trends. These results illustrate the

extreme sensitivity of the calculations to the geometries used.

Very influential experiments from Kebarle's lab came out in 1975-1976.[22-25] French and Kebarle[22] studied the pyrolysis of $C_2H_7^+$ and found an activation energy of 10.5 kcal/mole for dissociation into $C_2H_5^+ + H_2$. They concluded that $PA(C_2H_6)$ was greater than $PA(CH_4)$ by more than 10 kcal/mole. Assuming the activation energy for the reaction equals the enthalpy change, they found $\Delta H_f(C_2H_7^+)$ = 208.5 ± 2 kcal/mole and $PA(C_2H_6)$ = 137.4 ± 2 kcal/mole. This was confirmed by experiments done by Hiraoka and Kebarle[25] in which they claimed to observe both the classical and nonclassical forms as a function of temperature. At the lowest temperature range they found the reaction of $C_2H_5^+ + H_2 \rightarrow C_2H_7^+$ had an inverse temperature relationship implying it was exothermic. At higher temperatures, the temperature dependence became positive suggesting an endothermic relationship. Analyzing these temperature dependences led to the conclusions shown in Fig. 3. The bridged structure is more stable than the classical by 7.8 kcal/mole. This leads to ΔH_f(bridged $C_2H_7^+$) = 207.2 kcal/mole, ΔH_f(classical $C_2H_7^+$) = 215.0 kcal/mole, and $PA(C_2H_6$ -> bridged $C_2H_7^+)$ = 139.6 kcal/mole, $PA(C_2H_6$ -> classical $C_2H_7^+)$ = 131.8 kcal/mole. These values are summarized in Table I.

An experimental study by Houle and Beauchamp[26] of the difference between the adiabatic and vertical ionization potentials of ethyl radical led to an estimated 3 kcal/mole difference between the bridged and classical structures of $C_2H_5^+$ with the bridged being lower. Their assumption was that a vertical ionization of ethyl radical would lead to the classical structure of ethyl cation whereas the adiabatic ionization would end with the lower energy bridged structure which necessitates a large geometry change. Houle and Beauchamp obtained a heat of formation for $C_2H_5^+$ of 219.2 ± 1.1 kcal/mole. This is in some disagreement with the value of 215.3 ± 1.0 kcal/mole found by Baer,[27] who did a photoionization and photoion-photoelectron coincidence (PIPECO) study of $C_2H_5^+$ formation. It is conceivable that the very large geometry change between the ethyl radical and the bridged ethyl cation makes it impossible to obtain a true adiabatic ionization potential experimentally. Gellene, Kleinrock, and Porter[28] took the reverse approach in that they started with the ethyl cation and neutralized it using various metals. They claimed that 87-90% of their $C_2H_5^+$ beam was the bridged structure. From this they put a lower bound on the difference in energy between the bridged and classical structures as 0.8 kcal/mole. Mackay, Schiff, and Bohme[29] studied the energetics and kinetics of the protonation of ethane. They obtained

$\Delta H_f(C_2H_7^+)$ = 204.8 ± 1.3 kcal/mole and $PA(C_2H_6)$ = 142.1 ± 1.2 kcal/mole, which presumably corresponds to the bridged form.

More recent theoretical calculations have generally concluded that the bridged structure is more stable than the classical for all three of the carbonium ions: $C_2H_3^+$, $C_2H_5^+$, and $C_2H_7^+$. The energies for the two structures are closest for $C_2H_3^+$. Weber and McLean,[30-31] using configuration interaction (SDCI) and a double zeta plus polarization (DZ+P) basis set, found bridged and classical $C_2H_3^+$ structures to have energies within 1-2 kcal/mole, with the bridged form probably lower. Kohler and Lischka[32] included electron correlation using CEPA and found the bridged structure of protonated acetylene lower by 3.5-4.0 kcal/mole. Raghavachari, Whiteside, Pople, and Schleyer[33] found the bridged form lower by ~3.0 kcal/mole, and more recent calculations by Hirao and Yamabe[34] found the bridged structure of $C_2H_3^+$ to be lower by 1.30 kcal/mole using the symmetry-adapted-cluster method with zero point energy correction (SAC + ZPE). These values are in close agreement with the most recent calculations by Lee and Schaefer[35] who found an energy difference of 0.97 kcal/mole using CISDT (DZ + P). Calculations on $C_2H_5^+$ found larger energy differences. Lischka and Kohler[36] found the bridged structure lower by 7.3 kcal/mole using the ab initio CEPA method and 8.0 kcal/mole using semi-

empirical MINDO/3. Raghavachari et al.[33] found the classical structure was not a minimum on the potential surface at the best level of theory considered (MP4(SDQ) with a reoptimization of the geometries at the MP2 level). Using the geometries optimized at the HF level and MP4(SDQ), the bridged structure was lower than the classical by 5.2 kcal/mole. Hirao and Yamabe[34] found an energy difference of 4.11 kcal/mole. Following this trend, the bridged structure of $C_2H_7^+$ was also found to be significantly more stable than the classical structure. Raghavachari et al.[33] found an energy difference of 6.8 kcal/mole, while Hirao and Yamabe[34] found the bridged form lower by 4.0 kcal/mole. These results are also summarized in Table I.

In the last few years, calculations of vibrational frequencies have been done. Raine and Schaefer[37] calculated vibrational frequencies, intensities, and geometries using SCF with a DZ + P basis set of both the classical and nonclassical forms of $C_2H_3^+$. This was followed by a calculation by Lee and Schaefer[35] at a higher level of theory that gave similar frequency results. The motivation for repeating this calculation was to aid in the assignment of the spectrum experimentally observed by Crofton and Oka.[38] This infrared spectrum is now assigned as essentially that of the bridged structure, possibly with some complications associated with tunneling between

the nonclassical and classical forms. DeFrees and McLean[39] also completed vibrational frequency calculations of protonated acetylene. In addition, they calculated frequencies for nonclassical $C_2H_5^+$ and CH_5^+. In 1987, Komornicki and Dixon[40] calculated frequencies, intensities, and structures for CH_5^+. M. Dupuis[41] has probably done the highest level calculation on CH_5^+ to date. At our request, Dupuis has also calculated frequencies and intensities for classical and bridged protonated ethane. The frequencies, intensities, and assignments will be discussed later.

Finally, this brief history would not be complete without mentioning the astounding work of Kanter, Vager, Both, and Zajfman.[42] They succeeded in experimentally determining the structure of $C_2H_3^+$ through a Coulomb explosion of the $C_2H_3^+$ ion caused by the sudden loss of several electrons. The arrival times of the three protons and two carbon ions are detected both with X-Y spatial resolution and temporal resolution and analyzed to give average geometries. They find the nonclassical structure dominates their sample of $C_2H_3^+$.

Thus, it seems certain that the lower energy structure after protonating acetylene, ethylene, and ethane is the nonclassical bridged form. Our work concentrated on the spectroscopy of protonated ethane. After a descrip-

tion of the experimental setup and spectra obtained, arguments will be presented to convince the reader that spectra have been obtained for both the bridged and classical structures. Table II lists bond lengths and angles for both forms of $C_2H_7^+$ as calculated by Hirao and Yamabe and by Dupuis.

II. Experimental Details

The apparatus used is basically the same as described in previous chapters.[43] A schematic of the machine is given in Fig. 4. Briefly, the ions are formed in a corona discharge and then mass-selected in a sector magnet. The ion under study is trapped in an octopole radio-frequency ion trap for 1 msec during which time they are interrogated by a tunable IR laser. The laser scheme is such that the parent ion will dissociate into fragments when tuned to a resonant transition. One of those fragment ions is selected by a quadrupole mass filter and is counted by a Daly detection system.[44] Details of the source conditions and laser system now follow.

This experiment is unusual in that the ratio of H_2:C_2H_6 was systematically varied. Early on, it was seen that the spectrum was strongly dependent on the mixing ratio and backing pressure. The four cylinder conditions used were:

1. 55,000:1 $H_2:C_2H_6$
2. 8,700:1 $H_2:C_2H_6$
3. 42,500:1 $H_2:C_2H_6$
4. 49,000:1 $H_2:C_2H_6$

These will hereafter be referred to as cylinder 1-4. In addition, the pressure behind the nozzle was set at one of three values: 60 torr, 90 torr, and 150 torr. The gases used were Matheson ultra-high purity hydrogen (99.999%) and pure ethane from Spectra Gases (99.99%). In spite of this high purity, we found it helpful to remove residual water by flowing the gas through a molecular sieve trap (Linde 13X molecular sieve, 10 Å pore diameter) cooled in a dry ice/acetone bath before allowing the gas to enter the source.

A schematic of the corona discharge ion source is shown in Fig. 5. The discharge is struck between the nickel-plated iron needle and the copper walls of the source. The distance between the needle and the source body was 0.069 $\pm$ .003 in. The source body was composed primarily of copper for more efficient cooling from a refrigerant which was introduced from outside the machine and used to cool a copper block that was clamped around the base of the source. For this experiment, Freon-22 was used to cool the source to -28°C. This was necessary to freeze out impurity water contained in the gas inlet line. At the highest pressure, contamination was more of a

problem and the source had to be warmed up after running for only a few hours to allow the condensed water to be pumped off from the surfaces.

After the discharge is a small high pressure drift region which allows the ions to cool vibrationally through multiple collisions. A supersonic expansion through a 75μm nozzle cools the rotational temperature to $\leq$40K. About 7.5 mm downstream from the nozzle is a skimmer which separates the first and second regions of differential pumping. Typical pressures before and after the skimmer are 1.1×10^{-4} torr and 8.4×10^{-6} torr when run with a backing pressure of 90 torr. The voltage bias of the nozzle and skimmer were kept within 1.0 V of each other to minimize collisional heating by accelerating ions.

In the lower pressure region after the skimmer, the ions are gradually accelerated to a kinetic energy of 350 eV which they maintain (through the sector magnet) until directly before the ion trap. In order to keep the machine at ground potential, the ion source and associated optics and the ion trap are floated at +350 V. A stack of 12 plates evenly spaced decelerate the ions before entering the octopole trap.[45] In the trap, their kinetic energy is less than 0.5 eV. The octopole trap consists of eight molybdenum rods 50 cm long, 0.32 cm diameter, evenly spaced on a 1.25 cm diameter circle. Alternate rods have, at any moment, opposite phases of rf applied with typi-

cally 300 V peak-to-peak and a frequency of 7.4 MHz. During the 1 msec in which the ions are trapped, they are probed using infrared lasers.

Generally, two lasers are used. The first is a tunable Quanta-Ray Infrared Wavelength EXtender system (IR-WEX) which is scanned from 2490-4150 cm^{-1}. The infrared wavelength is generated in a lithium niobate crystal which takes the difference of a Quanta-Ray pulsed dye laser (PDL) output and Nd:YAG fundamental. Scanning is achieved by a computer controlled motor system which steps the drive for the dye laser grating. In the high resolution scans, an etalon was placed in the Nd:YAG cavity which reduced the IR linewidth from 1.2 cm^{-1} to 0.3 cm^{-1}. Pulse duration was 10 nsec with typically 0.5 mJ/pulse at 2800 cm^{-1} and 1 mJ/pulse at 3940 cm^{-1}.

The WEX output was combined with a cw MPB CO_2 laser using a custom designed beam combiner on a ZnSe substrate (CVI Laser Corporation). The CO_2 laser was run on the R(10) line of the $00^{o}1$-$10^{o}0$ band with 6-8 W at the output of the laser and with 3-4 W passing completely through the machine. This was used to selectively dissociate those ions vibrationally excited by the WEX. The method is based on the difference in the density of states near v = 0 and v = 1 which causes enhanced multiphoton dissociation (MPD) of v = 1 as compared to v = 0. Because spectroscopy is done in this apparatus through detection of fragment

ions, it is important to have a strong correlation between vibrational excitation of parent ions and formation of fragment ions. This has been achieved in this experiment by monitoring the fragment ion $C_2H_5^+$.

III. Results

Initial results were obtained using cylinder 1 with a backing pressure of 90 torr. The results obtained are shown in Fig. 6. All of the $C_2H_7^+$ spectroscopy was done by monitoring formation of $C_2H_5^+$ as a function of the WEX frequency. The dominant features are located at 2825, 2945, 3082, and 3128 cm^{-1}. The spectrum was taken from 2775 - 3300 cm^{-1}.

In hopes of obtaining higher ion counts, the second cylinder had a six times larger ethane to hydrogen ratio than cylinder 1. Unexpected results were obtained. With 90 torr backing pressure, not only did the $C_2H_7^+$ ion count not increase, but also several spectral features had disappeared. In a scan from 2470 to 3260 cm^{-1}, only three large features were seen. Their frequencies are 2945, 3082, and 3128 cm^{-1}. The large peak seen using cylinder 1 at 2825 cm^{-1} has almost completely disappeared, as shown in Fig. 7.

At this point, it was clear that something unusual was occurring. In order to reproduce the results taken with cylinder 1, a third cylinder was mixed with a H_2:C_2H_6

ratio similar to cylinder 1 (cylinder 1- 55,000:1, cylinder 3- 42,500:1). The peak at 2825 cm^{-1} reappeared although it was smaller than with cylinder 1 as might be expected from the slightly different mixing ratio. It was also discovered that with the CO_2 laser blocked and only the WEX being passed through the machine, the only feature seen from 2775 to 3265 cm^{-1} was this peak at 2825 cm^{-1}. When the pressure in the source was increased from 90 torr to 150 torr, the peak at 2825 cm^{-1} was the only one to disappear. Thus, there were three observations that led us to view the 2825 cm^{-1} peak as arising from a very different parent ion from the features at 2945, 3082, and 3128 cm^{-1}.

In order to investigate this more thoroughly, the scanning range was extended both to higher and lower frequencies and the spectra were taken at three different backing pressures. The pressures chosen were 60, 90, and 150 torr, and are shown in Figs. 8 and 9. At 60 torr, the 2825 cm^{-1} feature was larger than the three peaks at 2945, 3082, and 3128 cm^{-1}, whereas by 150 torr, the 2825 cm^{-1} band had disappeared. Note that the ratio of the other three features is independent of backing pressure. Five more features were found that disappeared with increasing backing pressure. Four were to the red of the previous scanning range and were located at 2521, 2601, 2683, and 2762 cm^{-1}. The fifth peak was well to the blue of these

at 3964 cm^{-1}. In order to test whether these peaks showed the same lack of sensitivity to whether the CO_2 laser was on or off, the spectrum from 2490 to 2800 cm^{-1} was taken with the CO_2 laser off. Like the 2825 cm^{-1} feature, the signal levels of these peaks were apparently unaffected by the absence of the CO_2 laser, implying that some of the parent ions are able to predissociate after the absorption of a single tunable IR photon.

While scanning to the blue of the original scanning range, several more features were seen that were independent of backing pressure. A broad intense band centered around 3845 cm^{-1} dominates this region. Two sharp features at 3667 and 3917 cm^{-1} are also quite prominent. The features at 3726 and 3762 cm^{-1} are much less intense. All five of these features appear pressure independent as seen in Fig. 9. In contrast to earlier results, however, these features are independent of whether the CO_2 laser is on or off. Frequencies of all of the experimentally observed peaks are given in Table III.

Attempts at higher resolution spectra were made by inserting the etalon in the YAG yielding approximately a factor of four reduction in linewidth. The bands centered at 2945.4 and 2762.2 cm^{-1} showed no resolvable structure within the signal-to-noise level, although their band envelopes are distinctly different (Figs. 10 and 11).

However, the band at 3964.0 cm^{-1} is clearly separated into a P, Q, R sub-band structure as shown in Fig. 12.

IV. Discussion

As mentioned in the introduction, Hiraoka and Kebarle[25] studied the thermochemistry of pentacoordinated carbonium ions. They claimed to observe both the bridged and classical forms of $C_2H_7^+$. Their potential energy diagram is reconstructed in Fig. 3. Their conclusion is that the bridged structure is 8 kcal/mole more stable than the classical form with a 5.2 kcal/mole barrier inbetween them. Thus, in order for the classical $C_2H_7^+$ to dissociate into $C_2H_5^+ + H_2$ it takes 4 kcal/mole (1400 cm^{-1}), whereas the bridged structure requires 13 kcal/mole (4500 cm^{-1}) to dissociate into $C_2H_5^+ + H_2$.

M. Dupuis has calculated vibrational frequencies for both the bridged and classical forms of $C_2H_7^+$.[41] Although the classical form frequencies were difficult to calculate due to the extended C-H bonds connecting the H_2 unit to the $C_2H_5^+$ moiety, the separation between the calculated frequencies should yield information even if their absolute values are inaccurate. Frequencies for both structures are shown in Tables IV and V. Refer to Table II for bond lengths and angles.

The experimental vibrational frequencies are listed in Table III. Both the backing pressure dependence and

CO_2 laser dependence are also included. The obvious question is why there seems to be two sets of peaks based on pressure dependence. Several possibilities must be considered: impurities, combination bands, hot bands, and the presence of two structures. The features below 3400 cm^{-1} will be considered separately from those above.

A. 2400-3400 cm^{-1}

First, let's consider impurities. Because the ions are mass-selected before doing the spectroscopy, any impurity peak must be from an ionic species of mass 31. Possibilities would include $N_2H_3^+$ and H_3CO^+. However, the impurity must not only be of mass 31, it must also have strong absorptions between 2500-2900 cm^{-1}, and must dissociate to mass 29. The fact that we pumped out the mixing cylinder extensively each time before adding pure H_2 and C_2H_6 further diminishes the possibility that the five features between 2500 and 2900 cm^{-1} are due to impurities.

The second possibility to consider is combination bands. This can be ruled out using energy considerations. The features below 2900 cm^{-1} are still present when the CO_2 laser is blocked. This evidence supports the theory that these features arise from a highly excited $C_2H_7^+$ that has a smaller dissociation energy than the features be-

tween 2900 and 3300 cm^{-1} which require the CO_2 laser to be on and are thought to be from ground state $C_2H_7^+$.

This leads to the possibility of hot bands. From energetic considerations, hot bands would be expected to need less energy to dissociate in agreement with the above described observations for these features below 2900 cm^{-1}. Two different types of hot bands are $v = 1 \rightarrow 2$ of a C-H stretch where all other vibrations are in the ground state ($v' = 0$), and $v = 0 \rightarrow 1$ of a C-H stretch where a different mode is excited ($v' \neq 0$). Note that three of the bands below 2900 cm^{-1} are more intense than the strongest C-H stretch. This makes the hot band hypothesis seem unlikely. In order to have a hot band intensity be stronger than the fundamental, the excitation of the "hot" bend or stretch would have to increase the transition moment of the C-H stretching vibration, since a population inversion is probably impossible.

The last consideration is the presence of both the bridged and classical structures. The classical structure is higher in energy than the bridged by 4-8 kcal/mole.[25,33,34] This lends credence to the idea that the bridged structure will not dissociate after being excited by the WEX unless the CO_2 laser is on, whereas the classical structure can dissociate. Thus, the five features below 2900 cm^{-1} seem to arise from the classical structure, and the features between 2900 and 3300 cm^{-1}

from the bridged structure. More evidence to support this assignment follows.

The five features at 2521, 2601, 2683, 2762, and 2825 cm^{-1} can be made to disappear both by raising the backing pressure and by increasing the relative amount of C_2H_6 to H_2. At the higher pressures, more collisions will occur behind the nozzle which logically leads to more efficient internal cooling of the nascent ions. This leads to strongly enhanced formation of the lower energy bridged structure over the classical form. An analogous argument can be made for the case with a higher C_2H_6:H_2 ratio, but the same backing pressure. Even though the number of collisions will be approximately the same, internally excited $C_2H_7^+$ is much more efficiently cooled through collisions with an ethane molecule than with a hydrogen molecule. Several mechanisms can contribute to this increased efficiency.[46,47] Due to the closer vibrational frequency match between C_2H_6 and $C_2H_7^+$ than between H_2 and $C_2H_7^+$, V → V transfer from the hot $C_2H_7^+$ will occur much more readily to ethane. Another factor is that ethane has a larger polarizability than hydrogen. This leads to an increased collision cross section through long-range ion-induced dipole forces. Also increasing the cross section is that ethane is physically larger than hydrogen. All of these factors will contribute to more efficient cooling by ethane than by hydrogen.

Comparison of theoretically calculated vibrational frequencies by Dupuis with the experimental spectrum further supports the bridged/classical theory. Referring to Table IV one sees that the SCF calculation for the bridged structure predicts six features above 2500 cm^{-1} with frequencies 3271, 3274, 3420, 3422, 3466, and 3466 cm^{-1}. These frequencies are expected to be 10% too high. Scaling them down yields the frequencies 2944, 2947, 3078, 3080, 3119, and 3119 cm^{-1}. Comparison with the experimental frequencies and intensities leads to the assignment of the 2945 cm^{-1} feature as mostly ν_6, the 3082 cm^{-1} to ν_3 and ν_4, and the 3128 cm^{-1} to ν_1 and ν_2. The agreement between the theoretical and experimental frequencies is excellent.

A comparison with the theoretical vibrational frequencies for the classical structure is also encouraging. The calculated frequencies and intensities are listed in Table V. The C-H bonds were treated at the SCF level, but the CH_1H_2 group was treated at the correlated level. Because of the difficulty of this calculation caused by the weakly bound H_2 group, absolute values for the frequencies may not be reliable. However, the separation between the asymmetric CH_a and CH_b peaks and the symmetric CH_a and CH_b peaks may prove more informative. This appears to be the case. The five experimental frequencies 2521, 2601, 2683, 2762, and 2825 cm^{-1} can be

tentatively assigned to the five scaled frequencies 2935, 2995, 3027, 3041, and 3091 cm^{-1}. The experimental separation between the asymmetric CH_a and CH_b is 63 cm^{-1} as compared to a theoretical value of 50 cm^{-1}. The separation between the symmetric CH_a and CH_b peaks is 80 cm^{-1} for the experimental data and 60 cm^{-1} for theory. Also note the similarity in the experimental band shapes between the asymmetric CH_b and symmetric CH_b bands. Both have clearly resolved shoulders shifted to the red side by 25-30 cm^{-1} with ~1/3 the intensity of the main very sharp peak. Comparing the band shapes of the asymmetric CH_a and symmmetric CH_a also shows similar envelopes. They also have shoulders but the red shift is only ~7 cm^{-1} and thus not well separated, and their intensities compared to the main peak are larger. The primary peaks are broader than the ones for CH_b.

Thus, it seems that based on a comparison of calculated peak separations and experimental separations and on band contours, the assignment of the experimental features between 2500 and 2900 cm^{-1} to the classical structure is reasonable. The most troubling aspect of this assignment is the magnitude of the experimentally observed redshift of the C-H stretches which is not predicted by theory. The C-H stretches in ethane lie between 2895 and 2985 cm^{-1}. A redshift of close to 400 cm^{-1} is, at first, quite disconcerting. Looking at the situation more carefully,

the classical structure of $C_2H_7^+$ can be approximated as a $C_2H_5^+$ loosely attaching a H_2. The C-H stretches observed correspond to vibrations in the $C_2H_5^+$ moiety. Much work has been done on the correlation between C-H stretch frequencies, bond lengths, and bond dissociation energies.[48] Caution must be employed when using bond energies to predict vibrational frequencies due to the possibility of a significant stabilization energy from the radical formed. This leads to a smaller dissociation energy than the frequency alone would seem to indicate. In this particular case, the stabilization energy does not seem to interfere. Instead, the primary complication comes from the interaction of the C-H bonds to give antisymmetric and symmetric stretching modes. The work quantitating a linear relationship between C-H frequencies and dissociation energies uses "isolated" frequencies which are found by deuterating all hydrogens except the one under study. Nonetheless, it is still expected that an estimate for the dissociation energy will serve as a guide for a reasonable first approximation to the stretch frequency. Using values from Table I for the difference between the classical and bridged $C_2H_5^+$ forms, a C-H bond energy in the classical structure of $C_2H_5^+$ is calculated to be 82-86 kcal/mole.[49] This is significantly weaker than that in ethane (97.4 kcal/mole) or methane (103.4 kcal/mole). Therefore, a significant redshift in the C-H stretch

frequencies in the classical $C_2H_7^+$ structure from those in ethane and methane is expected. From an equation given in Ref. 48, a C-H bond energy of 84 kcal/mole is predicted to correspond to a stretch frequency of 2770 cm^{-1}. This is between the two observed absorptions that have been assigned to antisymmetric CH_a and CH_b modes.

B. 3400-4200 cm^{-1}

The six features above 3400 cm^{-1} will now be discussed. The peaks at 3667, 3726, 3762, 3845, and 3917 cm^{-1} show no backing pressure dependence whereas the one at 3964 cm^{-1} disappeared at higher pressures. The CO_2 laser was not necessary for any of these features. Again, impurities, combination bands, hot bands, and the presence of two structures will be discussed.

Based on similar arguments to those given above, impurities are ruled out as the mechanism to explain the contrasting pressure behavior.

Combination bands are a real possibility to explain the five features that show no pressure dependence. Based on the reasoning above, these bands should arise from the bridged structure of $C_2H_7^+$, which has no predicted fundamentals above 3400 cm^{-1}. Therefore the observed peaks must come from combination bands or overtones. The lack of CO_2 laser dependence can be explained by realizing that the absorption frequencies (3667 to 3917 cm^{-1}) correspond

to energies (10.5-11.2 kcal/mole) very close to the expected dissociation energy (13 kcal/mole). If the ions initially contain 2-2.5 kcal/mole internal energy or if the measured dissociation energy is too high, then the CO_2 laser photons would not be necessary. Based on the vibrational frequencies calculated by Dupuis, an internal energy of 2-2.5 kcal/mole only requires an average vibrational temperature of 400-450 K. Even though the source is cooled with chloro-difluoromethane (Freon-22), a vibrational temperature after the discharge slightly above room temperature is possible.

Assigning the features between 3400-4200 cm^{-1} to hot bands is not logical because hot bands are redshifted from fundamentals.

Finally, the implication of two structures will be discussed. As argued in the preceeding section, the pressure dependence of some features implies a kind of collisional stabilization of an internally excited type of $C_2H_7^+$ ion. The fact that the feature at 3964 cm^{-1} disappears simultaneously with the five features below 2900 cm^{-1} strongly suggests that they originate from the same form of $C_2H_7^+$. Therefore, the peak at 3964 cm^{-1} is assigned to a classical $C_2H_7^+$ structure. The five features between 3600 and 3950 cm^{-1} show no pressure dependence, and thus all originate from the more stable bridged $C_2H_7^+$ structure. The fact that these features do not require

the CO_2 laser to be present is not an issue here as it was at the lower frequencies as has been discussed above.

Theory does not predict any fundamentals for either the classical or bridged structure above 3600 cm^{-1}.[41] The highest frequency in the classical structure should correspond to the H_1-H_2 stretch vibration of the H_2 moiety which is loosely bound to the $C_2H_5^+$ unit. The unscaled frequency for this motion is 3516 cm^{-1} as compared to 3171 cm^{-1} for CH_5^+ at a comparable level of theory.[41] (At higher levels of theory this mode is predicted to lie at 2797 and 2813 cm^{-1} for CH_5^+.)[41,40] The calculated geometries of the classical $C_2H_7^+$ and CH_5^+ are consistent with the frequency shift. The C-H_1 and C-H_2 bond distances are longer in $C_2H_7^+$ (1.295 and 1.315 Å)[41] than in CH_5^+ (1.261 Å)[41], and the H_1-H_2 bond distance is shorter in $C_2H_7^+$ (0.824 Å,[41] 0.833 Å[34]) than in CH_5^+ (0.853 Å,[41] 0.882 Å,[34] 0.869 Å[40]). Thus, it's clear that the H-H stretching vibration in $C_2H_7^+$ will be significantly to the blue of that in CH_5^+. Our results indicate that rather than being shifted by only a few hundred wavenumbers, the H-H stretching vibration has actually been shifted close to a thousand wavenumbers to 3964 cm^{-1}. In our previous work on the hydrogen cluster ions H_n^+ (n = 5, 7, 9, 11, 13, 15),[50,51] and on the hydrated hydronium cluster ions $H_3O^+ \cdot (H_2O)_n \cdot (H_2)_m$,[52] we were able to detect the H-H stretching vibration in the region from 3900-4120 cm^{-1}.

The redshift of the H-H stretching vibration from free H_2 (4161 cm^{-1}) was a gauge of the binding energy of the H_2 moiety to the rest of the ion. The most strongly bound cluster ion was H_5^+ which requires ~6 kcal/mole[53] to dissociate into $H_3^+ + H_2$. The redshift of the H_2 stretch was also greatest at 251 cm^{-1} placing the H_2 stretch at 3910 cm^{-1}. The H_7^+ ion was bound by roughly 3 kcal/mole[53] and showed a redshift of only 181 cm^{-1} putting it at 3980 cm^{-1}. Since the classical $C_2H_7^+$ is estimated to have a binding energy of ~4 kcal/mole,[25] this places it between H_5^+ and H_7^+. A first approximation to the H_2 moiety frequency, then, is between 3910 and 3980 cm^{-1}. Our peak observed at 3964 cm^{-1} fits nicely into this range.

This feature was also scanned at higher resolution as shown in Fig. 12. A P, Q, R bandshape emerges. $C_2H_7^+$ is a near symmetric top with the C-C bond as top axis. For such a molecule, a transition with a changing dipole moment parallel to the C-C axis would show a P, Q, R bandshape. The rotational constant, B, is calculated from the classical $C_2H_7^+$ geometry to be 0.55 cm^{-1}. In fact, the ripples on top of the P and R branches are spaced by 1.1 cm^{-1}, in excellent agreement with the expected 2B separation. Using assignments based on these facts, a rotational temperature of 20K is obtained.

The five features between 3600 and 3950 cm^{-1} are believed to originate from the bridged structure. The six

highest calculated frequencies[41] correspond to C-H stretches and can be grouped into three quasi-degenerate pairs. The next highest frequency, ν_7, corresponds to a side-to-side motion of the bridging proton with a scaled frequency of 2074 cm^{-1} and huge intensity of 20 $D^2/(Å^2 \cdot amu)$. The first overtone of this should have an observable intensity and lie close to 4000 cm^{-1}. We tentatively assign the feature at 3917 cm^{-1} to this first overtone. The peak observed at 3667 cm^{-1} has a similar band contour to the feature at 3917 cm^{-1}. The frequency corresponding to the motion of the bridging proton away from the C-C bond is calculated to lie at 1786 cm^{-1}. This leads to preliminary assignment of the 3667 cm^{-1} band as the combination band of the motion of the proton side-to-side and away from the C-C bond ($\nu_7 + \nu_8$). The two smaller features at 3726 and 3762 cm^{-1} are separated by 36 cm^{-1}, close to the separation of the fundamental C-H stretches observed at 3082 and 3128 cm^{-1}. The band contours and relative heights at the three pressures of these two pairs also matches well. This leads to an initial assignment to the combination band of these C-H stretches and ν_{17} which is calculated to have a very strong intensity of 10 $D^2/(Å^2 \cdot amu)$. Even a tentative assignment of the broad feature at 3845 cm^{-1} is difficult. The best guess at this point is a combination band of $\nu_7 + \nu_{14} + \nu_{17}$. The reason for the unusual broadness is

unknown. These preliminary assignments are listed in Table VI. Encouraging is the fact that the difference between the experimental frequencies and the theoretical frequencies with no anharmonic correction is between 193-257 cm^{-1} for binary combinations and 321 cm^{-1} for the ternary combination. Because the bridged structure calculated for $C_2H_7^+$ has C_2 symmetry, no combination bands or overtones can be ruled out on the basis of symmetry.

V. Conclusion

The spectrum of $C_2H_7^+$ has been presented. The spectrum shows a strong dependence on both the ratio of ethane to hydrogen and on the backing pressure used. Evidence has been presented in support of our belief that the different behavior can be attributed to the changing ratio of classical to bridged protonated ethane being probed spectroscopically. The observed infrared frequencies are compared with predicted frequencies for the classical and bridged structures.

REFERENCES

1. L. I. Yeh, M. Okumura, J. D. Myers, and Y. T. Lee, NAS Workshop on Molecular and Cluster Beam Science (National Academy Press, Washington, D.C. 1988) p. 57.

2. S. Winstein and D. Trifan, J. Am. Chem. Soc. **74**, 1147 (1952).

3. S. Winstein and D. Trifan, J. Am. Chem. Soc. **74**, 1154 (1952).

4. R. T. Morrison and R. N. Boyd, Organic Chemistry (Allyn and Bacon, Boston, 1973) p. 917-918.

5. H. C. Brown, Tetrahedron **32**, 179 (1976).

6. J. D. Roberts and J. A. Yancey, J. Am. Chem. Soc. **74**, 5943 (1952).

7. G. A. Olah, Acc. Chem. Res. **9**, 41 (1976).

8. S. Wexler and N. Jesse, J. Am. Chem. Soc. **84**, 3425 (1962).

9. F. H. Field, J. L. Franklin, and M. S. B. Munson, J. Am. Chem. Soc. **85**, 3575 (1963).

10. M. S. B. Munson, J. L. Franklin, and F. H. Field, J. Phys. Chem. **68**, 3098 (1964).

11. M. S. B. Munson and F. H. Field, J. Am. Chem. Soc. **87**, 3294 (1965).

12. G. A. Olah, G. Klopman, and R. H. Schlosberg, J. Am. Chem. Soc. **91**, 3261 (1969).

13. A. S. Blair, E. J. Heslin, and A. G. Harrison, J. Am. Chem. Soc. **94**, 2935 (1972).

14. W. A. Lathan, W. J. Hehre, and J. A. Pople, J. Am. Chem. Soc. **93**, 808 (1971).

15. P. C. Hariharan, W. A. Lathan, and J. A. Pople, Chem. Phys. Lett. **14**, 385 (1972).

16. S. L. Chong and J. L. Franklin, J. Am. Chem. Soc. **94**, 6347 (1972).

17. D. K. Bohme, P. Fennelly, R. S. Hemsworth, and H. I. Schiff, J. Am. Chem. Soc. **95**, 7512 (1973).

18. B. Zurawski, R. Ahlrichs, and W. Kutzelnigg, Chem. Phys. Lett. **21**, 309 (1973).

19. V. Dyczmons and W. Kutzelnigg, Theor. Chim. Acta **33**, 239 (1974).

20. P. K. Bischof and M. J. S. Dewar, J. Am. Chem. Soc. **97**, 2278 (1975).

21. H.-J. Kohler and H. Lischka, Chem. Phys. Lett. **58**, 175 (1978).

22. M. French and P. Kebarle, Can. J. Chem. **53**, 2268 (1975).

23. K. Hiraoka and P. Kebarle, J. Chem. Phys. **63**, 394 (1975).

24. K. Hiraoka and P. Kebarle, Can. J. Chem. **53**, 970 (1975).

25. K. Hiraoka and P. Kebarle, J. Am. Chem. Soc. **98**, 6119 (1976).

26. F. A. Houle and J. L. Beauchamp, J. Am. Chem. Soc. **101**, 4067 (1979).

27. T. Baer, J. Am. Chem. Soc. **102**, 2482 (1980).

28. G. I. Gellene, N. S. Kleinrock, and R. F. Porter, J. Chem. Phys. **78**, 1795 (1983).

29. G. I. Mackay, H. I. Schiff, and D. K. Bohme, Can. J. Chem. **59**, 1771 (1981).

30. J. Weber and A. D. McLean, J. Am. Chem. Soc. **98**, 875 (1976).

31. J. Weber, M. Yoshimine, and A. D. McLean, J. Chem. Phys. **64**, 4159 (1976).

32. H.-J. Kohler and H. Lischka, Theor. Chim. Acta **54**, 23 (1979).

33. K. Raghavachari, R. A. Whiteside, J. A. Pople, and P. v. R. Schleyer, J. Am. Chem. Soc. **103**, 5649 (1981).

34. K. Hirao and S. Yamabe, Chem. Phys. **89**, 237 (1984).

35. T. J. Lee and H. F. Schaefer III, J. Chem. Phys. **85**, 3437 (1986).

36. H. Lischka and H.-J. Kohler, J. Am. Chem. Soc. **100**, 5297 (1978).

37. G. P. Raine and H. F. Schaefer III, J. Chem. Phys. **81**, 4034 (1984).

38. M. Crofton and T. Oka (private communication).

39. D. J. DeFrees and A. D. McLean, J. Chem. Phys. **82**, 333 (1985).

40. A. Komornicki and D. A. Dixon, J. Chem. Phys. **86**, 5625 (1987).

41. M. Dupuis (private communication).

42. E. P. Kanter, Z. Vager, G. Both, and D. Zajfman, J. Chem. Phys. **85**, 7487 (1986).

43. See also: S. W. Bustamente, PhD thesis, University of California, Berkeley, California, 1983 and M. Okumura, PhD thesis, University of California, Berkeley, California, 1986.

44. N. R. Daly, Rev. Sci. Instrum. **31**, 264 (1960). See also, Y. T. Lee, J. D. McDonald, P. R. LeBreton, and D. R. Herschbach, ibid. **40**, 1402 (1969).

45. E. Teloy and D. Gerlich, Chem. Phys. **4**, 417 (1974).

46. J. T. Yardley, Introduction to Molecular Energy Transfer (Academic Press, New York, 1980).

47. R. D. Levine and R. B. Bernstein, Molecular Reaction Dynamics and Chemical Reactivity (Oxford University Press, New York, 1987).

48. D. C. McKean, Chem. Soc. Rev. **7**, 399 (1978). See also D. C. McKean, J. L. Duncan, and L. Batt, Spectrochim. Acta **29**, 1037 (1973).

49. H. M. Rosenstock, K. Draxl, B. W. Steiner, and J. T. Herron, J. Phys. Chem. Ref. Data **6**, Suppl. 1, 99, 102 (1977).

50. M. Okumura, L. I. Yeh, and Y. T. Lee, J. Chem. Phys. **88**, 79 (1988).

51. M. Okumura, L. I. Yeh, and Y. T. Lee, J. Chem. Phys. **83**, 3705 (1985).

52. M. Okumura, L. I. Yeh, J. D. Myers, and Y. T. Lee, J. Chem. Phys. **85**, 2328 (1986).

53. R. J. Beuhler, S. Ehrenson, and L. Friedman, J. Chem. Phys. **79**, 5982 (1983).

TABLE I. Relative energies of the classical (cl) and bridged (br) structures of $C_2H_3^+$, $C_2H_5^+$, and $C_2H_7^+$. Heats of formation for $C_2H_7^+$ and proton affinities for C_2H_6. Units are kcal/mole.

Reference	$C_2H_3^+$ cl-br	$C_2H_5^+$ cl-br	$C_2H_7^+$ cl-br	H_f $C_2H_7^+$	PA C_2H_6
Lathan et al.[a]		-7	9.8		140.1
Hariharan et al.[b]	-5.7	1			
Chong and Franklin[c]				218.8±1	127.0±1
Bohme et al.[d]					136<PA<159
Zurawski et al.[e]	7	9			
Bischof and Dewar[f]			15	cl 199.8 br 215	
Kohler and Lischka[g]			MINDO -11 SCF 8.5 CEPA 6.3		cl 138.3 br 143.4
French and Kebarle[h]				br 208.5±2	br 137.4±2
Hiraoka and Kebarle[i]			7.8	cl 215 br 207.2	cl 131.8 br 139.6
Houle and Beauchamp[j]		~3			

Mackay et al.[k]				204.8±1	142.1±1
Weber and McLean[l]	1-2				
Lischka and Kohler[m]	MINDO 5.3 CEPA 4.0	8.0 7.3			
Kohler and Lischka[n]	3.5-4.0				
Raghavachari et al.[o]	3.0	6.5	6.8		
Hirao and Yamabe[p]	1.30	4.11	4.03		cl 135.6 br 139.7
Lee and Schaefer[q]	0.97				

a. Reference 14.
b. Reference 15.
c. Reference 16.
d. Reference 17.
e. Reference 18.
f. Reference 20.
g. Reference 21.
h. Reference 22.
i. Reference 25.
j. Reference 26.
k. Reference 29.
l. Reference 30 and 31.
m. Reference 36.
n. Reference 32.
o. Reference 33.
p. Reference 34.
q. Reference 35.

TABLE II. Bond lengths and bond angles of the bridged and classical forms of protonated ethane as given by Hirao and Yamabe (Ref. 34), and Dupuis (Ref. 41). Bond lengths are given in Å, and bond angles are in degrees. H_a and H_b are on opposite carbons and H_p is the bridging proton in the nonclassical structure. In the classical structure, the two hydrogens in the H_2 moiety are labeled 1 and 2. The other two hydrogens on the same carbon are labeled H_b. Two of the hydrogens on the opposite carbon are labeled H_a and the third is labeled $H_{a'}$.

Bridged	Hirao and Yamabe	Dupuis
C-C	2.209	2.099
$C-H_p$	1.239	1.234
$C-H_a$, $C-H_b$	1.073-1.079	1.073-1.080
H_p to center of C-C	0.561	0.649
$C-H_p-C$	126.2°	116.5°

Classical	Hirao and Yamabe	Dupuis
C-C	1.525	1.544
$C-H_a$	1.081	1.080
$C-H_{a'}$	1.082	1.082
$C-H_b$	1.086	1.078
$C-H_1$, $C-H_2$	1.267	1.295, 1.315
H_1-H_2	0.833	0.824
H_1-C-H_2	38.4°	36.8°

TABLE III. Experimentally observed vibrational frequencies of $C_2H_7^+$. Frequency units are cm^{-1}.

Frequency	Shows pressure dependence	Remains when CO_2 is blocked
3964.0	Yes	Yes
3917	No	Yes
3845	No	Yes
3762	No	Yes
3726	No	Yes
3667	No	Yes
3128	No	No
3082	No	No
2945.4	No	No
2825	Yes	Yes
2762.2	Yes	Yes
2683	Yes	Yes
2601	Yes	Yes
2521	Yes	Yes

TABLE IV. Vibrational frequencies and intensities of the $C_2H_7^+$ bridged structure. Frequencies are in cm^{-1}, intensities are in $D^2/(Å^2 \cdot amu)$. Theoretical frequencies are from M. Dupuis, ref. 41. Scaled frequencies are in parentheses. Predicted symmetry is C_2.

ν	Species	Calc. freq	Int.	Observed freq.	Assignment
1	B	3466 (3119)	0.32		CH_a, CH_b asym stretch, out-of-phase
2	A	3466 (3119)	0.57	3128	CH_a, CH_b asym stretch, in-phase
3	A	3422 (3080)	0.35		CH_a, CH_b asym stretch, in-phase
4	B	3420 (3078)	0.65	3082	CH_a, CH_b asym stretch, out-of-phase
5	A	3275 (2947)	0.08		CH_a, CH_b sym stretch, in-phase
6	B	3272 (2944)	0.37	2945.4	CH_a, CH_b sym stretch, out-of-phase
7	B	2305 (2074)	20.12		Bridging proton side-to-side
8	A	1984 (1786)	0.29		Bridging proton - away from C-C bond
14	B	1345 (1210)	2.13		CH_a, CH_b deformation
17	B	1003 (900)	10.23		CH_a, CH_b rock

TABLE V. Vibrational frequencies and intensities of the $C_2H_7^+$ classical structure. Frequencies are in cm^{-1}, intensities are in $D^2/(Å^2 \cdot amu)$. Theoretical frequencies are from M. Dupuis, ref. 41. Scaled frequencies are in parentheses. Predicted symmetry is C_s.

ν	Species	Calc. freq	Int.	Observed freq.	Assignment
1	A'	3516 (3164)	0.94	3964.0	H_1-H_2 stretch
2	A"	3434 (3091)	0.31	2825	CH_b-CH_b asym stretch
3	A"	3379 (3041)	0.04	2762.2	CH_a-CH_a asym stretch
4	A'	3363 (3027)	0.06	2683	CH_a, stretch
5	A'	3328 (2995)	0.14	2601	CH_b-CH_b sym stretch
6	A'	3261 (2935)	0.04	2521	CH_a-CH_a sym stretch

TABLE VI. Preliminary assignments of the combination bands for the bridged structure of $C_2H_7^+$. Frequencies are in cm^{-1}. Scaled frequencies from ref. 41 are used with no anharmonic corrections. Predicted symmetry is C_2.

Experimental frequency	Preliminary assignment	Theoretical frequency	Species	Difference
3917	$2\nu_7$	4148	A	231
3845	$\nu_7 + \nu_{14} + \nu_{17}$	4166	B	321
3762	$\nu_2 + \nu_{17}$	4019	B	257
3726	$\nu_4 + \nu_{17}$	3978	A	252
3667	$\nu_7 + \nu_8$	3860	B	193

FIGURE CAPTIONS

Fig. 1a Acetolysis of both endo- and exo-norbornyl p-bromobenzenesulfonate yields the exo-norbornyl acetate. A "nonclassical" ion was proposed as the intermediate.

Fig. 1b Solvolysis of optically active exo-norbornyl p-bromobenzenesulfonate leads to loss of optical activity indicating a racemic product.

Fig. 2 Schematic of bridged and classical structures for protonated acetylene, ethylene, and ethane.

Fig. 3 Energy diagram based on the thermochemical studies of Ref. 25 for the bridged and classical forms of $C_2H_7^+$.

Fig. 4 Schematic of the experimental apparatus.

Fig. 5 The ions are created in a corona discharge ion source. Typical conditions are described in the text.

Fig. 6 Infrared spectrum of $C_2H_7^+$ taken using cylinder 1. The resolution of the IR-WEX is about 1.2 cm^{-1}.

Fig. 7 Spectrum of $C_2H_7^+$ taken using cylinder 2.

Fig. 8 Spectrum of $C_2H_7^+$ from 2500-3300 cm^{-1} taken using cylinders 3 and 4 at the backing pressures indicated. The features which disappear with increasing pressure are due to the classical structure of $C_2H_7^+$. The bands which are independent of pressure are from the more stable bridging structure of $C_2H_7^+$.

Fig. 9 Spectrum of $C_2H_7^+$ from 3400-4100 cm^{-1} taken using cylinders 3 and 4 at the backing pressures indicated. The feature at 3964.0 cm^{-1} disappears with increasing pressure and is assigned to the H-H stretch of the classical structure of $C_2H_7^+$.

Fig. 10 Higher resolution scan of the band at 2945.4 cm^{-1} ($\Delta\nu \approx 0.3$ cm^{-1}).

Fig. 11 Higher resolution scan of the band at 2762.2 cm^{-1}.

Fig. 12 Higher resolution scan of the band centered at 3964.0 cm^{-1}. P, Q, R branches are emerging with some partial rotational resolution. The

vibration excited is the H-H stretch in the classical structure of $C_2H_7^+$.

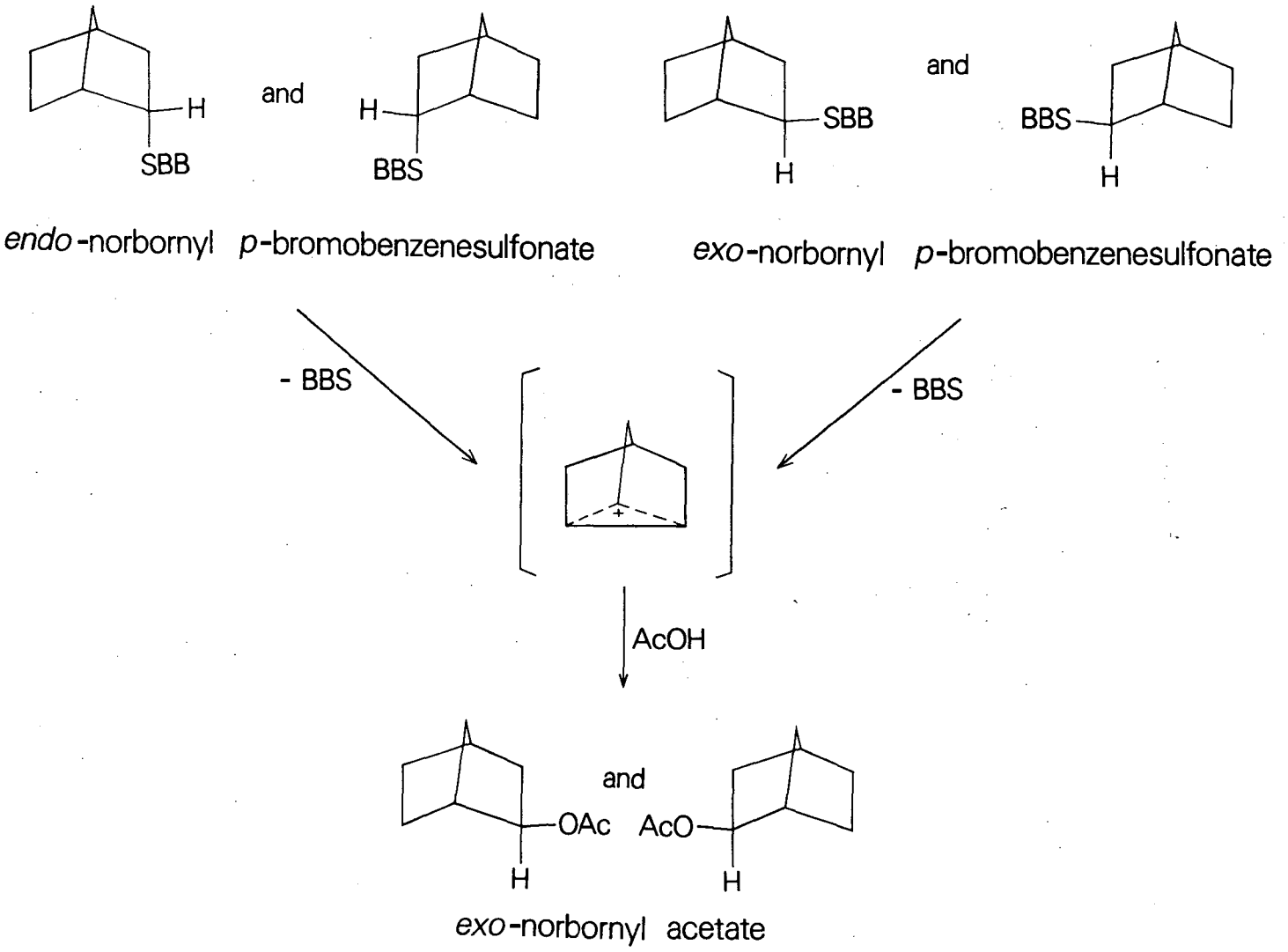

Figure 1a

XBL 887-2497

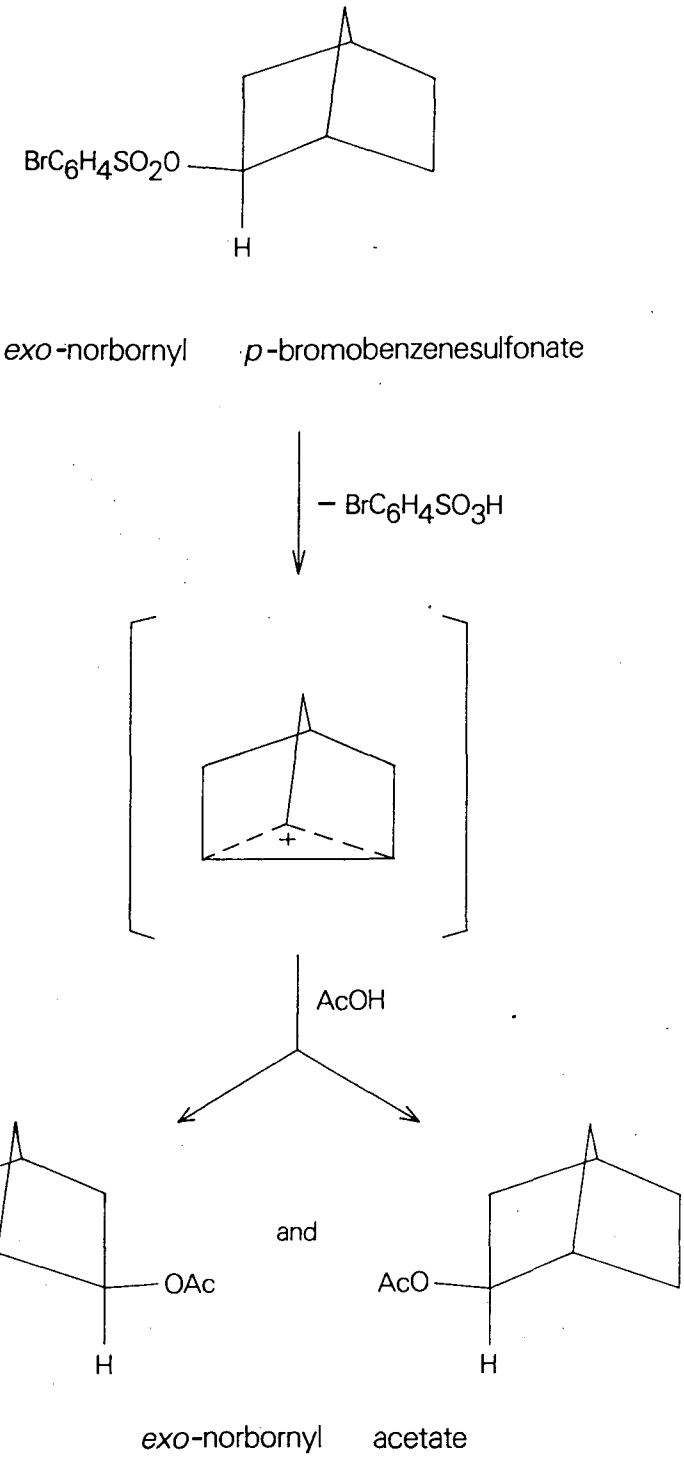

Figure 1b XBL 887-2494

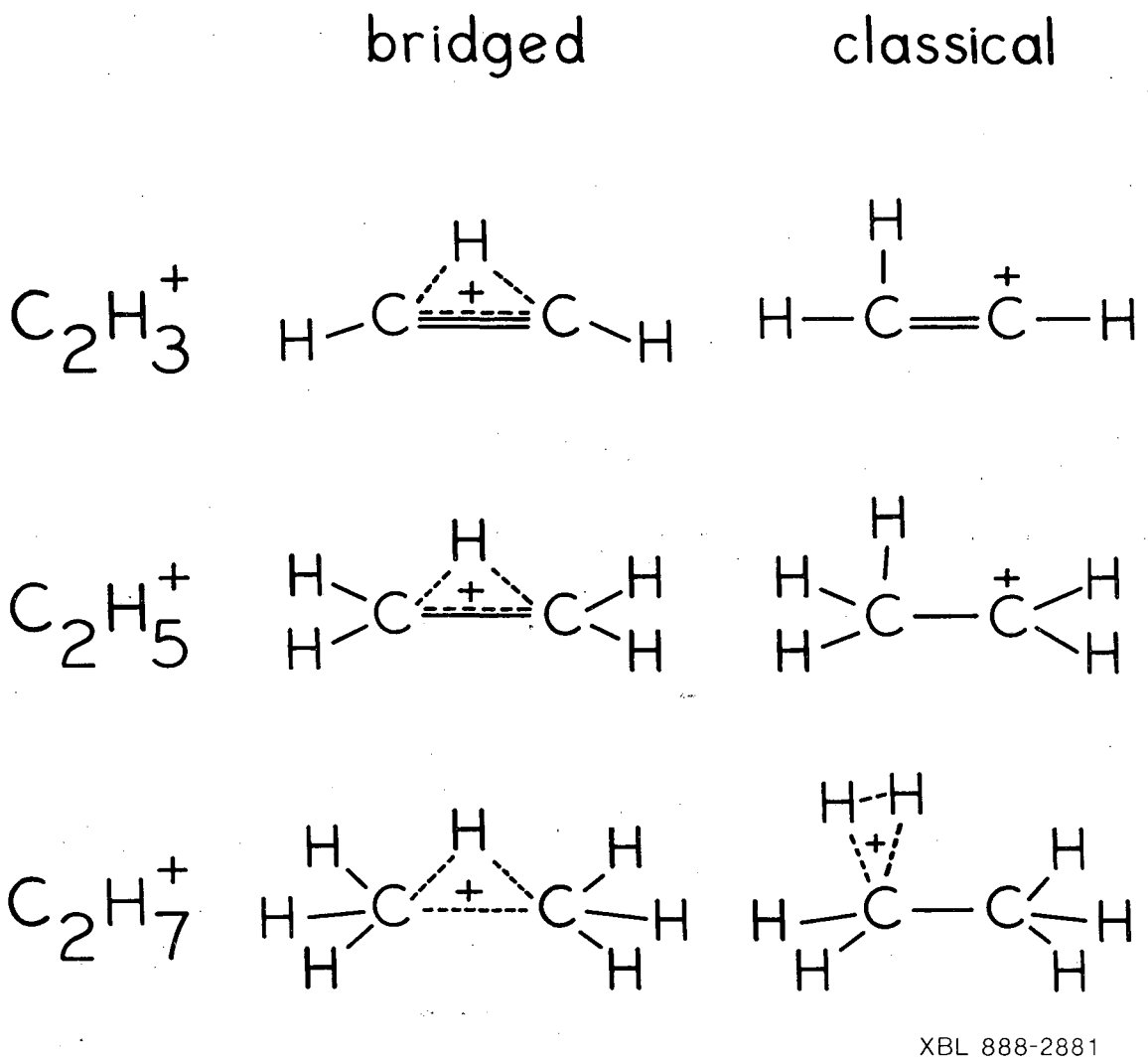

Figure 2

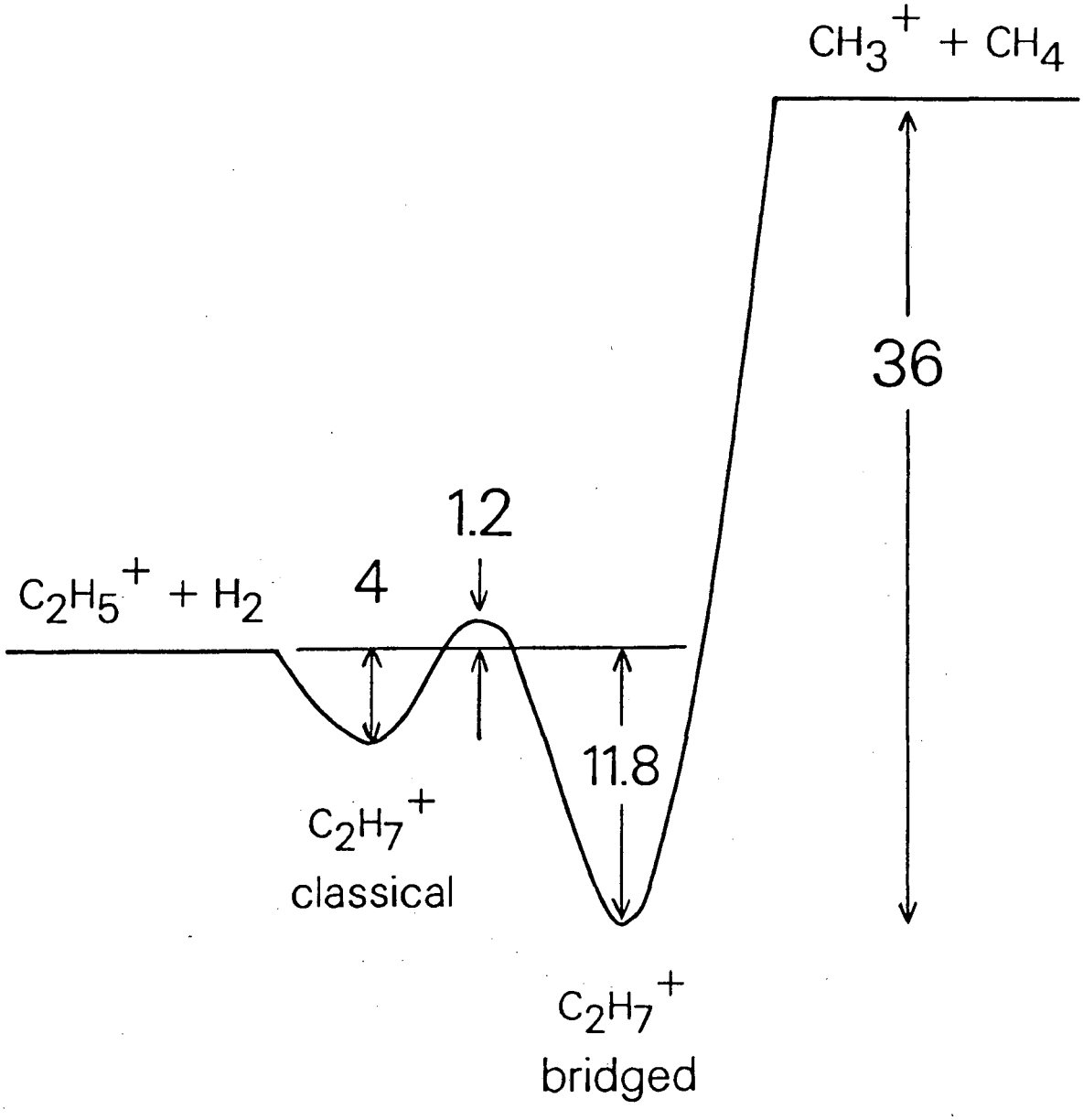

XBL 887-2558

Figure 3

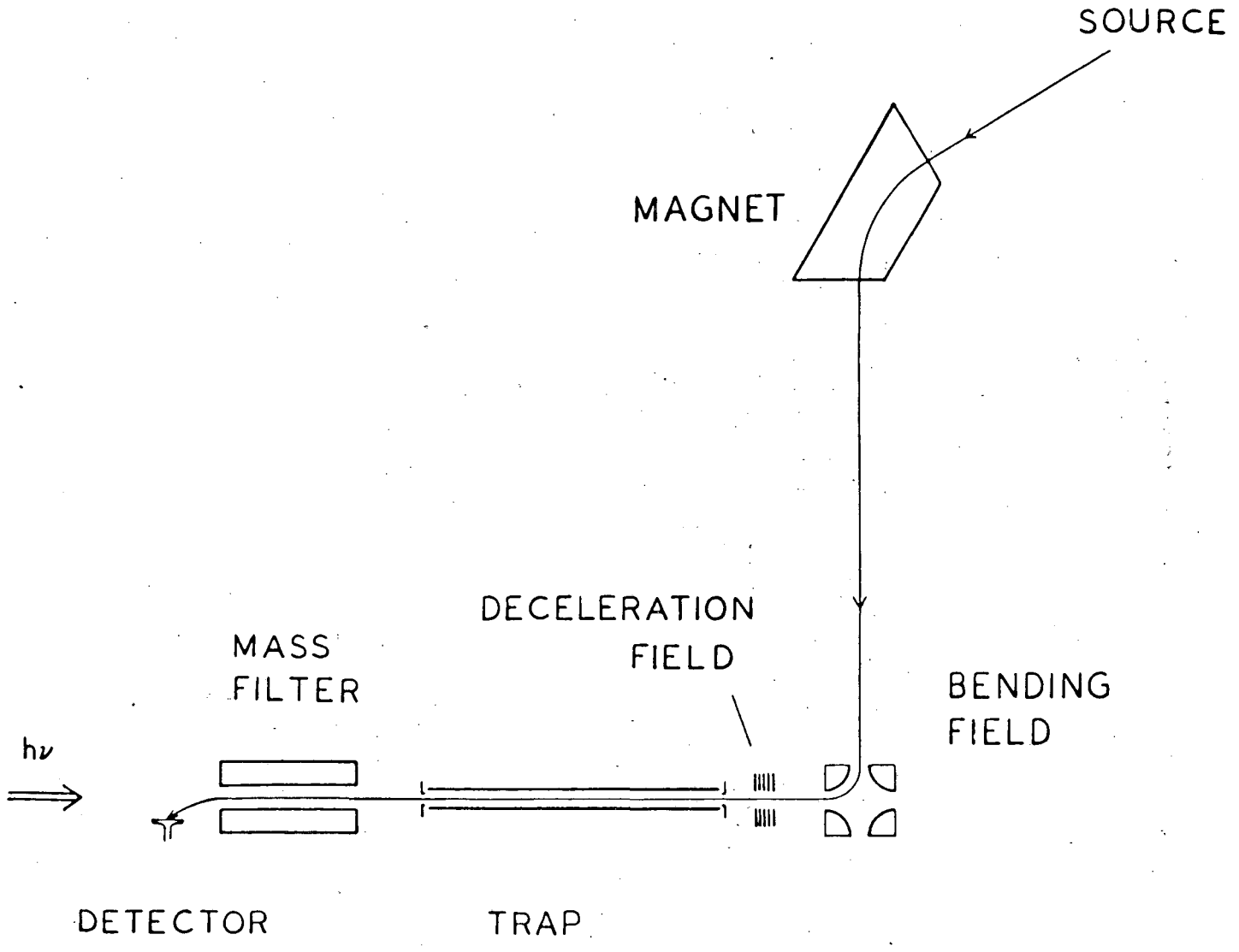

Figure 4

XBL 857-3143

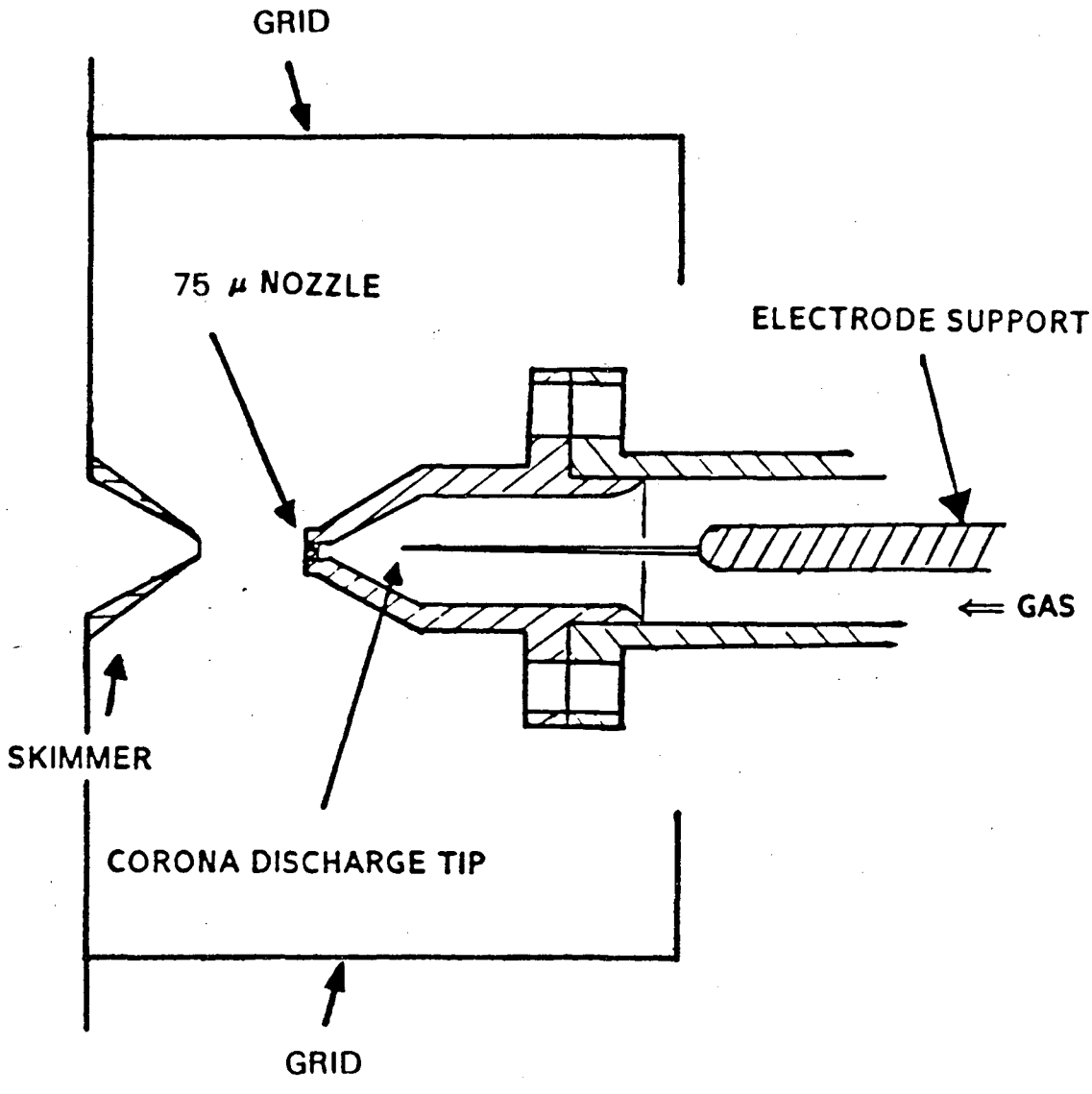

XBL 8711-4636 A

Figure 5

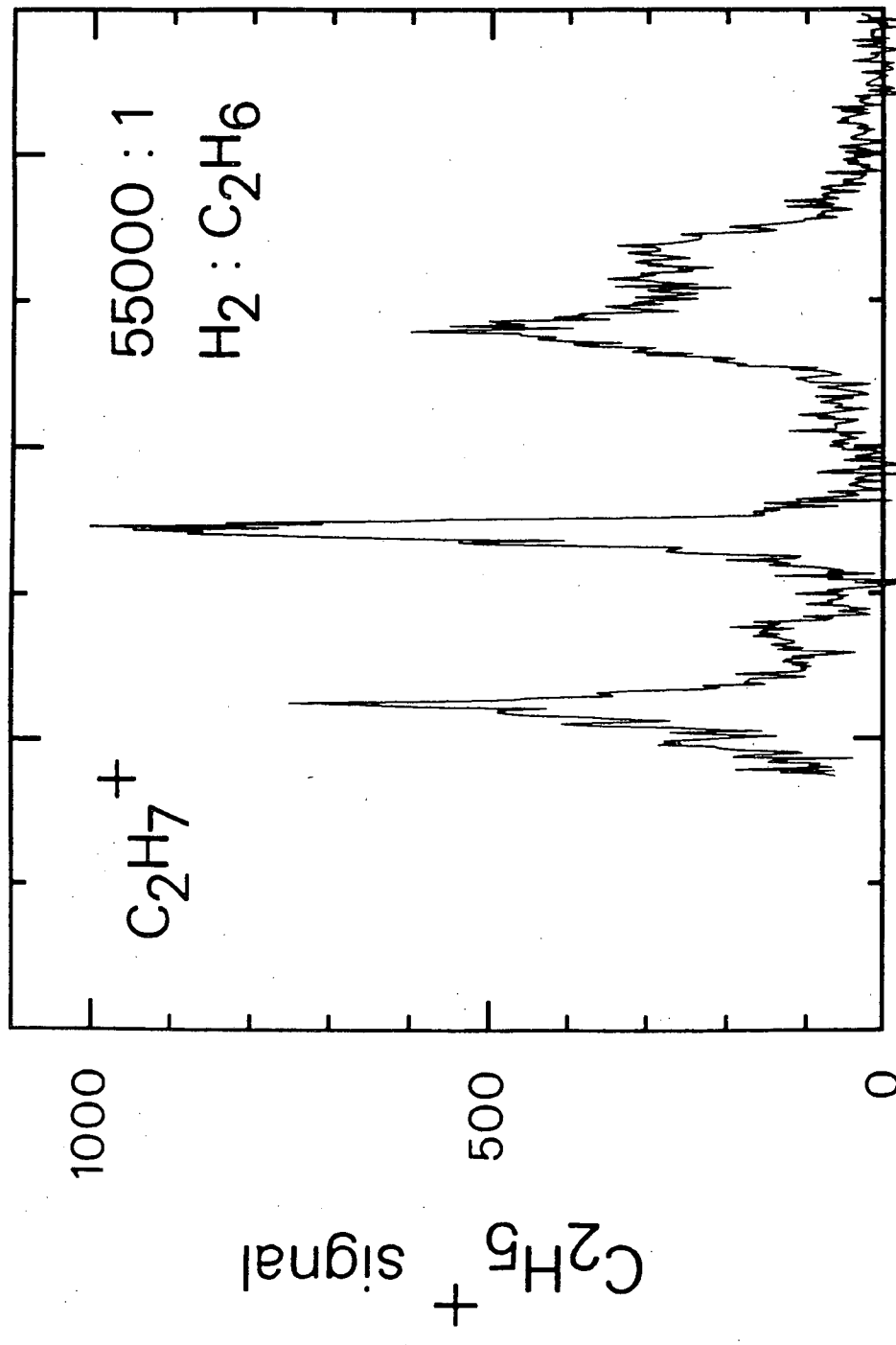

XBL 887-2529

Figure 6

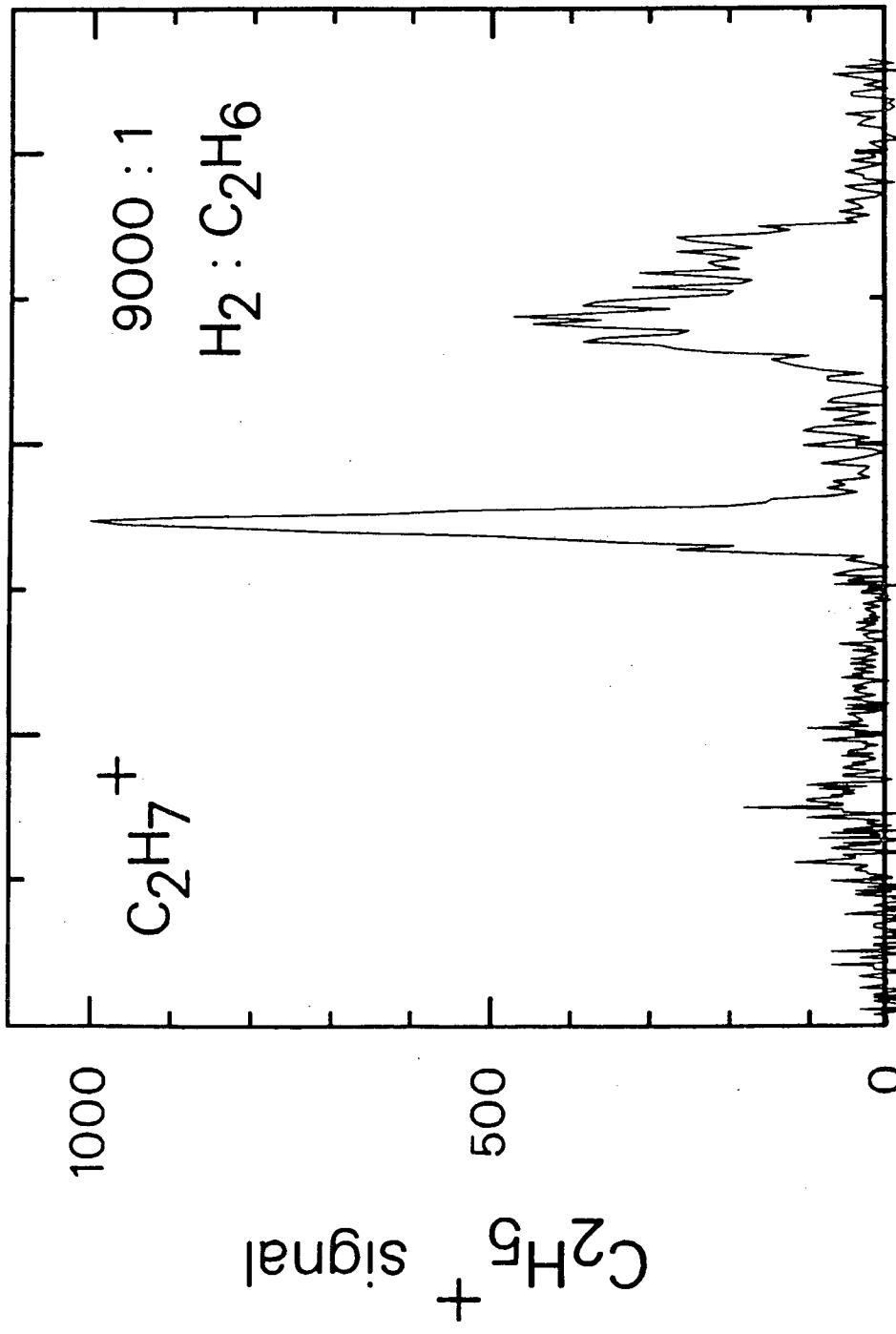

XBL 887-2528

Figure 7

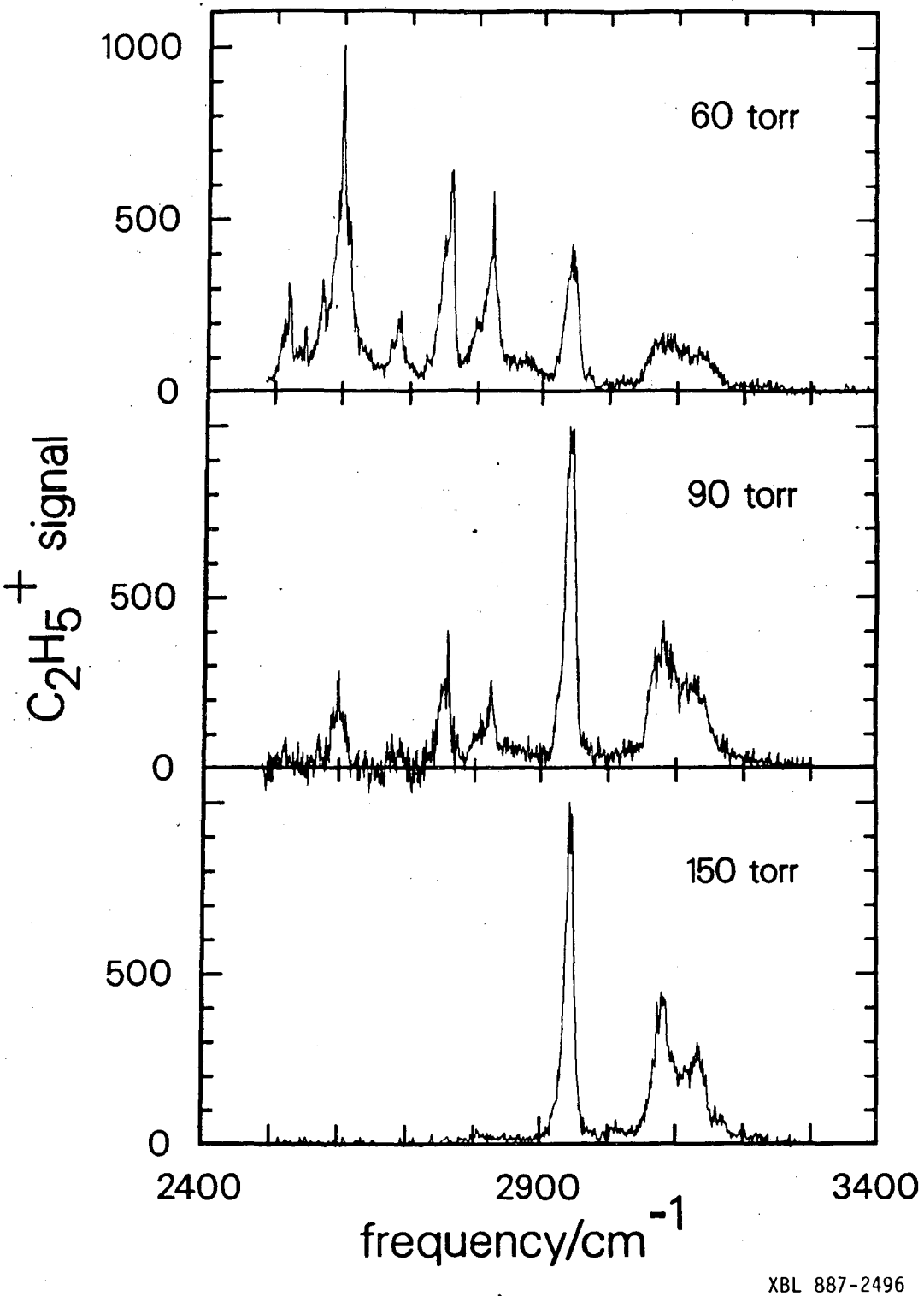

XBL 887-2496

Figure 8

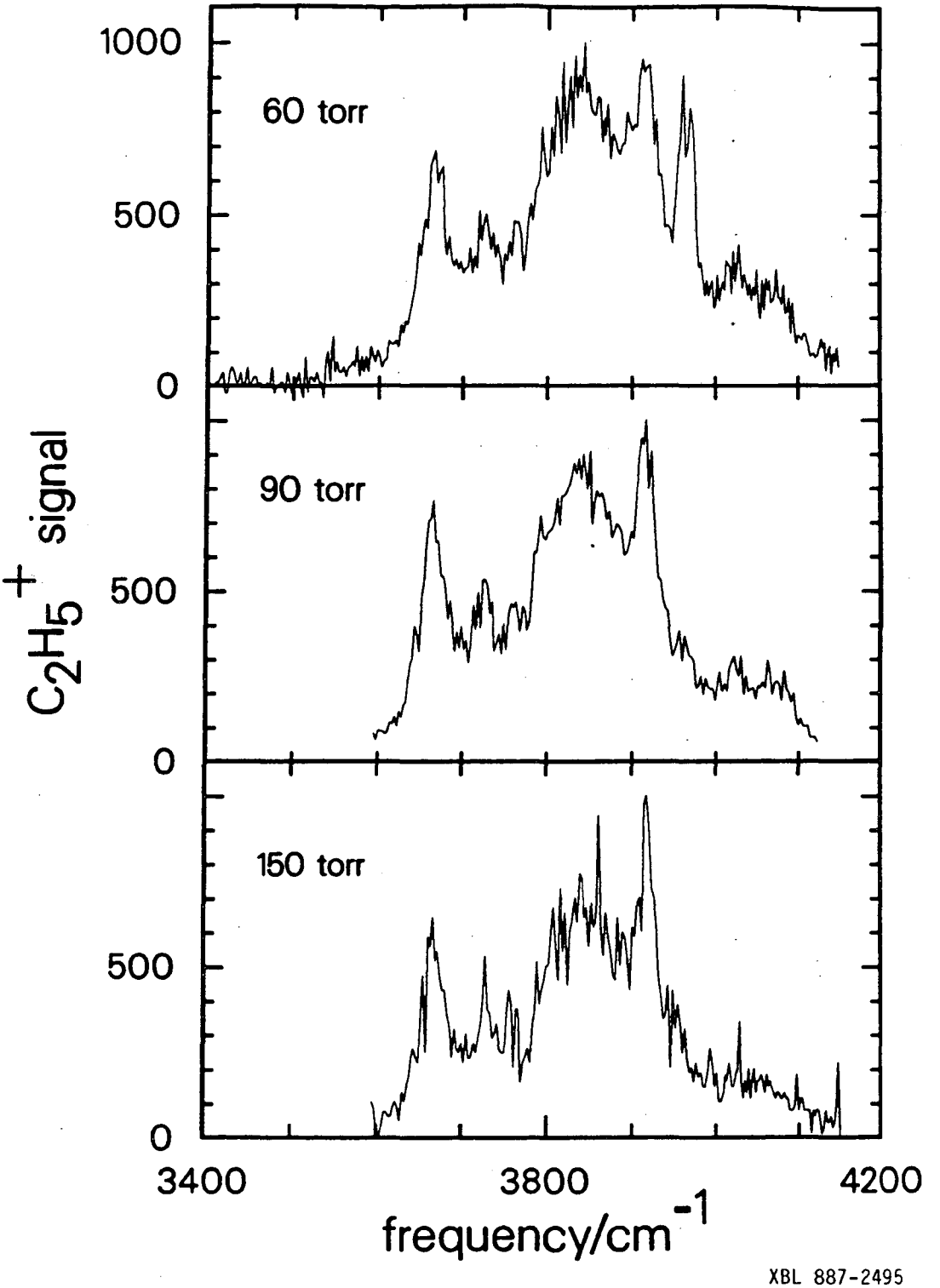

XBL 887-2495

Figure 9

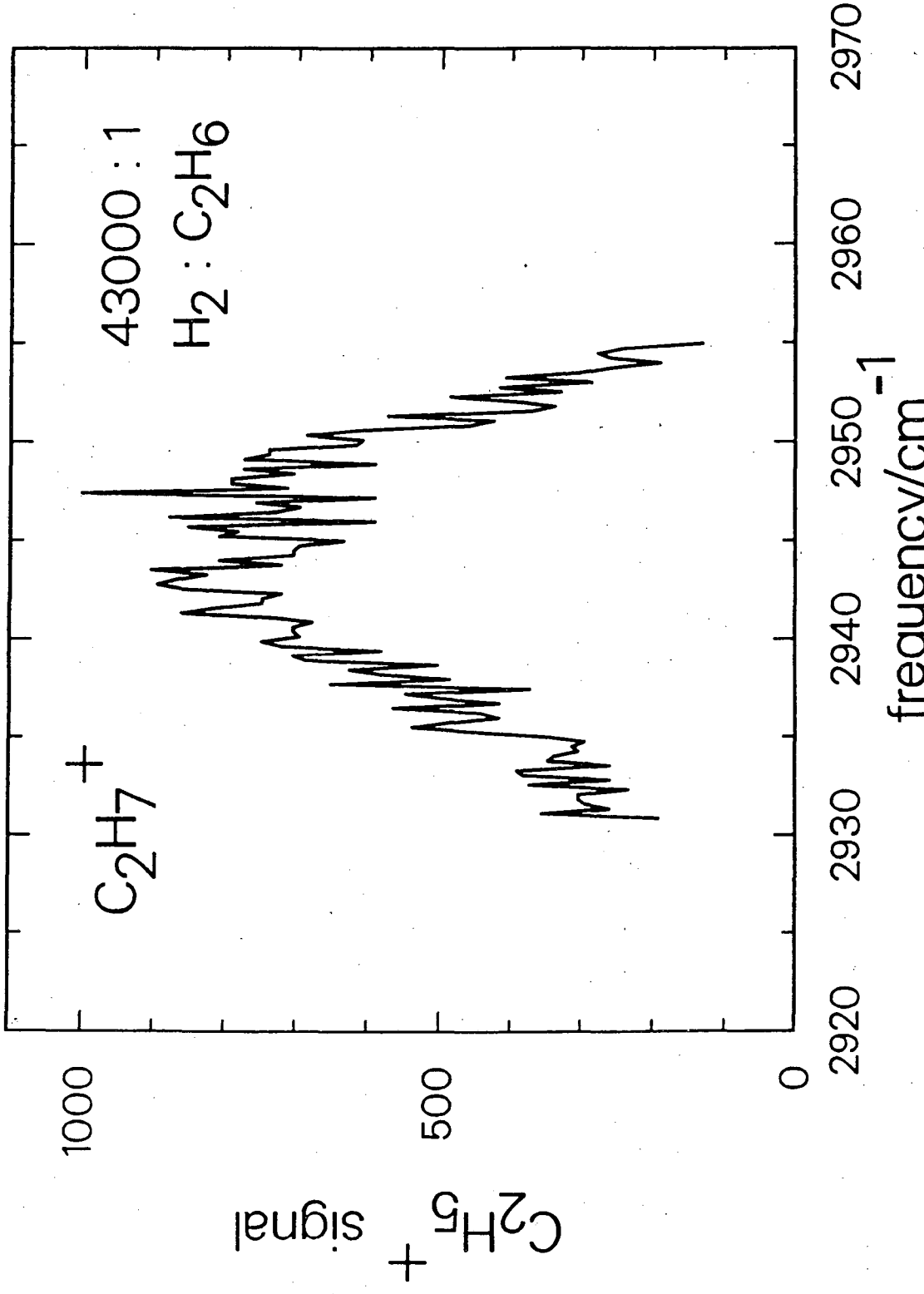

XBL 887-2527

Figure 10

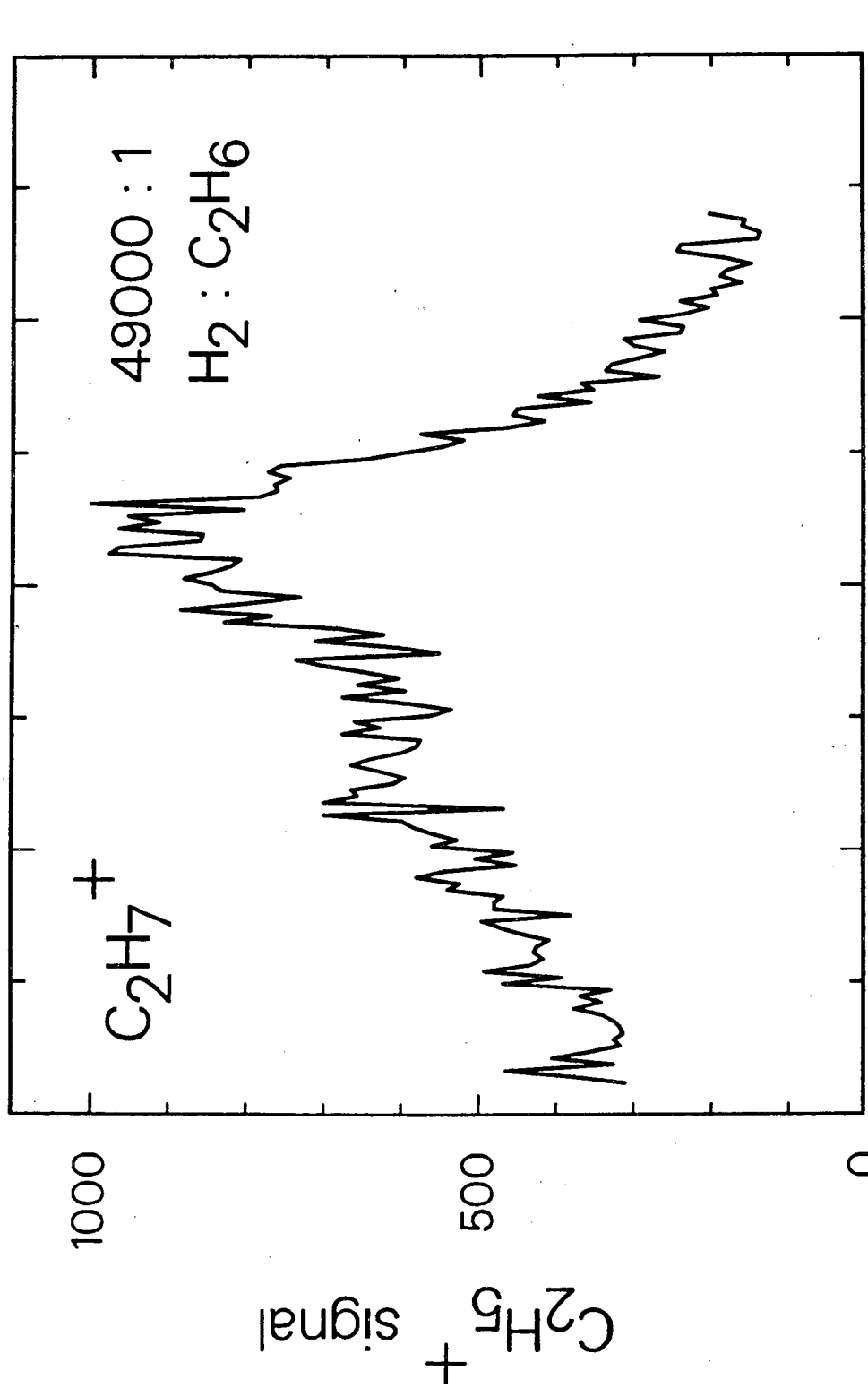

XBL 887-2526

Figure 11

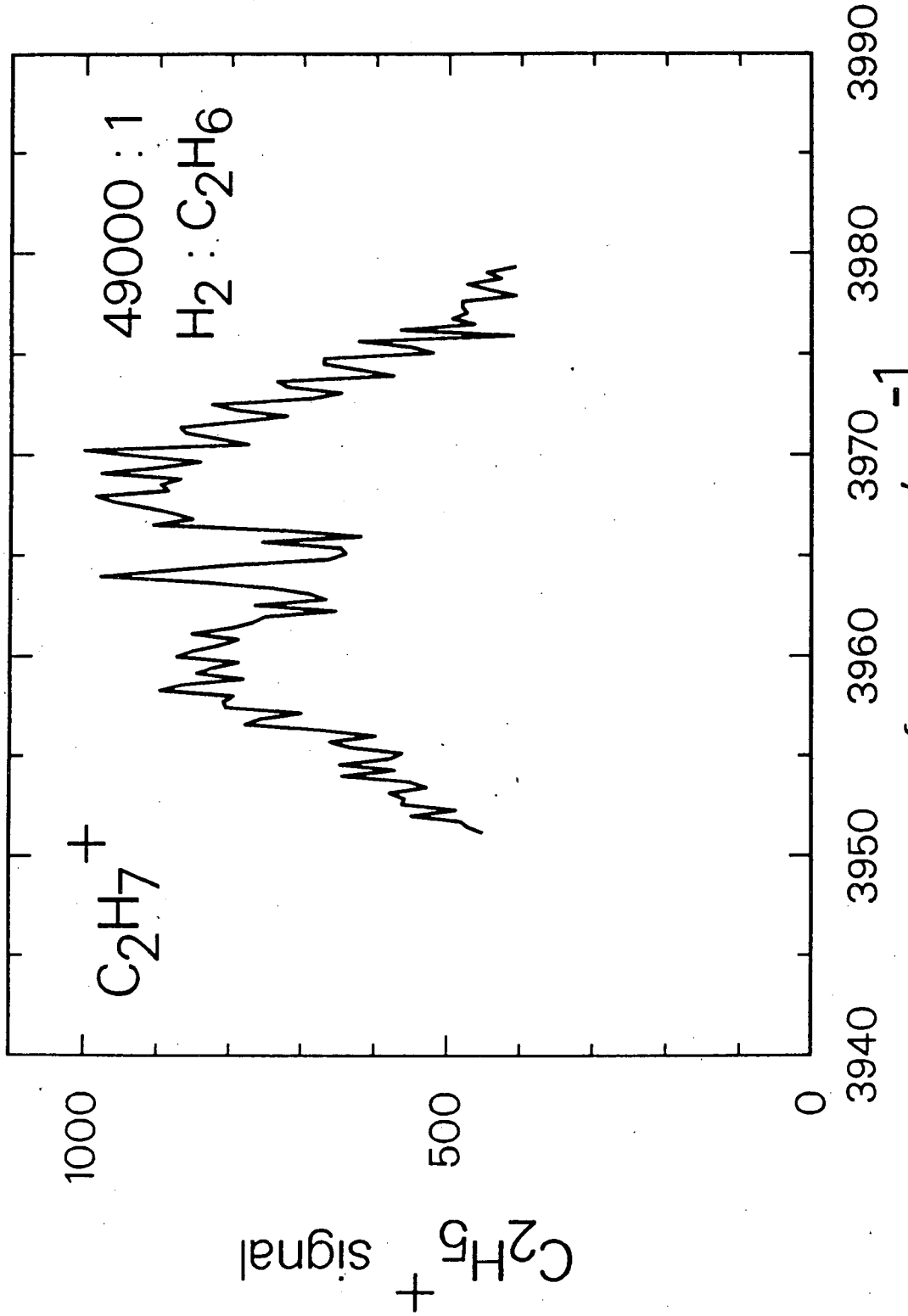

XBL 887-2530

Figure 12

LAWRENCE BERKELEY LABORATORY
TECHNICAL INFORMATION DEPARTMENT
1 CYCLOTRON ROAD
BERKELEY, CALIFORNIA 94720